

# Dissertation

submitted to the  
Combined Faculty of Natural Sciences and Mathematics  
of the  
Ruprecht-Karls-University Heidelberg  
for the degree of  
Doctor of Natural Sciences

Put forward by  
**Natalia Sánchez-Kuntz**  
born in: Mexico City, Mexico  
Oral examination: 29.11.2022

# An Entangled Vacuum and an Expanding Universe of Sound:

Pen, Paper, Numerics,  
and Condensate Traps

Referees: Prof. Dr. rer. nat. Stefan Flörchinger  
Prof. Dr. rer. nat. Maurits Haverkort



*Love is the strongest  
force in Nature.*

# Ein verschränktes Vakuum und ein expandierendes Klanguniversum: Stift, Papier, Zahlen und Kondensatfallen

## *Zusammenfassung*

In dieser Arbeit konzentrieren wir uns auf Bose-Einstein-Kondensate für zwei besondere Zwecke. Erstens als ein System, für das sich die Analyse der räumlichen Verschränkung aufgrund seiner zwei Regime (relativistisch/nichtrelativistisch) bezüglich der Dispersionsrelation von Bogoliubov-Quasiteilchen lohnt. Es ist daher ein vielversprechendes Szenario, um den Formalismus rund um die Berechnung von Verschränkungsentropien aus einem quantenfeldtheoretischen Ansatz heraus zu testen und einen Rahmen zu bieten, um Fragen im Zusammenhang mit seinen Divergenzen in einer relativistischen Quantenfeldtheorie weiter zu untersuchen. Wir liefern Ergebnisse für Kondensate ein- und zweidimensionaler räumlicher Geometrien, um eine selbstregulierte Theorie im Ultraviolett und eine Übereinstimmung mit der Literatur in allen erwarteten Ergebnissen zu finden. Darüber hinaus liefern wir neue Ergebnisse zum Übergangverhalten von nichtrelativistischen zu relativistischen Regimen. Unsere Berechnungen erfolgen unter Berücksichtigung eines unendlich ausgedehnten Kondensats. Das zweite Ziel ist die Implementierung des Kondensats als Quantensimulator für relativistische Felder in gekrümmten Raumzeiten, wobei Hintergrundgeometrien aufgebaut werden können, die sowohl räumlich gekrümmt als auch zeitabhängig sein können, um die Klasse der FLRW-Universen zu simulieren. Wir liefern das theoretische Konstrukt eines solchen Simulators und seine erfolgreiche experimentelle Umsetzung mit Ergebnissen zur Detektion der Teilchenproduktion in gekrümmten Raumzeiten. Beide Untersuchungsthemen sind für sich genommen interessant, aber zusammengenommen bieten sie die Möglichkeit, der Frage der Verschränkung in verschiedenen Raum-Zeit-Geometrien, einschließlich kausal getrennter Regionen, in einem experimentellen Kontext nachzugehen.

# **An entangled vacuum and an expanding universe of sound: pen, paper, numerics, and condensate traps**

## *Abstract*

In this work we focus on Bose-Einstein condensates for two particular purposes. First, as a system for which the analysis of spatial entanglement is worthwhile, given its two regimes (relativistic/nonrelativistic) regarding the dispersion relation of Bogoliubov quasiparticles. It is therefore a promising scenario to put to test the formalism around entanglement entropies computation from a quantum field theoretical approach, providing a setting to look further into questions related to its divergences in a relativistic quantum field theory. We put forward results for condensates of one- and two-dimensional spatial geometries, to find a self-regularised theory in the ultraviolet, and an agreement with the literature in all the expected results. Furthermore, we give new results regarding the crossover behaviour from nonrelativistic to relativistic regimes. Our calculations are done considering a condensate of infinite extent. The second aim is to implement the condensate as a quantum simulator for relativistic fields in curved spacetimes, building background geometries which can be both, spatially curved and time-dependent, being able to simulate the class of FLRW universes. We provide the theoretical construct of such a simulator, and its successful experimental implementation, with results related to the detection of particle production in curved spacetimes. Both topics of inquiry are interesting in and of themselves, while taken together they present the opportunity to look into the question of entanglement in different spacetime geometries, including causally disconnected regions, in an experimental context.

# Publications

---

1. Quantum field simulator for dynamics in curved spacetime.  
Viermann C, Sparrn M, Liebster N, Hans M, Kath E, Strobel H, Parra-López Á, Tolosa-Simeón M, **NSK**, Haas T, Floerchinger S, and Oberthaler MK, [arXiv:2202.10399](https://arxiv.org/abs/2202.10399) (2022). Accepted for publication.
2. Curved and expanding spacetime geometries in Bose-Einstein condensates.  
Tolosa-Simeón M, Parra-López Á, **NSK**, Haas T, Viermann C, Sparrn M, Hans M, Liebster N, Kath E, Strobel H, Oberthaler MK, and Floerchinger S, *Phys Rev A* **106**, 3 (2022).
3. Scalar quantum fields in cosmologies with  $2 + 1$  spacetime dimensions.  
**NSK**, Parra-López Á, Tolosa-Simeón M, Haas T, and Floerchinger S, *Phys Rev D* **105**, 10 (2022).
4. Spatial entanglement in interacting Bose-Einstein condensates.  
**NSK** and Floerchinger S, *Phys Rev A* **103**, 4 (2021).

# Contents

---

<b>1</b>	<b>Introduction</b>	<b>1</b>
<b>2</b>	<b>Theoretical starting point</b>	<b>4</b>
2.1	Condensation . . . . .	6
2.1.1	Bogoliubov theory from quantum statistics . . . . .	6
2.1.2	Symmetry broken phase in QFT . . . . .	10
2.2	Quantum simulators . . . . .	12
2.2.1	Cosmology: the system to simulate . . . . .	13
2.2.2	BEC: background of our simulator . . . . .	17
2.2.3	BEC: relativistic fields in curved spacetimes . . . . .	19
<b>3</b>	<b>Striking features</b>	<b>23</b>
3.1	Entanglement in QFT . . . . .	23
3.1.1	Entanglement entropy . . . . .	24
3.2	Particle production . . . . .	27
3.2.1	Symmetries in FLRW spacetimes . . . . .	27
3.2.2	Vacuum state in FLRW spacetimes . . . . .	27
<b>4</b>	<b>Entanglement in a BEC</b>	<b>32</b>
4.1	Three particular scenarios . . . . .	34
4.2	Dictionary to Fourier space . . . . .	35
4.2.1	In one dimension . . . . .	36
4.2.2	In two dimensions . . . . .	39
4.3	Analytical expressions . . . . .	43
4.3.1	For a one-dimensional system . . . . .	43
4.3.2	For a two-dimensional system . . . . .	47
4.4	Numerical results . . . . .	48
4.4.1	One-dimensional vacuum . . . . .	48
4.4.2	Two-dimensional vacuum . . . . .	51
<b>5</b>	<b>Table-top 2 + 1 cosmology</b>	<b>57</b>
5.1	Spatial curvature . . . . .	59
5.2	Expanding universe . . . . .	60
<b>6</b>	<b>Concluding remarks</b>	<b>69</b>

---

A Noninteracting BEC in a box	71
B Lower dimensional BEC	73
C Horizon problem and inflation	74
D Bogoliubov coefficients for polynomial expansion	75
E Experimental implementation	78
Bibliography	79

# Introduction

---

*It begins with one of the oldest storytelling devices, “Once there was, and once there was not...” This paradoxical phrase is meant to alert the soul of the listener that this story takes place in the world between worlds where nothing is as it first seems. So let us begin.*

When a system of bosons undergoes a phase transition in which the  $U(1)$  gauge symmetry is broken, the collective behaviour of the atoms gives rise to particular features worthwhile of examination and characterisation, as is the case for any particular phase of matter. In this situation we encounter the theory of Bose-Einstein condensates (BECs). This condensate phase involves the macroscopic occupation of the ground state, so that the background field has a nonvanishing expectation value when the system is in its ground state. Excitations on top of this vacuum state carry features of what has become a “matter bath”. In particular, their dispersion relation has two limits, a relativistic one in the low momentum regime, and a nonrelativistic one for higher energies.

The system thus comprises massless excitations for low momenta, phonons, and massive quasiparticles for high momentum modes. We use this promising scenario to look into the dynamics of relativistic fields in different types of backgrounds, which can be configured by playing around with the condensate properties [1–3]. We find also within BECs a good ground to test for features which would be typically divergent in the ultraviolet (UV), in particular we analyse entanglement entropies for these systems. These are the main topics of the present thesis, which aims at providing a starting point for the understanding, quantification, and experimental analysis of entanglement across simulated cosmological horizons [4–7]. Other themes to look into would be Hawking radiation [8] and the Unruh effect [9].

We provide here a precise calculation of spatial entanglement entropies in one- and two-dimensional BECs, a one-to-one mapping of the condensate structure to an FLRW universe — with freedom in the choice of spatial curvature — and clear benchmarks to certify the system as a successful simulator for relativistic fields in curved spacetimes. This thesis stems from the work developed in [10–13], and extends further for the case of spatial entanglement in two-dimensional condensates. Our work around  $d = 2 + 1$  dimensional models

for FLRW spacetimes is inspired and builds up on the already very proliferous analog gravity programme [14–23].

**This work is structured as follows:** in chapter 2 we provide the overall background for our work. In section 2.1 we give a brief overview of the theory behind weakly interacting BECs, using both a statistical approach, which derives in Bogoliubov theory (section 2.1.1), and a quantum field theoretical description of the symmetry broken phase (section 2.1.2). In section 2.2 we discuss the theory behind quantum simulators, with a particular focus on the evolution of relativistic fields on curved spacetimes. We provide the cosmological theory to be simulated in section 2.2.1 and go into the details that allow for such a simulation within BECs in section 2.2.2 and section 2.2.3.

In chapter 3 we put together the general treatment of the topics we want to look into, namely: entanglement in a quantum field theory (QFT) (section 3.1) and particle production in curved spacetimes (section 3.2).

We provide this as the main setting before going into the mathematical details needed to calculate entanglement in a nonrelativistic system (chapter 4) of one and two dimensions, to yield the numerical results, in section 4.4. We go into the theoretical predictions for the implementation of the quantum simulator in chapter 5, and provide also the experimental outcomes therein.

The intermittent quotes given in this work stem from two sources, the ones in purple from *Women Who Run With the Wolves*<sup>1</sup> and the ones in burgundy from *The Vajra Essence*<sup>2</sup>. All in all, if you'll embark, enjoy the ride.

**Units:** we employ natural units  $\hbar = c = k_B = 1$ . For this reason we use the wavevector  $k^\alpha$  in place of momentum  $p^\alpha$  throughout. SI units are only introduced to compare quantitatively experimental vs. theoretical results in chapter 5.

**Notation:** when the physics analysis is done in a spatial hypersurface  $\Sigma_t$  we use a D-dimensional integral over D-dimensional spatial volume, or conversely over D-dimensional conjugate momentum space<sup>3</sup>

$$\int_{\mathbf{x}} := \int_V d^D x \quad \int_{\mathbf{k}} := \frac{1}{(2\pi)^D} \int_{V_k} d^D k. \quad (1.1)$$

We denote spacetime vectors by  $\tilde{v} = (t, \mathbf{v})$ , and refer to spacetime dimension as  $d = D+1$ . When components are specified, we take away any redundant specification, therefore  $\tilde{v}^\alpha = v^\alpha$  denotes the  $\alpha$  component of the spacetime

<sup>1</sup>Pinkola-Estés C (Ballantine 1992).

<sup>2</sup>Wallace AB (Wisdom Publications 2017).

<sup>3</sup>We treat the metric determinant as implicit in the integral measure.

vector  $\tilde{v}$ . Just as above, we use the notation for spacetime integrals

$$\int_{\tilde{x}} := \int_{\mathcal{M}} d^d x \quad \int_{\tilde{k}} := \frac{1}{(2\pi)^d} \int_{\mathcal{M}_k} d^d k. \quad (1.2)$$

Derivatives with respect to any coordinate are expressed depending on convenience as

$$\frac{\partial}{\partial x^\mu} f := \partial_\mu f := f_{,\mu}. \quad (1.3)$$

We have also the particular cases of derivative with respect to coordinate time, conformal time, and spatial coordinate

$$\partial_0 f := \dot{f}, \quad \frac{\partial}{\partial \eta} f := f', \quad \text{and} \quad \partial_i := \nabla_i \quad (1.4)$$

respectively.

**Conventions:** greek indices run from 0 to  $d$  while latin indices run from 1 to  $d$ . Fourier transforms are carried out with the sign convention

$$\begin{aligned} f(\mathbf{k}) &= \int_{\mathbf{x}} e^{-i\mathbf{k}\mathbf{x}} f(\mathbf{x}) & \text{and} & & f(\mathbf{x}) &= \int_{\mathbf{k}} e^{i\mathbf{k}\mathbf{x}} f(\mathbf{k}), \\ f(\tilde{k}) &= \int_{\tilde{x}} e^{i(\omega t - \mathbf{k}\mathbf{x})} f(\tilde{x}) & \text{and} & & f(\tilde{x}) &= \int_{\tilde{k}} e^{-i(\omega t - \mathbf{k}\mathbf{x})} f(\tilde{k}). \end{aligned} \quad (1.5)$$

Talking about sign conventions, we use the metric signature  $\eta^{00} = -1$  and  $\eta^{ij} = \delta^{ij}$ , here specified by the Minkowski metric. We use Einstein's sum convention for repeated indices.

**A note on style:** my personal aim in this work is to provide the reader with the important outcomes of the corresponding research projects, framing those outcomes in the current physics understanding for which they are relevant. Here we explore three main areas of physics: condensed matter, quantum field theory, and cosmology. All of them have an immense background, with equal amount of literature. My wish is to make this a self-contained work, without overwhelming the reader with both information and literature, so I opt to take a minimalistic approach. Rather than providing extensive resources, I will provide the most characteristic, most representative, or neatest example (in my view) of the specific topics to be illustrated. Alongside, I will provide the outline of the theoretical construct, without the detail that is found in an extensive presentation such as a graduate lecture, textbook, or review, but mentioning the important building blocks, to connect the advanced notions with the ground they grow from.

## Theoretical starting point

---

Where to begin? From the harmonic oscillator to a chain of many oscillators? From the Hamiltonian formalism, to its Legendre transform and into Lagrangian mechanics? Canonical quantisation and continuum limit of the theory's degrees of freedom? Maybe rather setting the ground for statistical physics? Ergodic principle, second law, universality, symmetries... what have you?!

To the newcomer all of the above are good starting points; though one can guess that not many newcomers would be wandering around these pages, not with the interest to gain much from the work developed here, at least. To the learned ones, the above route would sound like a broken record of that tune played over and over in their 90's favourite radio frequency. REM? Something of the sort if you, like me, are a culturally western bug. A more exciting learning process for the newcomer, if any curiosity has suddenly arisen, would be to dive into the world wide web for videos and wikipedia articles explaining the above concepts (or, for example, into references [24, 25]). A less boring avenue for the learned reader is to go straight to the point: having in mind all the above building blocks, we turn now to more enticing matters, condensed matter.

While Fermi statistics is also relevant for the discussion of condensed matter, here we will exclusively focus on bosonic matter as our many-body subject. Although going to spinor fields extends the topic to broader situations and phenomena, we will focus on scalar bosons, with the aim to go as deep as possible into the handle and knowledge of this regime.

Well, wait, we do need some building blocks. Let us provide the relevant theoretical tools, as a way to also introduce the notation we employ throughout. Unsurprisingly, we begin with commutation relations for bosonic field operators,

$$\begin{aligned} [\phi(x), \pi(x')] &= i\delta(x - x') & [\phi_k, \pi_{k'}] &= i\delta_{kk'} \\ [\hat{a}_k, \hat{a}_{k'}^\dagger] &= \delta_{kk'} & [\hat{a}_k, \hat{a}_{k'}] &= 0, \end{aligned} \quad (2.1)$$

introducing the quantum field  $\phi$ , its conjugate momentum  $\pi$ , and the creation and annihilation operators  $\hat{a}$ ,  $\hat{a}^\dagger$ . The field and its conjugate momentum are related by

$$\pi(x) = \frac{\delta\mathcal{L}}{\delta\dot{\phi}(x)}, \quad (2.2)$$

where  $\mathcal{L}$  is the Lagrangian density. The creation and annihilation operators form an algebra which is irreducibly represented in Fock space. That is, any vector (state) in Fock space can be reached by repeated application of the objects of the algebra. *What is this Fock space anyway?* Well, if one can find a way to write down the Hamiltonian of the theory in diagonal form with operators  $\hat{a}_k, \hat{a}_k^\dagger$  — obtained by a canonical transformation of the fields —, then the ground state of that Hamiltonian — if it has one — is precisely the (unique) vacuum state in Fock space  $|0\rangle_{\hat{a}}$ , defined as the only state annihilated by all  $\hat{a}_k$ . All states in Fock space are eigenstates of the Hamiltonian, and the description of the many-body system turns from one of fields to that of quasiparticles. These quasiparticles encompass the relevant collective behaviour of the system.

**Fock space**

A good way to illustrate this is with a chain of oscillators with mass  $m$ , average spacing  $a$ , and spring constant  $k_s$ , written in the Lagrangian formalism as

$$\mathcal{L}(\phi, \partial_\mu \phi) = \frac{m}{2} \dot{\phi}^2(x) - \frac{k_s a^2}{2} (\partial_x \phi(x))^2, \quad (2.3)$$

or through the Hamiltonian density, its Legendre transform, as

$$\mathcal{H}(\phi, \partial_\mu \phi) = \pi \dot{\phi} - \mathcal{L} \Big|_{\dot{\phi}=\dot{\phi}(\phi, \pi)} = \frac{1}{2m} \pi^2(x) + \frac{k_s a^2}{2} (\partial_x \phi(x))^2. \quad (2.4)$$

The latter can be integrated out to obtain the Hamiltonian of a set of independent oscillators,

$$\hat{H} = \sum_k \frac{1}{2m} \pi_k \pi_{-k} + \frac{m\omega_k^2}{2} \phi_k \phi_{-k} = \sum_k \omega_k \left( \hat{a}_k^\dagger \hat{a}_k + \frac{1}{2} \right). \quad (2.5)$$

In this last step we took the Hamiltonian density (2.4) to Fourier space, and the canonical transformation

$$\hat{a}_k = \sqrt{\frac{m\omega_k}{2}} \left( \phi_k + \frac{i}{m\omega_k} \pi_{-k} \right), \quad \hat{a}_k^\dagger = \sqrt{\frac{m\omega_k}{2}} \left( \phi_{-k} - \frac{i}{m\omega_k} \pi_k \right) \quad (2.6)$$

to diagonalise the Hamiltonian. Thus, the chain constructed here can be regarded as a system of  $n$  independent oscillators with different frequencies. That is, an  $n$ -particle state  $|n\rangle_{\hat{a}}$  in Fock space with energy  $\sum_k \omega_k (n_k + 1/2)$ , determined by the Hamiltonian (2.5) through the eigenvalue equation

$$\hat{N}_k |n\rangle_{\hat{a}} = n_k |n\rangle_{\hat{a}}, \quad \hat{N}_k := \hat{a}_k^\dagger \hat{a}_k. \quad (2.7)$$

**Occupation number operator**

The system is therefore completely described by its modes  $k$  and the number of quasiparticles  $n_k$  in each mode; the defined operator  $\hat{N}_k$  is thus called the occupation number operator.

In the above we used a discrete momentum basis, which corresponds to a chain of oscillators of finite size, but this need not be the case. Anyhow, one

goes from position space to momentum space through a discrete or continuous Fourier transform (1.5), depending on the spatial region one is interested in analysing (of finite or infinite extent, correspondingly).

Let us now turn to the topic of condensation. Here we refer to condensation as the transition to a phase where the global  $\mathbf{U}(1)$  symmetry of a system of bosons is broken, which occurs under precise thermodynamic conditions. This concept will be cleared out in the following.

## 2.1 Condensation

The characteristic feature of a condensate is the macroscopic occupation of the (one-particle) lowest energy eigenstate. That this is equivalent to  $\mathbf{U}(1)$  symmetry breaking has extensively been discussed; sound proofs, summaries, and conclusions around this discussion can be found in [26–29]. Mathematically, they show that the Bogoliubov prescription of assigning a number  $\sqrt{N_0} \sim \sqrt{N}$  to the creation (annihilation) operator of the lowest energy eigenstate, gives rise — in the thermodynamic limit ( $N \rightarrow \infty$ ,  $V \rightarrow \infty$ ,  $N/V \rightarrow n$ ) — to a theory described by a Hamiltonian where the  $\mathbf{U}(1)$  symmetry is absent. This symmetry is restored when the ground state is not macroscopically occupied, where  $\hat{a}_0$ ,  $\hat{a}_0^\dagger$  recover their operator character.

Provided we have a many-body system, there are two natural approaches to analyse it. First is the path drawn by quantum statistics, which — for a weakly interacting gas at low temperatures — culminates in Bogoliubov theory; second we have the description coming from a quantum field theoretical formalism, giving rise to the same results, once the broken-symmetric-phase is considered. We shall expand on both of them.

### 2.1.1 Bogoliubov theory from quantum statistics

In order to set the thermodynamic aspects of condensation, we discuss the case of a free gas in a box in [appendix A](#). Here we will introduce weak interactions and work with what is known for the condensed regime, basically the macroscopic occupation of the ground state below critical temperature. We will focus now on a three dimensional system, and go into the specific considerations regarding lower spatial dimensions in [appendix B](#).

The Hamiltonian we are interested in includes two-body interactions, which can be described through the two-body Hamiltonian

$$\hat{h}(\mathbf{r}, \mathbf{r}') = \hat{a}^\dagger(\mathbf{r})\hat{a}^\dagger(\mathbf{r}')V(\mathbf{r} - \mathbf{r}')\hat{a}(\mathbf{r})\hat{a}(\mathbf{r}') \quad (2.8)$$

depicting a two-to-two scattering process. Within the many-body system, we take into account the repetition of this process by every pair of particles, distributed over all possible positions in the spatial extent of our sample, plus the

Hamiltonian that characterises each individual particle, so that the complete system is described by

$$\begin{aligned}\hat{H} &= \int_{\mathbf{r}} \frac{1}{2m} \nabla \hat{a}^\dagger(\mathbf{r}) \nabla \hat{a}(\mathbf{r}) + \frac{1}{2} \int_{\mathbf{r}, \mathbf{r}'} \hat{a}^\dagger(\mathbf{r}) \hat{a}^\dagger(\mathbf{r}') V(\mathbf{r} - \mathbf{r}') \hat{a}(\mathbf{r}) \hat{a}(\mathbf{r}') \\ &= \sum_{\mathbf{k}} \frac{\mathbf{k}^2}{2m} \hat{a}_{\mathbf{k}}^\dagger \hat{a}_{\mathbf{k}} + \frac{1}{2V} \sum_{\mathbf{k}, \mathbf{k}', \mathbf{q}} V_{\mathbf{q}} \hat{a}_{\mathbf{k}+\mathbf{q}}^\dagger \hat{a}_{\mathbf{k}'-\mathbf{q}}^\dagger \hat{a}_{\mathbf{k}} \hat{a}_{\mathbf{k}'}.\end{aligned}\quad (2.9)$$

Note that we have introduced the creation and annihilation operators in position space, obtained by the basis transformation

$$\hat{a}(\mathbf{r}) = \sum_{\mathbf{k}} \langle \mathbf{r} | \mathbf{k} \rangle \hat{a}_{\mathbf{k}} = \frac{1}{\sqrt{V}} \sum_{\mathbf{k}} e^{i\mathbf{k}\mathbf{r}} \hat{a}_{\mathbf{k}}, \quad (2.10)$$

and expressed the two particle potential in Fourier space by the identification

$$V_{\mathbf{q}} = \int_{\mathbf{r}} e^{-i\mathbf{q}\mathbf{r}} V(\mathbf{r}). \quad (2.11)$$

If we focus on the interaction process at low energies, we can work with the lowest momentum mode of the potential, given by  $\mathbf{q} = 0$  in the Fourier expansion. The Hamiltonian is then

$$\hat{H} = \sum_{\mathbf{k}} \frac{\mathbf{k}^2}{2m} \hat{a}_{\mathbf{k}}^\dagger \hat{a}_{\mathbf{k}} + \frac{V_0}{2V} \sum_{\mathbf{k}, \mathbf{k}', \mathbf{q}} \hat{a}_{\mathbf{k}+\mathbf{q}}^\dagger \hat{a}_{\mathbf{k}'-\mathbf{q}}^\dagger \hat{a}_{\mathbf{k}} \hat{a}_{\mathbf{k}'} \quad (2.12)$$

where  $V_0$  determines the s-wave scattering length in perturbation theory up to a certain order of approximation (Born approximation). If we would consider only zero momentum modes ( $\mathbf{k} = \mathbf{k}' = \mathbf{q} = 0$ ), then the above expression would yield the energy of the ground state,

$$E_0 = \frac{V_0 N^2}{2V} \quad (2.13)$$

which is realised at zero temperature. In this situation, the expected occupation number of atoms in the condensate equals the total number of particles,  $N_0 = N$ .

One can derive from the ground state energy (2.13) the equation of state for the BEC, and hence determine the speed of sound

$$P = -\frac{\partial E_0}{\partial V} = \frac{V_0 n^2}{2}, \quad mc^2 = \frac{\partial P}{\partial n} = V_0 n \quad \Rightarrow \quad c = \sqrt{\frac{V_0 n}{m}}; \quad (2.14) \quad \text{Speed of sound}$$

where the density  $n = N/V$  has been introduced.

When going to next order in momenta one considers that the total number of particles will be given by

$$\hat{a}_0^\dagger \hat{a}_0 + \sum_{\mathbf{k} \neq 0} \hat{a}_{\mathbf{k}}^\dagger \hat{a}_{\mathbf{k}} = N, \quad (2.15)$$

so that

$$\hat{a}_0^\dagger \hat{a}_0 \hat{a}_0^\dagger \hat{a}_0 + 2\hat{a}_0^\dagger \hat{a}_0 \sum_{\mathbf{k} \neq 0} \hat{a}_{\mathbf{k}}^\dagger \hat{a}_{\mathbf{k}} = N^2 + \mathcal{O}_{\mathbf{k}}(2) \quad (2.16)$$

at first order in momenta. Consequently, we have for the Hamiltonian in (2.12)

$$\begin{aligned} \hat{H} &= \frac{V_0}{2V} \left( \hat{a}_0^\dagger \hat{a}_0^\dagger \hat{a}_0 \hat{a}_0 + N \sum_{\mathbf{k} \neq 0} 4\hat{a}_{\mathbf{k}}^\dagger \hat{a}_{\mathbf{k}} + \hat{a}_{\mathbf{k}} \hat{a}_{-\mathbf{k}} + \hat{a}_{\mathbf{k}}^\dagger \hat{a}_{-\mathbf{k}}^\dagger \right) + \sum_{\mathbf{k}} \frac{\mathbf{k}^2}{2m} \hat{a}_{\mathbf{k}}^\dagger \hat{a}_{\mathbf{k}} \\ &= \frac{V_0 n}{2} \left( N + \sum_{\mathbf{k} \neq 0} 2\hat{a}_{\mathbf{k}}^\dagger \hat{a}_{\mathbf{k}} + \hat{a}_{\mathbf{k}} \hat{a}_{-\mathbf{k}} + \hat{a}_{\mathbf{k}}^\dagger \hat{a}_{-\mathbf{k}}^\dagger \right) + \sum_{\mathbf{k}} \frac{\mathbf{k}^2}{2m} \hat{a}_{\mathbf{k}}^\dagger \hat{a}_{\mathbf{k}}. \end{aligned} \quad (2.17)$$

This expression is evidently not diagonal in the Fock space spanned by the algebra  $\hat{a}_{\mathbf{k}}, \hat{a}_{\mathbf{k}}^\dagger$ . The way to go to an algebra of operators which diagonalises (2.17) is through a Bogoliubov transformation,

**Bogoliubov  
transformation**

$$\begin{pmatrix} \hat{a}_{\mathbf{k}} \\ \hat{a}_{-\mathbf{k}}^\dagger \end{pmatrix} = \begin{pmatrix} \alpha_{\mathbf{k}} & \beta_{-\mathbf{k}}^* \\ \beta_{\mathbf{k}} & \alpha_{-\mathbf{k}}^* \end{pmatrix} \begin{pmatrix} \hat{b}_{\mathbf{k}} \\ \hat{b}_{-\mathbf{k}}^\dagger \end{pmatrix}. \quad (2.18)$$

The Bogoliubov coefficients  $\alpha_{\mathbf{k}}$  and  $\beta_{\mathbf{k}}$  must satisfy

$$|\alpha_{\mathbf{k}}|^2 - |\beta_{-\mathbf{k}}|^2 = 1 \quad (2.19)$$

so that the bosonic commutation is preserved in the algebra of operators  $\hat{b}_{\mathbf{k}}, \hat{b}_{\mathbf{k}}^\dagger$ . This condition and enforcing the coefficients of nondiagonal terms (those in front of  $\hat{b}_{\mathbf{k}}^\dagger \hat{b}_{-\mathbf{k}}^\dagger$  and  $\hat{b}_{\mathbf{k}} \hat{b}_{-\mathbf{k}}$  in the Hamiltonian) to vanish, fully determines the shape of  $\alpha_{\mathbf{k}}$  and  $\beta_{\mathbf{k}}$  [25]

$$\alpha_{\mathbf{k}} = \left( \frac{\mathbf{k}^2/2m + V_0 n}{2\epsilon(\mathbf{k})} + \frac{1}{2} \right)^{1/2} \quad \beta_{-\mathbf{k}} = - \left( \frac{\mathbf{k}^2/2m + V_0 n}{2\epsilon(\mathbf{k})} - \frac{1}{2} \right)^{1/2}, \quad (2.20)$$

where  $\epsilon(\mathbf{k})$  is the Bogoliubov dispersion relation,

**Bogoliubov  
dispersion  
relation**

$$\epsilon(\mathbf{k}) = \sqrt{\frac{\mathbf{k}^2}{2m} \left( \frac{\mathbf{k}^2}{2m} + 2V_0 n \right)}. \quad (2.21)$$

By direct substitution in (2.17) one can see that the coefficients in front of  $\hat{b}_{\mathbf{k}}^\dagger \hat{b}_{\mathbf{k}}$  give rise to the term in the Hamiltonian

$$\begin{aligned} & \sum_{\mathbf{k}} \left[ (|\alpha_{\mathbf{k}}|^2 + |\beta_{\mathbf{k}}|^2) (\mathbf{k}^2/2m + V_0 n) + 2(\alpha_{\mathbf{k}} \beta_{\mathbf{k}}) V_0 n \right] \hat{b}_{\mathbf{k}}^\dagger \hat{b}_{\mathbf{k}} \\ & = \sum_{\mathbf{k}} \epsilon(\mathbf{k}) \hat{b}_{\mathbf{k}}^\dagger \hat{b}_{\mathbf{k}} \end{aligned} \quad (2.22)$$

while the ones which do not involve any quasiparticle give rise to the ground state energy,

$$E_0 = \frac{V_0 N n}{2} + \sum_{\mathbf{k}} \left[ |\beta_{\mathbf{k}}|^2 (\mathbf{k}^2/2m + V_0 n) + (\alpha_{\mathbf{k}} \beta_{\mathbf{k}}) V_0 n \right]. \quad (2.23)$$

To conclude, we introduce the s-wave scattering length  $a_s$  related to the interaction coupling constant  $\lambda$  through

$$a_s = \frac{m}{4\pi} \lambda. \quad (2.24)$$

**3D s-wave  
scattering  
length**

This scattering length can be obtained from the scattering amplitude calculated up to some order of approximation in the Born series [25, 30]. When going up to second order in the potential, the result yields for the coupling

$$\lambda = V_0 - \frac{V_0^2}{V} \sum_{\mathbf{k} \neq 0} \frac{m}{\mathbf{k}^2} \rightarrow V_0 = \lambda \left( 1 + \frac{\lambda}{V} \sum_{\mathbf{k} \neq 0} \frac{m}{\mathbf{k}^2} \right) \quad (2.25)$$

where we have expressed  $V_0$  in the same order of approximation. Since we are working up to first order in momenta,  $V_0 = \lambda$  goes into the Bogoliubov dispersion relation, and the term proportional to  $\lambda^2$  enters only the ground state energy. The Hamiltonian can be written down explicitly as,

$$\begin{aligned} \hat{H} & = \frac{\lambda N n}{2} + \frac{1}{2} \sum_{\mathbf{k}} \left[ \epsilon(\mathbf{k}) - \frac{\mathbf{k}^2}{2m} - \lambda n + \frac{(\lambda n)^2 m}{\mathbf{k}^2} \right] \\ & + \sum_{\mathbf{k}} \sqrt{\mathbf{k}^2 \left( \left( \frac{\mathbf{k}}{2m} \right)^2 + c^2 \right)} \hat{b}_{\mathbf{k}}^\dagger \hat{b}_{\mathbf{k}} \end{aligned} \quad (2.26)$$

in this order of approximation. The dispersion relation in front of the Bogoliubov quasiparticles implies that for low momenta  $|\mathbf{k}| \ll mc$  the dispersion relation becomes relativistic  $\epsilon = c|\mathbf{k}|$ , while for  $|\mathbf{k}| \gg mc$  the dispersion relation goes to that of nonrelativistic quasiparticles  $\epsilon = \mathbf{k}^2/2m$ . The magnitude of the momentum at the transition region defines the healing length as  $|\mathbf{k}| \sim 1/\xi$ , with

$$\xi = \frac{1}{\sqrt{2m\lambda n}}, \quad (2.27)$$

**Healing  
length**

which is an important parameter to determine the acoustic regime as opposed to the nonrelativistic one. In this way,  $\xi$  sets a characteristic length scale for Bose-Einstein condensates.

### 2.1.2 Symmetry broken phase in QFT

Let us now paint the same picture from the QFT perspective. Since we are considering an interacting theory of complex scalar fields, it is natural to start with a  $\varphi^4$  action for relativistic fields,

$$S = - \int_{\bar{x}} (\partial^\mu \varphi^* \partial_\mu \varphi + m^2 \rho) + \frac{\lambda_r}{2} \rho^2 \quad (2.28)$$

with  $\rho = \varphi^* \varphi$ . As we will work in the low energy regime, we consider the nonrelativistic limit of the theory by looking into the free part of the action. This is equivalent to finding the nonrelativistic limit of the Klein-Gordon equation,

$$(\partial^\mu \partial_\mu - m^2) \varphi = 0 \quad (2.29)$$

and substituting for the free part in (2.28). It is a textbook exercise [31] to find that the nonrelativistic version is precisely Schrödinger's equation,

$$\left( i\partial_0 + \frac{\nabla^2}{2m} \right) \Phi = 0 \quad (2.30)$$

for the rescaled field  $\varphi = \frac{1}{\sqrt{2m}} e^{-imt} \Phi$ . The nonrelativistic theory can then be written down as

**Nonrelativistic  
action**

$$S = \int_{\bar{x}} \Phi^* \left( i\partial_0 + \frac{\nabla^2}{2m} \right) \Phi - \frac{\lambda}{2} (\Phi^* \Phi)^2 \quad (2.31)$$

where  $\lambda$  is related to the coupling of the relativistic theory through  $\lambda = \lambda_r/4m^2$ . For an homogenous field,  $\Phi = \phi_0$  constant in spacetime, the above action finds a minimum of the potential at  $\phi_0 = 0$ , yielding a vanishing vacuum expectation value. Nevertheless, if one adds an offset energy term, for example in the form of a chemical potential, the Lagrangian density of the theory is then

$$\begin{aligned} \mathcal{L} &= \Phi^* \left( i\partial_0 + \frac{\nabla^2}{2m} \right) \Phi + \mu \Phi^* \Phi - \frac{\lambda}{2} (\Phi^* \Phi)^2 \\ &\stackrel{\Phi=\phi_0}{=} \mu \phi_0^* \phi_0 - \frac{\lambda}{2} (\phi_0^* \phi_0)^2 \end{aligned} \quad (2.32)$$

**Vacuum  
expectation  
value**

so that the field that solves for an extremum in the Lagrangian is  $\phi_0 = e^{i\alpha} \sqrt{\mu/\lambda}$ . Although the Lagrangian is still symmetric under a  $\mathbf{U}(1)$  transformation of the field, when the vacuum expectation value is non-zero, a choice of phase  $\alpha$  is

made and perturbation theory is done around this background field: this is how the global symmetry is spontaneously broken.

To describe the excitations around this background one can expand around  $\phi_0$  either in density and phase variables or in real and imaginary parts. Symmetry breaking leads to a Nambu-Goldstone mode, which in one case corresponds to the phase perturbation, and in the other to the imaginary part of the linear expansion. We take the latter approach, as it is directly related to the Bogoliubov quasiparticles. This is easily made evident from the dispersion relation of the fields. Taking  $\alpha = 0$  we have the linearised expansion,

$$\Phi(\tilde{x}) = \phi_0 + [\varphi_1(\tilde{x}) + i\varphi_2(\tilde{x})] / \sqrt{2}; \quad (2.33)$$

plugging this into the action corresponding to (2.32), we get

$$\begin{aligned} S &= \int_{\tilde{x}} \frac{\mu^2}{2\lambda} - \frac{1}{2}(\varphi_1, \varphi_2) \begin{pmatrix} -\frac{\nabla^2}{2m} + 2\lambda n & \partial_0 \\ -\partial_0 & -\frac{\nabla^2}{2m} \end{pmatrix} \begin{pmatrix} \varphi_1 \\ \varphi_2 \end{pmatrix} \\ &= \int_{\tilde{k}} \frac{\mu^2}{2\lambda} - \frac{1}{2}(\varphi_1, \varphi_2) \begin{pmatrix} \frac{\mathbf{k}^2}{2m} + 2\lambda n & -i\omega \\ i\omega & \frac{\mathbf{k}^2}{2m} \end{pmatrix} \begin{pmatrix} \varphi_1 \\ \varphi_2 \end{pmatrix} \end{aligned} \quad (2.34)$$

with  $n = |\phi_0|^2$ . By taking the determinant of the inverse propagator and equating it to zero, we find the Bogoliubov dispersion relation — (2.21), with  $\omega = \epsilon(\mathbf{k})$  and the  $V_0 = \lambda$  correspondence — for the excitations related to the perturbation fields  $\varphi_{1,2}$ .

We can read out from the action (2.34) the emergence of a massless field  $\varphi_2$  (the Nambu-Goldstone mode), and see also that  $\varphi_1$  and  $\varphi_2$  are each other's conjugate field, i.e.,

$$\pi_1 = \frac{\delta \mathcal{L}}{\delta \dot{\varphi}_1(x)} = \varphi_2, \quad \pi_2 = \frac{\delta \mathcal{L}}{\delta \dot{\varphi}_2(x)} = -\varphi_1. \quad (2.35)$$

It is therefore convenient to rescale the fields

$$\varphi_2 \rightarrow \varphi_2 / \sqrt{2m} = \phi, \quad \pi_2 \rightarrow \sqrt{2m} \pi_2 = \pi \quad (2.36)$$

and rewrite the action (2.34) as

$$\begin{aligned} S &= \int_{t, \mathbf{k}} \frac{\mu^2}{2\lambda} - \frac{1}{2} (A\pi_{-\mathbf{k}}\pi_{\mathbf{k}} - \pi_{-\mathbf{k}}\partial_0\phi_{-\mathbf{k}} - \pi_{\mathbf{k}}\partial_0\phi_{\mathbf{k}} + B\phi_{-\mathbf{k}}\phi_{\mathbf{k}}) \\ &\text{with } A = \frac{\mathbf{k}^2}{4m^2} + c^2 \quad \text{and } B = \mathbf{k}^2, \end{aligned} \quad (2.37)$$

using the expression of the speed of sound introduced in (2.14). By solving the Euler-Lagrange equations for  $\pi_{-\mathbf{k}}$  we find that  $\partial_0\phi_{-\mathbf{k}} = A\pi_{\mathbf{k}}$  and by substituting

into the action we obtain

**Full  
Bogoliubov  
action**

$$S = \int_{t,\mathbf{k}} \frac{\mu^2}{2\lambda} - \frac{1}{2} (-A\pi^2 + B\phi^2). \quad (2.38)$$

From here one can easily determine the Hamiltonian density,

$$\begin{aligned} \mathcal{H} = A\pi^2 - \mathcal{L} &= -\frac{\mu^2}{2\lambda} + \frac{1}{2} (A\pi_{-\mathbf{k}}\pi_{\mathbf{k}} + B\phi_{-\mathbf{k}}\phi_{\mathbf{k}}) \\ &= -\frac{\mu^2}{2\lambda} + \sqrt{AB} \left( \hat{b}_{\mathbf{k}}^\dagger \hat{b}_{\mathbf{k}} + \frac{1}{2} \right). \end{aligned} \quad (2.39)$$

We have taken the opportunity to introduce the creation and annihilation operators

$$\hat{b}_{\mathbf{k}} = \left( \frac{B}{4A} \right)^{1/4} \left( \phi_{\mathbf{k}} + i\sqrt{\frac{A}{B}}\pi_{-\mathbf{k}} \right), \quad \hat{b}_{\mathbf{k}}^\dagger = \left( \frac{B}{4A} \right)^{1/4} \left( \phi_{-\mathbf{k}} - i\sqrt{\frac{A}{B}}\pi_{\mathbf{k}} \right) \quad (2.40)$$

and encounter again the Bogoliubov dispersion relation  $\sqrt{AB} = \epsilon(\mathbf{k})$ . While the action (2.38) describes the full Bogoliubov theory, when working in the low momentum regime one can approximate  $A \approx c^2$  and rewrite the action (using  $\partial_0\phi = A\pi$ ) as

**Acoustic  
approximation**

$$S = \int_{\tilde{x}} \frac{\mu^2}{2\lambda} - \frac{1}{2} \left( -\frac{(\partial_0\phi)^2}{c^2} + (\nabla\phi)^2 \right) \quad (2.41)$$

which is the action of a massless relativistic scalar field. Of course, now we have  $\sqrt{AB} = c|\mathbf{k}|$  for the dispersion relation of the excitations of this field. This fact inspires the construction of simulators for relativistic quantum fields in different background geometries. Different geometries can be engineered by making the speed of sound  $c$  a spacetime dependent quantity, meaning that the structure of the background field  $\phi_0$  must now be space and/or time dependent, as developed in [section 2.2.2](#).

## 2.2 Quantum simulators

The history of fluids simulating spacetime metrics can be traced back to Unruh's proposal [9]. A quest for building different types of simulators, both classical and quantum, which stand for scenarios which are far from experimental reach has taken a plethora of roads, with successful proposals and outcomes. The specific case of an acoustic regime emerging from a many-body setting is particularly inviting for the simulation of relativistic fields on a certain background, given that the action of each of these two scenarios has the same mathematical structure, so an analog treatment is possible. We therefore encounter here a great opportunity to look deeper into cosmology, as it pertains the dynamics of relativistic quantum fields in curved spacetimes.

## 2.2.1 Cosmology: the system to simulate

*Therefore space, self, others, and all sense objects are of one taste — they are certainly not separate. Moreover, it is the luminosity of space itself, and nothing else, that makes appearances manifest.*

Let us begin by specifying the particular instance of cosmology that we wish to simulate with the condensed matter systems at hand. Cosmology studies a wide range of phenomena involved in the formation and evolution of the universe with all its energy/matter content. At its core it is a theory of fields and geometry: it comprises the evolution of these fields living in particular backgrounds, better known as “spacetimes”. A spacetime is a  $d$ -dimensional manifold endowed with a Lorentz metric, i.e., it can be described by a coordinate chart with one “temporal” coordinate and  $D$  “spatial” coordinates. The particular feature of a Lorentz metric is that timelike and spacelike distances have opposite signs; a Lorentz metric is thus defined by its signature,  $(1, D)$  — this sets the tone.

Apart from the signature, the geometry of spacetime is determined by its matter content, as expressed through Einstein’s equations: in the absence of matter, spacetime is flat, in the presence of matter, spacetime is curved,

$$G_{\alpha\beta} := R_{\alpha\beta} - \frac{1}{2}Rg_{\alpha\beta} = 8\pi G_N T_{\alpha\beta}. \quad (2.42) \quad \text{Einstein's equations}$$

Some important objects have sneaked in: the Ricci tensor and scalar ( $R_{\alpha\beta}$  and  $R$ ), Newton’s constant in  $D$  dimensions ( $G_N$ ), the energy momentum tensor ( $T_{\alpha\beta}$ ), and of course, Einstein’s tensor ( $G_{\alpha\beta}$ ); further details about them will be given soon. Back to the notion of curvature: let us remember that this geometrical property is manifest in the acceleration of bodies residing in a given spacetime, or what is formally known as “geodesic deviation”. Simply put, geodesics are the natural straight trajectories drawn by “free falling” objects in a certain spacetime, if through time they “accelerate” either towards or away from each other, then they must be drawn upon curved backgrounds. A brief explanation of this idea is given in [Figure 2.1a](#) and caption therein. Acceleration between geodesics is quantified by

$$a^\mu = u^\alpha \nabla_\alpha (u^\beta \nabla_\beta h^\mu) = R^\mu{}_{\alpha\beta\gamma} u^\alpha u^\beta h^\gamma, \quad (2.43)$$

where we see the Riemann tensor  $R^\mu{}_{\alpha\beta\gamma}$  emerge as the defining parameter for the curvature of the  $d$ -dimensional manifold. Here, as shown in [Figure 2.1a](#),  $\tilde{u}$  is the geodesics’ tangent vector, while  $\tilde{h}$  is the deviation vector. Time for a crash course on geodesics: what defines a straight line in a manifold which can be curved all over the place? Well, the “geodesic equation”, the solution of which are those curves that “parallel transport” their own tangent vector, which is what characterises a “shortest distance” trajectory. The geometrical

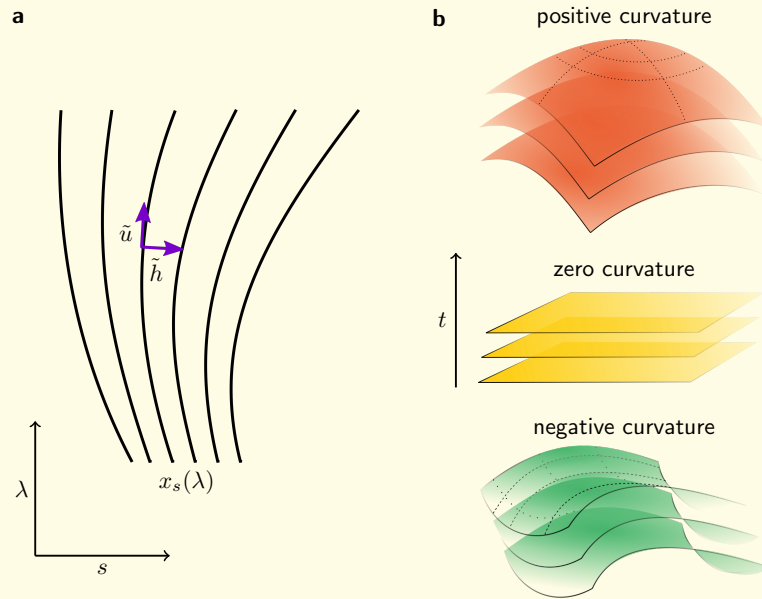


**Figure 2.1 | A look into curvature.** Depicted in **a** is a family of geodesics parametrised by  $s$ . The geodesic  $x_s(\lambda)$  has the neighbouring geodesic  $x_{s+\delta s}(\lambda)$ . It also has a tangent vector  $\tilde{u}$  and one orthogonal to it,  $\tilde{h}$ , connecting the two geodesics. Acceleration (or curvature) is the notion of the change of  $\tilde{h}$  when moving tangentially to  $\tilde{u}$ . In **b** we show the natural foliation of all three possible spatially curved isotropic universes. Each of the surfaces depicted in a group is defined by a constant time parameter  $t$ .

object which tells us how things are parallel transported along a manifold is “the connection”. Fast forward in our crash course: in general relativity we work with the Levi-Civita connection, whose components (in some coordinate basis) are given by the Christoffel symbols  $\Gamma^\alpha_{\beta\gamma}$  so that the geodesic equation for a curve  $x(\lambda)$ , parametrised by  $\lambda$  reads

$$\frac{d^2 x^\alpha}{d\lambda^2} + \Gamma^\alpha_{\beta\gamma} \frac{dx^\beta}{d\lambda} \frac{dx^\gamma}{d\lambda} = 0. \quad (2.44)$$

Let us now properly introduce the Ricci tensor and scalar,

$$R_{\alpha\beta} := R^\mu_{\alpha\mu\beta}, \quad R := g^{\alpha\beta} R_{\alpha\beta}; \quad (2.45)$$

done. With these objects we can now talk about the geometry of spacetime, but we do not know anything yet about  $g_{\alpha\beta}$  — or  $T_{\alpha\beta}$  for that matter — so we are missing both sides of Einstein’s equations (2.42). Luckily enough we can approximate our universe as a homogeneous and isotropic spacetime. Homogeneity means that matter distribution is everywhere the same, and isotropy, that the universe looks the same in every direction around any point one is standing at.

**Cosmological principle**

To think about it, this appears to be not much about luck but about balance, for why would there be any preference in a certain location or direction, if one takes into account symmetric initial conditions? — actually this is not so trivial, and brings about what is known as “the horizon problem” together with the need for an inflationary period in the early universe; we give a brief account of this in [appendix C](#). It is nevertheless lucky for us, given that all the equations simplify enormously just by this observation, the cosmological principle.

Taking the cosmological principle as guiding principle for the geometry of spacetime ( $g_{\alpha\beta}$ ), the first thing to note is that there exists a natural foliation of this spacetime through spacelike hypersurfaces  $\Sigma_t$ . What does this mean? Well, that one can describe this spacetime by a set of “sheets”  $\Sigma_t$  orthogonal to a timelike flow, as presented in [Figure 2.1b](#).

This allows to select coordinates (the coordinate chart of “isotropic observers”) in which the metric components are simply  $g_{00} = -1$ ,  $g_{0i} = g_{i0} = 0$ , and  $g_{ij} = h_{ij}(t)$ , where  $h_{ij}(t)$  is the metric induced by  $g_{\alpha\beta}$  on the spatial hypersurfaces  $\Sigma_t$ . Isotropy requires that the spatial hypersurfaces have a constant curvature,  $\kappa$ , and that they are related to each other simply by a rescaling of distances  $a(t)$ . Thus, introducing the scale factor  $a(t)$ , the spatial line element is given by

$$h_{ij}(t)dx^i dx^j = a^2(t) \left( \frac{dr^2}{1 - \kappa r^2} + r^2 d\Omega^2 \right) = a^2(t) \gamma_{ij} dx^i dx^j. \quad (2.46)$$

In this way, for the spacetime metric, we get the FLRW line element

$$ds^2 = -dt^2 + a^2(t) \gamma_{ij} dx^i dx^j. \quad (2.47) \quad \text{FLRW line element}$$

Finally, we can start to have some fun calculating Christoffel symbols, and all the geometric quantities up to the Einstein tensor, then by Einstein’s equation (2.42) and a certain matter distribution dictated by  $T_{\alpha\beta}$ , obtain Friedman’s equations to determine the scale factor  $a(t)$  as a function of time.

First, let us give general expressions for the nonvanishing components of the Levi-Civita connection in an FLRW universe,

$$\begin{aligned} \Gamma^{\alpha}_{\beta\gamma} &= \frac{1}{2} g^{\alpha\lambda} (g_{\lambda\beta,\gamma} + g_{\lambda\gamma,\beta} - g_{\beta\gamma,\lambda}) \\ \Rightarrow \Gamma^0_{ii} &= \frac{1}{2} g^{ii,0}, \quad \Gamma^i_{i\mu} = \frac{1}{2} g^{ii} g^{ii,\mu}, \quad \text{and} \quad \Gamma^i_{jj} \stackrel{i \neq j}{=} -\frac{1}{2} g^{ii} g^{jj,i}. \end{aligned} \quad (2.48)$$

For the Ricci tensor we have

$$R_{\alpha\beta} = \Gamma^{\lambda}_{\alpha\beta,\lambda} - \Gamma^{\lambda}_{\alpha\lambda,\beta} + \Gamma^{\lambda}_{\lambda\rho} \Gamma^{\rho}_{\alpha\beta} - \Gamma^{\rho}_{\alpha\lambda} \Gamma^{\lambda}_{\beta\rho} \quad (2.49)$$

and for the Ricci scalar, we simply calculate the trace  $R^{\alpha}_{\alpha}$ . We explicitly derive these quantities for a 2 + 1-dimensional spacetime in [chapter 5](#); in general,

Einstein's tensor (2.42) in  $D$  spatial dimensions for an FLRW metric can be determined to be

$$\begin{aligned} G_{00} &= \frac{D(D-1)}{2a^2}(\dot{a}^2 + \kappa) \\ G_{ii} &= -\frac{D-1}{a^2} \left[ \ddot{a}a + \frac{D-2}{2}(\dot{a}^2 + \kappa) \right] g_{ii}. \end{aligned} \quad (2.50)$$

Now, the energy momentum tensor of a homogenous and isotropic universe is simply

$$T_{\alpha\beta} = \epsilon (u_\alpha u_\beta) + P (u_\alpha u_\beta + g_{\alpha\beta}) \quad (2.51)$$

**Energy  
momentum  
tensor**

where the matter content is modelled by a fluid with velocity  $\tilde{u}$ , having the components  $u^0 = 1, u^i = 0$  for an observer moving with the flow (the isotropic observer we have followed all along). We have introduced here the energy density  $\epsilon$  and the effective pressure  $P$ . The conservation law  $\nabla_\alpha T^\alpha_\beta = 0$  imposed on this shape of  $T_{\alpha\beta}$  yields the evolution equation for the energy density

$$\dot{\epsilon} + D \frac{\dot{a}}{a} (\epsilon + P) = 0. \quad (2.52)$$

Now we have all the tools we need to analyse three different scenarios: radiation dominated ( $T^\alpha_\alpha = 0$ ), matter dominated ( $P = 0$ ), and dark energy dominated ( $P = -\epsilon$ ). Defining the quantity  $w := P/\epsilon$ , a general solution for the evolution of the energy density in terms of the scale factor  $a(t)$  is obtained,

$$\epsilon \propto a^{-D(1+w)}. \quad (2.53)$$

Here we can read out that the energy density, for any spatial dimension:

- scales inversely to the volume multiplied by  $1/a(t)$  (due to energy redshift in time) for a radiation dominated scenario, where  $w = 1/D$ ;
- scales inversely to the volume for a matter dominated scenario,  $w = 0$ ;
- remains constant in time for a dark energy dominated universe,  $w = -1$ .

We will forget about the proportionality constants in Einstein's equation and look only into the dependence of the scale factor with respect to time. To do so we remember the equation corresponding to  $G_{00}$  and put together radiation ( $\gamma$ ), matter (M), and dark energy ( $\Lambda$ ) dominated situations,

$$(\dot{a}^2 + \kappa) \propto \begin{cases} a^{1-D} \\ a^{2-D} \\ a^2 \end{cases} \xrightarrow[\text{D=3}]{\kappa=0} a(t) \propto \begin{cases} t^{1/2} & \gamma \\ t^{2/3} & \text{M} \\ e^{Ht} & \Lambda, \end{cases} \quad (2.54)$$

which are the famous solutions for different expansion epochs in our universe, including in particular our current state of expansion ( $\Lambda$  dominated), with the Hubble rate  $H = \dot{a}/a$ . One can look into [32, 33] for further knowledge about  $d = 3 + 1$  dimensional FLRW universes with nonvanishing spatial curvature in the context of inflation.

Let us pause a bit from calculations and remember our present motivation: to simulate FLRW manifolds in the lab. We will do this in  $2 + 1$  dimensions, so in chapter 5 we give the solutions analogous to (2.54) in the lower spatial dimension  $D = 2$ . We show therein that a simulation can be built for the general situation  $a(t) \propto t^\gamma$  and put this into practice. The emergent spacetime can further be manipulated to have either vanishing, positive, or negative curvature, the theoretical implementation of which is summarised in section 5.1.

Trapping condensates, though, and playing around with the parameters as the theory dictates, is not enough to actually certify that the corresponding spacetime has emerged in such a trapping situation. One has to come up with measurable quantities that depend on the spatial curvature  $\kappa$  or the type of expansion  $a(t)$ , which are theoretically distinguishable for the different scenarios, and obtain an agreement with the predictions. For the former we analyse phonon propagation in spatially curved metrics, and for the latter we make use of the phenomenon of particle production presented in section 3.2. Time to move forward then.

## 2.2.2 BEC: background of our simulator

The universes that are to be (were!) created in the lab with the proposal presented here are effectively of two spatial dimensions: that is, we work with a pancake trapping of the condensate. To describe this geometry it is convenient to go to cylindrical coordinates, and impose tight confinement in the  $z$ -direction. The confinement is realised by adding an external potential  $V$  to the action (2.31), while the coupling strength  $\lambda$  is made time-dependent to simulate an expanding (but could also be contracting) universe. Additionally, the linear splitting of the field (2.33) now includes a spatially-dependent background to simulate spatial surfaces of different curvatures. Putting all this into equations, we have for the action

$$S = \int_{\tilde{r}} \Phi^* \left( iD_0 + \frac{D^i D_i}{2m} - V \right) \Phi - \frac{\lambda}{2} (\Phi^* \Phi)^2 \quad (2.55)$$

with  $\tilde{r} = (t, r, \varphi)$ ; for the trapping potential

$$V(t, \mathbf{r}) = \frac{m}{2} \omega^2(t) f(\mathbf{r}) \quad (2.56)$$

where, for example  $f(\mathbf{r}) = r^2$  would mimic a harmonic trap, in which case  $\omega(t)$  plays the role of a trapping frequency; and for the 2D coupling

2D coupling

$$\lambda(t) = \sqrt{\frac{8\pi\omega_z}{m}} a_s(t), \quad (2.57)$$

where  $\omega_z$  is the trapping frequency in the  $z$ -direction. Let us take a quick look into the action (2.55). Notice that we have introduced covariant derivatives  $D_\mu$ , covariant with respect to gauge transformations, of course. That is, we have a gauge field related to the  $\mathbf{U}(1)$  symmetry given by  $A_\mu = \partial_\mu \alpha(t, \mathbf{r})$ , where  $\alpha$  defines the gauge transformation  $U(t, \mathbf{r}) = e^{-i\alpha(t, \mathbf{r})}$ . The gauge field then determines the covariant derivative as

$$D_\mu = \partial_\mu + iA_\mu. \quad (2.58)$$

Let us apply these considerations to the background field, described by the condensate wavefunction

$$\phi_0(t, \mathbf{r}) = \sqrt{n_0(t, \mathbf{r})} e^{iS_0(t, \mathbf{r})}, \quad (2.59)$$

and let us focus on a static situation, where the density does not depend on time, so that  $n_0(t, \mathbf{r}) := n_0(\mathbf{r})$ . Additionally one can choose (by symmetry) the setting in which  $\nabla S_0 = 0$ ; this is the frame in which the condensate is at rest. A general description for a condensate with superfluid velocity  $\mathbf{v} \propto \nabla S_0$  is given in [12].

The action (2.55) provides two equations of motion for the background field. One of them is a continuity equation, which is trivial, since the background density  $n_0$  is time-independent and the superfluid velocity  $\mathbf{v}$  is zero. The second equation is

$$\begin{aligned} 0 &= \left( -D_0 S_0(t) + \frac{D^i D_i}{2m} - V(t, \mathbf{r}) - \lambda(t) n_0(\mathbf{r}) \right) \phi_0(t, \mathbf{r}) \\ &= \left( -\partial_0 S_0(t) + \frac{\nabla^2}{2m} - V(t, \mathbf{r}) - \lambda(t) n_0(\mathbf{r}) \right) \phi_0(t, \mathbf{r}) \end{aligned} \quad (2.60)$$

where we have chosen  $A_\mu = 0$ . If we apply the gauge transformation  $U(t) = e^{-iS_0(t)}$

$$\begin{aligned} \phi_0(t, \mathbf{r}) &\rightarrow e^{-iS_0(t)} \phi_0(t, \mathbf{r}) = \sqrt{n_0(\mathbf{r})} \\ \partial_0 &\rightarrow \partial_0 + i\partial_0 S_0(t) = \partial_0 - i\mu(t) \end{aligned} \quad (2.61)$$

we get of course the same equations of motion — trivial continuity and (2.60) —, but now with the chemical potential  $\mu(t) = -\partial_0 S_0(t)$  explicitly written down in the action, as was done in (2.32).

We can go further by implementing the Thomas-Fermi approximation, which amounts to neglecting the quantum pressure term  $\propto \nabla^2 \sqrt{n_0(\mathbf{r})}$ , and find that (2.60) reduces to

$$\begin{aligned} n_0(\mathbf{r}) &= \frac{\mu(t)}{\lambda(t)} - \frac{m\omega^2(t)}{2\lambda(t)} f(\mathbf{r}) \\ &= n \left( 1 - \frac{f(\mathbf{r})}{R^2} \right), \end{aligned} \quad (2.62) \quad \text{Background density}$$

with the size parameter  $R$

$$R^2 = \frac{2n\lambda(t)}{m\omega^2(t)}. \quad (2.63)$$

We work with the general assumption  $f(r=0) = 0$ , so that  $n_0(0) = n$  is the condensate density at the centre of the trap. When the trapping potential is that of a harmonic trap —  $f(\mathbf{r}) = r^2$  — we recover the Thomas-Fermi density profile, where the size parameter corresponds to the Thomas-Fermi radius  $R_{\text{TF}}$ .

Thomas-Fermi radius

Let us pause a bit and reflect on the experimental implementation of the above description. We have said that one can have a time-dependent interaction  $\lambda(t)$  by adjusting the scattering length, this is done by tuning to and playing around a convenient Feshbach resonance of the sample [34]. As the system is governed by a repulsive interaction, then lowering  $\lambda$  would have an effect on the size parameter  $R$  (shrinking) if nothing is done to the trapping frequency. So, to have a condensate of constant radius, one changes  $\omega(t)$  accordingly. Lowering the trapping frequency, makes the sample “relax” onto a larger size, lower repulsion makes it stay at constant size. Voilà.

### 2.2.3 BEC: relativistic fields in curved spacetimes

We have learnt before that a relativistic field is born from the fluctuations on top of a condensate background, involved in the linear splitting

$$\Phi(t, \mathbf{r}) = \phi_0(t, \mathbf{r}) + [\varphi_1(t, \mathbf{r}) + i\varphi_2(t, \mathbf{r})] / \sqrt{2}. \quad (2.64)$$

To derive the action for the fluctuating fields  $\varphi_i$  we perform the gauge transformation (2.61) so that the background field is purely real, and plug the linear splitting (2.64) into the action (2.55) with  $D_0 = \partial_0 - i\mu(t)$ ,

$$\begin{aligned} S &= \int_{\tilde{r}} \frac{(\mu - V)^2}{2\lambda} + \sqrt{2n_0}(\mu - V)\varphi_1 - \lambda \left( \frac{\mu - V}{\lambda} \right) \sqrt{2n_0}\varphi_1 \\ &\quad - \frac{1}{2}(\varphi_1, \varphi_2) \begin{pmatrix} -\frac{\nabla^2}{2m} + 2(\mu - V) & \partial_0 \\ -\partial_0 & -\frac{\nabla^2}{2m} \end{pmatrix} \begin{pmatrix} \varphi_1 \\ \varphi_2 \end{pmatrix}. \end{aligned} \quad (2.65)$$

The first line in (2.65) includes the background part and terms linear in the fluctuations, which at the end cancel out. In the second line we find the action quadratic in the fluctuations analogous to (2.34), but with the trapping potential, space-, and time-dependencies included. It is useful to keep in mind the relation  $\lambda(t)n_0(\mathbf{r}) = \mu(t) - V(t, \mathbf{r})$  obtained in (2.60). Following the same steps as before, i.e. rescaling fields as in (2.36) and so on, we obtain for the low momenta regime an action analogous to (2.41)

$$\begin{aligned} S &= -\frac{1}{2} \int_{\tilde{r}} -\lambda(t)n_0^2(\mathbf{r}) + \left( -\frac{(\partial_0\phi)^2}{c^2(t, \mathbf{r})} + (\nabla\phi)^2 \right) \\ &= -\frac{1}{2} \int_{\tilde{r}} -\lambda(t)n_0^2(\mathbf{r}) + \sqrt{g} g^{\alpha\beta} \partial_\alpha\phi \partial_\beta\phi, \end{aligned} \quad (2.66)$$

with the spacetime-dependent speed of sound,

Spacetime  
dependent  
speed of  
sound

$$c^2(t, \mathbf{r}) = \frac{\lambda(t)n_0(\mathbf{r})}{m} = \frac{\lambda(t)n}{m} \left( 1 - \frac{f(\mathbf{r})}{R^2} \right) \quad (2.67)$$

and the acoustic metric  $g_{\alpha\beta}(t, \mathbf{r})$ ,

$$(g^{\alpha\beta}) = \begin{pmatrix} -1 & 0 \\ 0 & c^2\delta^{ij} \end{pmatrix} \quad (g_{\alpha\beta}) = \begin{pmatrix} -1 & 0 \\ 0 & \delta_{ij}/c^2 \end{pmatrix}. \quad (2.68)$$

In (2.66) we used the definition  $\sqrt{g} := \sqrt{-\det(g_{\alpha\beta})} = 1/c^2$ . Again, a broader result which considers a condensate with finite fluid velocity  $\mathbf{v}$  is given in [12]. One can already see in (2.67) that the speed of sound can induce a spacetime curvature, which can be the intrinsic curvature of the foliation, if  $c$  is only space dependent, merely the extrinsic curvature, if it is only time dependent, and both if it depends on both parameters. In chapter 5 we discuss how this is implemented, the theoretical predictions of the implementation, and the corresponding experimental results. Within the discussion we hold there, it is already convenient to rewrite the linear expansion of the fields (2.64) with the rescaled field  $\phi$  and its derivative in place of the fluctuations, under the acoustic approximation  $\epsilon(\mathbf{k}) = c|\mathbf{k}|$ . This reads,

$$\Phi(t, \mathbf{r}) = \phi_0(t, \mathbf{r}) - \left[ \frac{\dot{\phi}(t, \mathbf{r})}{2\sqrt{m}c^2} - i\sqrt{m}\phi(t, \mathbf{r}) \right], \quad (2.69)$$

with the space- and time-dependent speed of sound  $c$ , as given in (2.67).

Let us wrap up by putting forward the line element of the spacetime manifold in which the field  $\phi(t, \mathbf{r})$  resides, which is naturally given by

$$\begin{aligned} ds^2 &= -dt^2 + \frac{1}{c^2(t, \mathbf{r})} (dr^2 + r^2d\varphi^2) \\ &= -dt^2 + a^2(t) \left( 1 - \frac{f(\mathbf{r})}{R^2} \right)^{-1} (dr^2 + r^2d\varphi^2), \end{aligned} \quad (2.70)$$

where a time-dependent scale factor

$$a^2(t) := \frac{m}{\lambda(t)n} \quad (2.71) \quad \text{Condensate scale factor}$$

has been introduced! We immediately see that if the condensate is homogeneous —  $f(\mathbf{r})$  identically zero,  $R \rightarrow \infty$ , but more realistically in a box trap, or in a small enough region around the centre of the trap — we recover the line element (2.47) with  $\kappa = 0$ , i.e. the FLRW metric of a spatially flat hypersurface. One can also choose  $f(\mathbf{r}) = \pm 2r^2 - r^4/R^2$  and through the coordinate transformation

$$u(r) = \frac{r}{1 \mp \frac{r^2}{R^2}}, \quad (2.72)$$

find that the line element reduces to

$$ds^2 = -dt^2 + a^2(t) \left( \frac{du^2}{1 - \kappa u^2} + u^2 d\varphi^2 \right). \quad (2.73)$$

This is an exact mapping to an FLRW universe with spatial curvature  $\kappa = \mp 4/R^2$  and is discussed in [12] with more detail.

As a prelude to chapter 5 we anticipate now that harmonic and inverted harmonic traps, where  $f(\mathbf{r}) = \pm r^2$ , induce the line element

$$\begin{aligned} ds^2 &= -dt^2 + a^2(t) \left( 1 \mp \frac{r^2}{R^2} \right)^{-1} (dr^2 + r^2 d\varphi^2) \\ &\approx -dt^2 + a^2(t) \left( \frac{du^2}{1 - \kappa u^2} + u^2 d\varphi^2 \right). \end{aligned} \quad (2.74)$$

We arrive to the last expression through a coordinate transformation and subsequent approximation,

$$u(r) = \frac{r}{\left( 1 \mp \frac{r^2}{R^2} \right)^{1/2}}, \quad \frac{du^2}{\left( 1 \pm \frac{u^2}{R^2} \right)^2} \approx \frac{du^2}{1 \pm 2\frac{u^2}{R^2}}. \quad (2.75)$$

This derivation then leads to a successful implementation of trapping potentials that simulate a spatial curvature  $\kappa = \mp 2/R^2$ , as long as one remains close to the central region of the trap. In Figure 2.2 we depict the coordinate transformation for the different trapping potentials in terms of the size parameter  $R$  (here equivalent to the Thomas-Fermi radius  $R_{\text{TF}}$ ). We also show the emergent spatial metric (radial component  $\gamma_{11} = a^{-2}g_{11}$ ) for harmonic and inverse harmonic traps, and we compare the latter to the radial component of the FLRW line element, which we recover under the approximation put forward in Eq. (2.75).

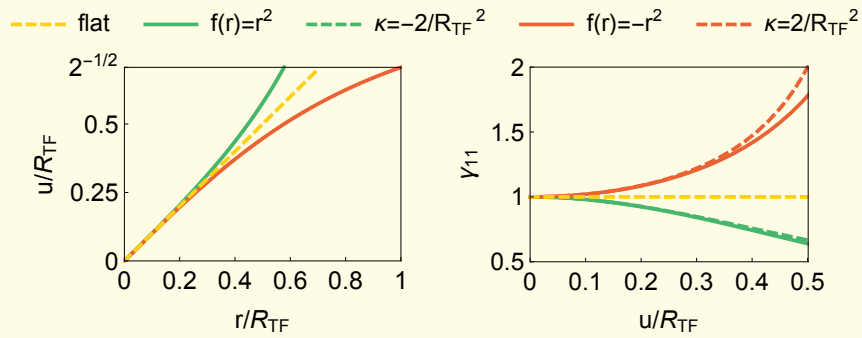


**Figure 2.2 | Line element for different trapping potentials.** On the left side we show the coordinate transformation between the lab coordinate  $r$  and the reduced circumference coordinate  $u$ . On the panel to the right we depict the shape of the emergent metric depending on different trapping potentials. The exact value of  $\gamma_{11}$  with a spatial curvature of  $\mp 2/R_{\text{TF}}^2$  is given in dashed lines, while the one obtained through harmonic and inverse harmonic traps is given in solid lines. We include the line element of a flat situation, to show the region in which a spatially curved manifold can be approximated as flat.

## Striking features

---

In the above we have reviewed the topics of Bose-Einstein condensation, the fluctuations on top governed by Bogoliubov's dispersion relation, their low energy corner following a relativistic behaviour, an emergent curved spacetime geometry with the speed of sound (phonons) in place of the speed of light (photons), and the basic principles of curved spacetimes from the point of view of cosmology.

In this chapter we wish to look deeper into some particular aspects of quantum field theory. We will go first into the topic of entanglement, with the goal of applying this knowledge to Bogoliubov fields, and second, we will look into specific features of relativistic quantum fields in curved backgrounds, to aim for their simulation with BECs. We hence set here the theoretical ground for both of our main topics of inquiry.

### 3.1 Entanglement in QFT

Well, well, well, if it isn't entanglement! that thought provoking phenomenon entering the world of physics at the beginning of last century with the birth, of course, of quantum mechanics. But as much as there are a lot of nice stories there, we must come back to the present moment and rather talk about how this concept has been developed in the realm of QFT. When we go into QFT we are instantly hopping into a description which talks about any system in terms of its properties either at any point in space, or for all values of momentum. Any bounded system has a fundamental vacuum state on top of which all the relevant physics happens. But the vacuum state is relevant in itself, given that it is already the seed for any phenomena to arise: what will arise and how, depends on the characterisation of this vacuum.

In terms of entanglement, it was found early in the days that two regions of a system in its vacuum state are in fact highly (not only, but divergently) entangled. The Reeh-Schlieder theorem [35] already shows the impossibility to regard the vacuum as a product state of two complementary spatial regions, pointing to the highly entangled nature of the algebra of operators (the proof of which can be found in [36]). Later it was shown that the vacuum state of a relativistic quantum field theory violates Bell's inequalities [37–40], to find

afterwards that the entanglement entropy associated to a spatial region in a relativistic quantum field theory displays both ultraviolet (UV) and infrared (IR) divergences [41, 42]. We point to the recent review [43] as a rather complete discussion on entanglement, its divergencies within QFT, and ways of dealing with them — such as lattice regularisation — together with the incursion into finding universal quantities that survive in the continuum limit.

### 3.1.1 Entanglement entropy

The quantification of entanglement is of course done by means of entanglement entropies. Entropies in general quantify the lack of information present in a certain state of the system. The amount of entropy in a system can be due to entanglement, or merely to the nature of the statistics of the internal degrees of freedom comprising the system. Entropies that refer to entanglement entail the missing information in a certain system  $A$ , due to its separation from another system  $B$ . Were they put together, this entropy would vanish. When they are separated — in Hilbert subspaces, not necessarily spatially separated —,  $A$  is said to be entangled with  $B$ , and the amount of entanglement can be determined through von Neumann and Rényi entanglement entropies.

If we look into spatial entanglement, we may use the Rényi entropy to quantify entanglement between some region  $A$  and its complement region  $B$  (such that  $A$  and  $B$  together form a Cauchy hypersurface of spacetime, for example a constant time hypersurface),

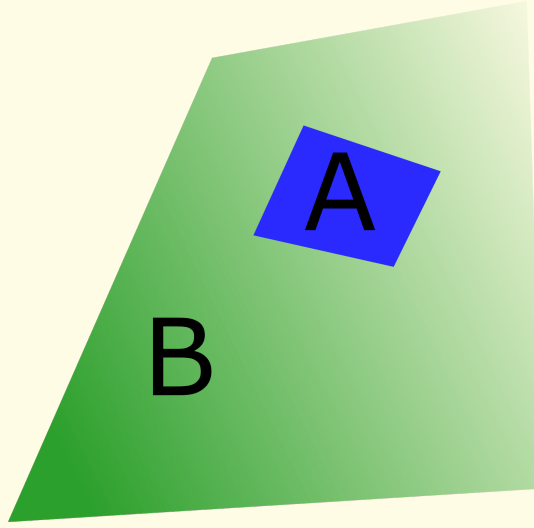
$$S_\alpha(\rho_A) = -\frac{1}{\alpha-1} \ln \text{Tr}\{\rho_A^\alpha\} \xrightarrow{\alpha \rightarrow 1} S_1(\rho_A) = -\text{Tr}\{\rho_A \ln \rho_A\}. \quad (3.1)$$

Rényi and  
von Neumann  
entanglement  
entropies

Therein we also provide the von Neumann entanglement entropy, which is the Rényi entanglement entropy in the limit  $\alpha \rightarrow 1$ . Furthermore, we introduced the density matrix  $\rho_A$ , which is the reduced density matrix obtained by tracing out the degrees of freedom of system  $B$  from the density matrix of the whole system,  $\rho_A = \text{Tr}_B\{\rho\}$ . This is a rather tricky procedure in QFT, nevertheless.

The approach to determine the actual amount of entanglement entropy (3.1) within many-body systems has been twofold. A direct calculation can be done for Gaussian states through the eigenvalues of the reduced density matrices  $\rho_A$ , analogous to the determination of the symplectic eigenvalues of the covariance matrix [7, 44–48]. Another path can be taken in the case of conformal field theories, using what is known as the “replica trick” [42, 49, 50], which is extended to derivations by means of holographic correspondence in [50]; see also [51] for an overview on results obtained with these methods. Both approaches have proved successful, and agree with each other in those systems which have lend themselves to both procedures.

In particular, the area law of entanglement entropy [6, 52] has been reconstructed for D-dimensional systems within AdS/CFT, and its deformation into



logarithmic growth with the size of the system for one-dimensional scenarios has been calculated for a diversity of systems. These include spin chains (or coupled harmonic oscillators) and bosonic and fermionic systems of infinite extent or with particular boundary conditions (periodic, Dirichlet, Neumann). Solutions have been found with both the direct eigenvalue calculation of reduced density matrices [53, 54] and through the replica trick [55, 56]. In particular, the entanglement entropy associated to an interval of length  $L$  in a  $1 + 1$  dimensional conformal field theory is known to be given by

$$S_1(L) = \frac{c}{3} \ln \left( \frac{L}{\epsilon} \right) + \text{const.} \quad (3.2)$$

Here  $c$  plays the role of the the conformal central charge and  $\epsilon$  is a small length that regularises the divergences. Although originally believed to be of UV origin (and as can be thought of by looking at the shape of Eq. (3.2)), it was shown in [54] that these divergences actually occur in the IR limit, due to zero modes. Moreover, the additive constant in (3.2) is not universal and can in general depend on the details of both the UV and IR regularisation schemes.

The path we will follow in this work is that of direct calculation of the eigenvalues of reduced density matrices. In QFT the degrees of freedom are of course the fields themselves. The density matrix for the state at some time  $t$  is a functional of the fields,  $\rho[\phi_+, \phi_-]$ . One may define a projection operator  $P$  such that  $P\phi(x) = \phi(x)$  for positions  $x$  in the region  $A$  and  $P\phi(x) = 0$  for positions  $x$  in the complement region  $B$ . The reduced density matrix for the region  $A$  reads then

$$\rho_A[\phi_+, \phi_-] = \frac{1}{Z_B} \int \mathcal{D}\tilde{\phi} \rho[P\phi_+ + (1 - P)\tilde{\phi}, P\phi_- + (1 - P)\tilde{\phi}] \quad (3.3)$$

where  $Z_B$  is chosen such that  $\text{Tr}\{\rho_A\} = 1$ .

As one may expect, in the case of Gaussian states, the entropy depends only on connected two-point correlation functions. These enter the calculation through a matrix of statistical equal-time correlation functions,

$$\text{Matrix } a \quad [a(t)]_{\mathbf{nm}} = \text{Tr}_o[\Delta_{\phi\phi}^S(t)]_{\text{no}}[\Delta_{\pi\pi}^S(t)]_{\text{on}} - \frac{1}{4}\delta_{\mathbf{nm}}, \quad (3.4)$$

whose eigenvalues are related to the symplectic eigenvalues  $\lambda_{\mathbf{n}}$  of the covariance matrix as  $a_{\mathbf{nm}} = (\lambda_{\mathbf{n}}^2 - 1/4)\delta_{\mathbf{nm}}$ , once the matrix  $a_{\mathbf{nm}}$  is diagonalised. The construction leading to the shape of  $a_{\mathbf{nm}}$  and the relation to the symplectic eigenvalues is discussed in detail in Ref. [46].

For the present development we encounter a system for which mixed statistical correlation function of fields  $\phi$  and their conjugate momenta  $\pi$  vanish,  $\langle\phi\pi + \pi\phi\rangle = 0$ . In such a situation Rényi entanglement entropies can be calculated through

$$S_\alpha = \frac{1}{(\alpha - 1)} \{ \text{Tr} \ln ((a_+)^{\alpha} - (a_-)^{\alpha}) \}, \quad (3.5)$$

with

$$a_+ = \sqrt{a + \frac{1}{4}} + \frac{1}{2} \quad \text{and} \quad a_- = \sqrt{a + \frac{1}{4}} - \frac{1}{2}. \quad (3.6)$$

The above expression for  $S_\alpha$  reduces to the von Neumann entropy by taking the limit  $\alpha \rightarrow 1$ , to obtain

$$S_1 = \text{Tr} \{ (a_+) \ln (a_+) - (a_-) \ln (a_-) \}. \quad (3.7)$$

Our goal is to investigate spatial entanglement in an interacting Bose-Einstein condensate with the tools provided here. In this case we have the matrix  $a$  (3.4) in position representation, with the corresponding statistical equal-time correlation functions, provided for a system of Bogoliubov quasiparticles in chapter 4. It is worthwhile to note that Eq. (3.7) holds both, for the global von Neumann entropy as well as for entanglement entropies. The only difference in the latter case is that the matrix or operator trace in (3.7) and the integral over positions in (3.4) need to be restricted accordingly. In the case of spatial entanglement, one looks at a specific region  $A$ , so that

$$a(\mathbf{x}, \mathbf{y}) = \int_{\mathbf{z} \in A} \Delta_{\phi\phi}^S(\mathbf{x}, \mathbf{z}) \Delta_{\pi\pi}^S(\mathbf{z}, \mathbf{y}) - \frac{1}{4}\delta(\mathbf{x} - \mathbf{y}) \quad (3.8)$$

amounts to the partial trace of the density matrix of the complete system. This integral in position space becomes a sum over discrete momentum, once it is translated to Fourier space. In chapter 4 we go through the determination of this matrix  $a$  in discrete momentum space and the results it yields for entanglement entropy in Bogoliubov systems of 1 and 2 spatial dimensions.

## 3.2 Particle production

*O Vajra of Mind, tell me, when you first arose, what was your source? Did you come from the earth, or from water and fire, or from air and space, or did you originate from any of the eight cardinal or intermediate directions, or from above or below? Investigate whence you arose and that which arises, and analyze! Likewise, investigate where you are now and who is there, and analyze!*

The adventurous reader would have arrived here directly from [section 2.2.1](#) wanting to learn all about particle production [[57–60](#)], so let us go straight into the topic.

### 3.2.1 Symmetries in FLRW spacetimes

We mentioned in passing before that particle production is due to the absence of a timelike Killing vector field  $\xi$ . So what is this object? A Killing vector field singles out the symmetries of a certain geometry defined by  $g_{\alpha\beta}$ . Specifically, the Lie derivative of the metric with respect to  $\xi$  vanishes. This is phrased in the [conformal](#) Killing equation,

$$g_{\alpha\nu} \xi^\alpha_{;\mu} + g_{\mu\alpha} \xi^\alpha_{;\nu} + \xi^\alpha g_{\mu\nu,\alpha} = \omega g_{\mu\nu}. \quad (3.9)$$

If  $w(x) = 0$ , the solution  $\xi^\alpha(x)$  defines a Killing vector field. It parametrises an infinitesimal change of coordinates,  $x^\alpha \rightarrow x'^\alpha = x^\alpha + \epsilon \xi^\alpha(x)$ , for which the metric remains unchanged. In the case of  $\omega(x) \neq 0$ , the invariance of the metric remains up to an overall conformal factor  $\Omega^2(x) = 1 - \epsilon \omega(x)$ , and we obtain the weaker version, a conformal Killing vector field.

By looking into [\(3.9\)](#), one can see that an FLRW metric with time dependent scale factor does not have a timelike Killing vector field, but it has a timelike conformal Killing vector field, with  $\omega = 2\dot{a}$ , whose components are given by  $\xi^0 = a$  and  $\xi^i = 0$ . The absence of a timelike Killing vector field implies that under time evolution energy is not conserved, this drives the time dependence of the Hamiltonian of the theory, which implies the absence of an “objective” ground or vacuum state. This lies behind the phenomenon of particle production, as we will now discuss.

### 3.2.2 Vacuum state in FLRW spacetimes

As our interest is specifically in  $d = 2 + 1$  scenarios, we will develop the concept of particle production within that frame. For the time being we will focus on the phenomenon of particle production when  $\kappa = 0$ , since in this section we want to gain insight about the phenomenon itself, not a plethora of possible

situations. A theoretical extension to particle production in spatially curved and time dependent  $2 + 1$  backgrounds is given in [11] and used in chapter 5.

We have then lights, camera,

$$\begin{aligned} S[\phi] &= -\frac{1}{2} \int_{\tilde{x}} \sqrt{g} \partial^\mu \phi \partial_\mu \phi \\ &= -\frac{1}{2} \int_{\tilde{x}} -a^2 (\partial_0 \phi)^2 + (\nabla \phi)^2, \end{aligned} \quad (3.10)$$

for the  $2 + 1$  dimensional FLRW metric, with  $\sqrt{g} = a^2$ . It is a sensible choice to change to conformal time  $a d\eta = dt$  so that the metric can be written down as a Minkowski metric — rescaled by  $a$  —,  $g_{\mu\nu} = a^2(\eta) \eta_{\mu\nu}$ . Or, talking in terms of the line element,

$$ds^2 = a^2(\eta) (-d\eta^2 + dx^i dx_i). \quad (3.11)$$

This calls directly for a rescaling of the fields  $\phi \rightarrow \sqrt{a} \phi = \chi$  so that the action for the rescaled fields in conformal time has the shape

$$\begin{aligned} S[\chi] &= -\frac{1}{2} \int_{\eta, \mathbf{x}} -(\partial_\eta \chi)^2 + (\nabla \chi)^2 + \left( \frac{a'^2 - 2a''a}{4a^2} \right) \chi^2 \\ &= -\frac{1}{2} \int_{\eta, \mathbf{k}} \chi_{-\mathbf{k}}(\eta) \left[ \chi_{\mathbf{k}}''(\eta) + \left( \mathbf{k}^2 + \frac{a'^2 - 2a''a}{4a^2} \right) \chi_{\mathbf{k}}(\eta) \right]. \end{aligned} \quad (3.12)$$

Here one can easily read out the effect of a time dependent background geometry, coming in as a time dependent effective mass

**Effective  
mass**

$$M^2(\eta) = \frac{a'^2 - 2a''a}{4a^2} \quad (3.13)$$

acquired by the relativistic field  $\chi$ . We can write down the equations of motion for  $\chi_{\mathbf{k}}(\eta)$ ,

$$0 = -2 \frac{\delta S}{\delta \chi_{-\mathbf{k}}} = \chi_{\mathbf{k}}'' + [\mathbf{k}^2 + M^2(\eta)] \chi_{\mathbf{k}} \quad (3.14)$$

and define a time dependent frequency  $\omega_{\mathbf{k}}^2(\eta)$  for the term in square brackets (note that fields who share the magnitude of  $\mathbf{k}$  share the same frequency  $\omega_k(\eta)$ ). Yes, we are dealing again with a harmonic oscillator.

It should be straightforward then to find a Fock space whose algebra of operators diagonalises the Hamiltonian of the fields  $\chi_{\mathbf{k}}(\eta)$ . Of course it is tempting to write down the Hamiltonian at a certain time  $\eta_0$  already as

**Instantaneous  
Hamiltonian**

$$\begin{aligned} \hat{H}(\eta_0) &= \frac{1}{2} \int_{\mathbf{k}} \Theta_{-\mathbf{k}}(\eta_0) \Theta_{\mathbf{k}}(\eta_0) + \omega_{\mathbf{k}}^2(\eta_0) \chi_{-\mathbf{k}}(\eta_0) \chi_{\mathbf{k}}(\eta_0) \\ &= \int_{\mathbf{k}} \omega_{\mathbf{k}}(\eta_0) \left( \hat{d}_{\mathbf{k}}^\dagger \hat{d}_{\mathbf{k}} + \frac{1}{2} \right) \end{aligned} \quad (3.15)$$

using the relation between the field and its conjugate momentum  $\Theta_{\mathbf{k}} = \chi'_{-\mathbf{k}}$ . This last expression of the Hamiltonian is arrived at through some expansion of the fields (and the corresponding one for  $\Theta_{\mathbf{k}}$ )

$$\chi_{\mathbf{k}}(\eta) = v_k(\eta)\hat{d}_{\mathbf{k}} + v_k^*(\eta)\hat{d}_{-\mathbf{k}}^\dagger, \quad \Theta_{\mathbf{k}}(\eta) = v'_k(\eta)\hat{d}_{-\mathbf{k}} + v_k'^*(\eta)\hat{d}_{\mathbf{k}}^\dagger \quad (3.16)$$

**Mode  
expansion**

which precisely diagonalises  $\hat{H}$  at the particular time  $\eta = \eta_0$ , but not at all times. This implies the condition at time  $\eta_0$  for  $v_k(\eta)$

$$v_k(\eta_0) = \frac{1}{\sqrt{2\omega_k(\eta_0)}} \quad v'_k(\eta_0) = -i\sqrt{\frac{\omega_k(\eta_0)}{2}} \quad (3.17)$$

up to an irrelevant phase factor, so we recover the usual harmonic oscillator expressions

$$\chi_{\mathbf{k}}(\eta_0) = \frac{1}{\sqrt{2\omega_k(\eta_0)}}(\hat{d}_{-\mathbf{k}}^\dagger + \hat{d}_{\mathbf{k}}), \quad \Theta_{\mathbf{k}}(\eta_0) = i\sqrt{\frac{\omega_k(\eta_0)}{2}}(\hat{d}_{\mathbf{k}}^\dagger - \hat{d}_{-\mathbf{k}}). \quad (3.18)$$

As the frequency  $\omega_k$  evolves, at time  $\eta_1$  the Hamiltonian is of diagonal form for some other set of creation and annihilation operators

$$\hat{H}(\eta_1) = \int_{\mathbf{k}} \omega_k(\eta_1) \left( \hat{c}_{\mathbf{k}}^\dagger \hat{c}_{\mathbf{k}} + \frac{1}{2} \right). \quad (3.19)$$

These are related to the  $\hat{d}_{\mathbf{k}}$  operators through, yes!, a Bogoliubov transformation (2.18). We see that the vacuum state  $|0\rangle_{\hat{d}}$  defined by  $\hat{d}_{\mathbf{k}}|0\rangle_{\hat{d}} = 0$  is only a vacuum state at time  $\eta_0$ , different from  $|0\rangle_{\hat{c}}$  at time  $\eta_1$ , hence its given name: “instantaneous vacuum”.

The field is now expanded in terms of these operators as

$$\chi_{\mathbf{k}}(\eta) = u_k(\eta)\hat{c}_{\mathbf{k}} + u_k^*(\eta)\hat{c}_{-\mathbf{k}}^\dagger, \quad (3.20)$$

with  $u_k(\eta)$  fulfilling the condition at time  $\eta_1$

$$u_k(\eta_1) = \frac{1}{\sqrt{2\omega_k(\eta_1)}}, \quad u'_k(\eta_1) = -i\sqrt{\frac{\omega_k(\eta_1)}{2}}, \quad (3.21)$$

again, up to an irrelevant phase factor.

Of course, if the frequency is constant, both Hamiltonians coincide,  $\alpha = 1$ ,  $\beta = 0$ , the vacuum state is well defined throughout; everything fits in. In that case, the field  $\chi$  as a solution to (3.14) is a sum of oscillatory modes, normalised by  $1/\sqrt{2\omega}$ , i.e.,

$$\chi_{\mathbf{k}}(\eta) = \frac{1}{\sqrt{2\omega}} \left( e^{-i\omega\eta}\hat{d}_{\mathbf{k}} + e^{i\omega\eta}\hat{d}_{-\mathbf{k}}^\dagger \right) \quad \leftrightarrow \quad v_k(\eta) = \frac{e^{-i\omega\eta}}{\sqrt{2\omega}}, \quad (3.22)$$

with  $\omega = |\mathbf{k}|$ .

**Mode functions**

Now let us take a deeper look into the expansion coefficients  $v_k(\eta)$  in (3.16) (or  $u_k(\eta)$  in (3.20)), known as the ‘‘mode functions’’. First of all, they are solutions to the second order differential equation (3.14). Second, as the creation and annihilation operators obey the bosonic commutation relations (2.1), the mode functions must satisfy

$$\text{Wr}[v_k, v_k^*] := v_k v_k'^* - v_k' v_k^* = i, \quad (3.23)$$

in order for the commutator  $[\chi_{\mathbf{k}}, \Theta_{\mathbf{k}'}] = i\delta(\mathbf{k} - \mathbf{k}')$  to be properly normalised. And third, by equating (3.16) to (3.20) and expressing the  $\hat{d}_{\mathbf{k}}$  operators in terms of  $\hat{c}_{\mathbf{k}}$  ones (doesn't hurt to remember how):

$$\begin{pmatrix} \hat{d}_{\mathbf{k}} \\ \hat{d}_{-\mathbf{k}}^\dagger \end{pmatrix} = \begin{pmatrix} \alpha_{\mathbf{k}} & \beta_{-\mathbf{k}}^* \\ \beta_{\mathbf{k}} & \alpha_{-\mathbf{k}}^* \end{pmatrix} \begin{pmatrix} \hat{c}_{\mathbf{k}} \\ \hat{c}_{-\mathbf{k}}^\dagger \end{pmatrix}, \quad (3.24)$$

one obtains the relation between mode functions

$$u_k = \alpha_k v_k + \beta_k v_k^* \quad \text{and} \quad v_k = \alpha_k^* u_k - \beta_k u_k^*. \quad (3.25)$$

We took here into account that the mode functions are independent of the direction of  $\mathbf{k}$ . With the above one can determine the Bogoliubov coefficients,

$$\alpha_k = \text{Wr}[u_k, v_k^*]/i, \quad \beta_k = -\text{Wr}[u_k, v_k]/i. \quad (3.26)$$

which relate the Hamiltonian between times  $\eta_0$  and  $\eta_1$  and, therefore, the vacuum state  $|0\rangle_{\hat{d}}$  at time  $\eta_0$  with the vacuum state  $|0\rangle_{\hat{c}}$  at time  $\eta_1$ .

To compare both vacua, one can calculate the expectation value of the occupation number operator for  $\hat{c}_{\mathbf{k}}$ -quasiparticles in the state  $|0\rangle_{\hat{d}}$ . This yields,

**Occupation at different times**

$$\langle \hat{c}_{\mathbf{k}}^\dagger \hat{c}_{\mathbf{k}} \rangle_{\hat{d}} = \langle (\alpha_k \hat{d}_{-\mathbf{k}}^\dagger - \beta_k \hat{d}_{\mathbf{k}}) (\alpha_k^* \hat{d}_{\mathbf{k}} - \beta_k^* \hat{d}_{-\mathbf{k}}^\dagger) \rangle_{\hat{d}} = |\beta_k|^2 \quad (3.27)$$

which expresses the amount of quasiparticles at time  $\eta_1$  present in the vacuum state defined at time  $\eta_0$ . This is the phenomena of particle production at play: as the system evolves, a given definition of a vacuum state at a certain time becomes populated at later times.

We provide the above expressions also in coordinate time in Table 3.1, to be well prepared for the experimental setting. An important thing to note is that the concept of effective mass squared is only valid in the conformal time point of view, but can nevertheless be related to the scale factor given in coordinate time. Of course, the Bogoliubov coefficients are independent of the approach taken to analyse a certain physical situation.

object	conformal time	coordinate time
fields	$\chi_{\mathbf{k}}(\eta) = \sqrt{a}\phi_{\mathbf{k}}$	$\phi_{\mathbf{k}}$
mode functions	$v_k(\eta) = \sqrt{a}v_k(t)$	$v_k(t)$
mode equation	$v_k'' = -(\mathbf{k}^2 + M^2(\eta))v_k$	$\ddot{v}_k + 2\frac{\dot{a}}{a}\dot{v}_k = -\frac{\mathbf{k}^2}{a^2}v_k$
effective mass squared	$(a'^2 - 2a''a)/4a^2$	$-(\dot{a}^2 + 2\ddot{a}a)/4$
at constant scale factor $\eta = t/a$		
frequency	$\omega(\eta) = k$	$\omega(t) = k/a$
oscillatory modes	$v_k(\eta) = e^{-i\omega\eta}/\sqrt{2\omega}$	$v_k(t) = e^{-i\omega t}/a\sqrt{2\omega}$

**Table 3.1** | **Fields and mode functions** in an FLRW spacetime. Relevant quantities describing the system are provided in both, conformal and coordinate time. We focus on the mode functions, which serve as expansion coefficients for the fields in terms of creation and annihilation operators. As such, they are solutions to the mode equation, which is equivalent to the Klein-Gordon equation for the fields. Additionally we provide an emergent effective mass, present in the dynamics of the system when its evolution is analysed in conformal time. Finally, though seemingly trivial, we solve the mode equation for the particular situation in which the scale factor is constant, as this will be of use for the experimental setting implemented in our simulation.

## Entanglement in a BEC

Let us now go into the question of spatial entanglement in a Bose-Einstein condensate. To get into the topic, we begin with a review of entanglement in a noninteracting condensate in a box of volume  $V$ . As we have discussed in [appendix A](#), the condensate has a ground state where all particles occupy the zero mode  $N_0 = N$ , which is a particle number eigenstate of the Hamiltonian. In this context, the formalism of quantum mechanics is sufficient to determine the entanglement entropy. Furthermore, since we are dealing with a nonrelativistic system, divergencies will naturally not be present.

Following the discussion in [\[10\]](#) one splits the box into two regions,  $A$  and  $B$ , with relative volumes  $w = V_A/V$  and  $1 - w = V_B/V$ . The reduced density matrix for subsystem  $A$  is obtained

$$\rho_A = \text{Tr}_B\{\rho\} = \sum_{\nu=0}^{N_0} \binom{N_0}{\nu} w^\nu (1-w)^{N_0-\nu} |\nu\rangle\langle\nu|, \quad (4.1)$$

where  $|\nu\rangle$  denotes a state with  $\nu$  particles in region  $A$ . Evidently, the subsystem described by [\(4.1\)](#) is in a mixed state, except in the limiting cases  $w = 1$ ,  $w = 0$ , and  $N_0 = 0$ , — which correspond to  $V_A = V$ ,  $V \rightarrow \infty$ , or a vanishing condensate.

Since the density matrix is already in diagonal form, it is straightforward to calculate the entropy. One can simply read out from the probability distribution the eigenvalues to trace over, and determine the von Neumann entropy [\(3.1\)](#) for subsystem  $A$ . In particular, for large  $N_0$  in a binomial distribution, one arrives to the result,

$$S_1(\rho_A) = \frac{1}{2} \ln(2\pi e N_0 w(1-w)) + \mathcal{O}(1/N_0). \quad (4.2)$$

It is interesting to also analyse the limiting case of small volume  $V_A$ , taking the limit  $w \rightarrow 0$  together with  $N_0 \rightarrow \infty$  in such a way that  $M = wN$ , the expected particle number in region  $A$ , remains finite. In that case the binomial distribution approaches a Poisson distribution,

$$\binom{N_0}{\nu} w^\nu (1-w)^{N_0-\nu} \rightarrow \frac{M^\nu}{\nu!} e^{-M} \quad (4.3)$$

Reduced  
density matrix  
for a particle  
number  
eigenstate

Entanglement  
entropy at  
large number  
of particles

whose entanglement entropy takes the form

$$\begin{aligned} S_1(\rho_A) &= M [1 - \ln(M)] + e^{-M} \sum_{\nu=0}^{\infty} \frac{M^\nu \ln(\nu!)}{\nu!} \\ &= M [1 - \ln(M)] + \frac{\ln(2)}{2} M^2 - \frac{\ln(4/3)}{6} M^3 + \mathcal{O}(M^4). \end{aligned} \quad (4.4)$$

**Entanglement  
entropy for  
expected  
particle  
number  $M$  in  
region  $A$**

Note that the power series on the right hand side in the first line has infinite radius of convergence. For  $M \ll 1$  it is dominated by the first few terms as written out in the second line. While the above result is exact, for the case  $M \gg 1$  one can take a different route to arrive to the approximate result for the entropy,

$$S_1(\rho_A) = \frac{1}{2} \ln(2\pi e M) - \frac{1}{12M} - \frac{1}{24M^2} - \frac{19}{360M^3} + \mathcal{O}(1/M^4). \quad (4.5)$$

One finds, in particular, that the above results depend only on the expected particle number  $M$  in region  $A$ , and not on the relative volume  $w$ . For  $M \rightarrow 0$  one sees in (4.4) that  $S_1(\rho_A) \rightarrow 0$ , as it should be. Therefore, for states with a fixed number of noninteracting particles in the ground state, the entanglement is essentially an entanglement of particle number. Indeed, if one measures particle number in subsystem  $A$  to give a certain value  $\nu$ , one can immediately infer the particle number in the complement subsystem  $B$  as  $N_0 - \nu$ . One can actually extend the above considerations to states where particle number is fluctuating, such as coherent states [61]. A coherent state describing a noninteracting Bose-Einstein condensate at non-zero chemical potential, but zero temperature, shows then no entanglement between spatial regions at all. This is in agreement with the fact that no information can be gained from measuring particle number locally in a subregion.

We will see now that things change again in the presence of interactions. To begin the analysis, we go back to our familiar Lagrangian (2.32) describing a complex nonrelativistic scalar field  $\Phi(x)$ . As seen before, this provides the action (2.34) to quadratic order for the perturbations by means of the linear expansion (2.33). From there, one directly finds the propagator of the fluctuating fields,

$$G(\tilde{k}) = \frac{1}{-\omega^2 + \frac{\mathbf{k}^2}{2m} \left( \frac{\mathbf{k}^2}{2m} + 2\lambda n \right)} \begin{pmatrix} \frac{\mathbf{k}^2}{2m} & i\omega \\ -i\omega & \left( \frac{\mathbf{k}^2}{2m} + 2\lambda n \right) \end{pmatrix} \quad (4.6)$$

**Bogoliubov  
propagator**

which has poles on the Bogoliubov dispersion relation (2.21). We introduce the spectral density  $\rho_{ij}(k^0, \mathbf{k})$  for the different field components, which is related to the propagator through

$$G_{ij}(\omega, \mathbf{k}) = \int_{-\infty}^{\infty} dk^0 \frac{\rho_{ij}(k^0, \mathbf{k})}{k^0 - \omega}. \quad (4.7)$$

It in turn determines the spectral correlation functions (see e.g. [62]),

$$\Delta_{ij}^n(\tilde{k}) = 2\pi\rho_{ij}(\omega, \mathbf{k}). \quad (4.8)$$

By substituting in (4.7) with the corresponding elements of the propagator (4.6), one obtains the four components of the spectral density matrix  $\rho_{\phi\phi}$ ,  $\rho_{\pi\phi}$ ,  $\rho_{\phi\pi}$ , and  $\rho_{\pi\pi}$  (these are given in [10], with a  $\phi \leftrightarrow \pi$  switching of the fields). Furthermore, in thermal equilibrium, the statistical correlation functions  $\Delta_{ij}^S(\tilde{k})$  are related to the spectral correlation functions  $\Delta_{ij}^n(\tilde{k})$  through the fluctuation-dissipation relation,

$$\Delta_{ij}^S(\tilde{k}) = \left[ \frac{1}{2} + n_B(\omega) \right] \Delta_{ij}^n(\tilde{k}), \quad (4.9)$$

with the Bose-Einstein thermal distribution function  $n_B(\omega) = 1/(e^{\omega/T} - 1)$ .

Specifically we find the equal-time statistical correlation functions

**Statistical  
correlation  
functions**

$$\begin{aligned} \Delta_{\phi\phi}^S(\mathbf{x} - \mathbf{y}) &= \int_{\mathbf{k}} \left[ \frac{1}{2} + n_T(\mathbf{k}) \right] \sqrt{\frac{\mathbf{k}^2 + 2/\xi^2}{\mathbf{k}^2}} e^{i\mathbf{k}(\mathbf{x}-\mathbf{y})}, \\ \Delta_{\pi\pi}^S(\mathbf{x} - \mathbf{y}) &= \int_{\mathbf{k}} \left[ \frac{1}{2} + n_T(\mathbf{k}) \right] \sqrt{\frac{\mathbf{k}^2}{\mathbf{k}^2 + 2/\xi^2}} e^{i\mathbf{k}(\mathbf{x}-\mathbf{y})}, \end{aligned} \quad (4.10)$$

and vanishing mixed correlation functions  $\Delta_{\phi\pi}^S$  and  $\Delta_{\pi\phi}^S$ . Here  $n_T(\mathbf{k})$  is the Bose-Einstein distribution evaluated on the Bogoliubov dispersion relation; in this work we specifically focus on the ground state where  $n_T(\mathbf{k}) = 0$ .

## 4.1 Three particular scenarios

**Entropy of  
the complete  
system**

Let us put together three particular situations in which the entanglement entropy (spoiler alert) vanishes. The first one is rather trivial, but shows that in fact the complete system is in a pure state. That is, we analyse the case where the volume of region  $A$  equals the volume of the complete system. Since we are dealing with a condensate of infinite extent, what would be a discrete sum over momenta (for a finite region  $A$ ) becomes an integral. Hence the matrix  $a$ , as defined by (3.8), is given by

$$a(\mathbf{x}, \mathbf{y}) = \int_{\mathbf{k}} e^{i\mathbf{k}(\mathbf{x}-\mathbf{y})} \Delta_{\phi\phi}^S(\mathbf{k}) \Delta_{\pi\pi}^S(\mathbf{k}) - \frac{1}{4} \delta(\mathbf{x} - \mathbf{y}) = 0, \quad (4.11)$$

by direct substitution with (4.10). Utilising Eq. (3.7) one finds that this yields zero entropy,  $S_1 = 0$ . In a thermal state, i.e., with non-vanishing occupation number  $n_T(\mathbf{k}) \neq 0$ , one finds instead the corresponding entropy for a free gas of quasiparticles.

The other two situations are particularly interesting. The affirmation is: for a noninteracting condensate ( $V_0 = \lambda = 0$ ) or one with vanishing density ( $n = 0$ ) all the following statements hold,

- the Bogoliubov dispersion relation (2.21) becomes nonrelativistic,  $\epsilon(\mathbf{k}) \rightarrow \mathbf{k}^2/2m$ ;
- the Bogoliubov coefficients (2.20) become  $\alpha_{\mathbf{k}} = 1$  and  $\beta_{\mathbf{k}} = 0$ , so that the annihilation and creation operators  $\hat{b}_{\mathbf{k}}$  and  $\hat{b}_{\mathbf{k}}^\dagger$  (which stand for Bogoliubov quasiparticles) are equal to  $\hat{a}_{\mathbf{k}}$  and  $\hat{a}_{\mathbf{k}}^\dagger$  (the bosonic ones);
- the Hamiltonian describes a gas of free bosons;
- the ground state energy as determined by (2.26) becomes zero,  $E_0 \rightarrow 0$ ;
- the healing length (2.27) becomes infinite,  $\xi \rightarrow \infty$ ;
- at zero temperature, the equal-time statistical correlation functions given in (4.10) simplify to  $\Delta_{\phi\phi}^S(\mathbf{x} - \mathbf{y}) = \Delta_{\pi\pi}^S(\mathbf{x} - \mathbf{y}) = \delta(\mathbf{x} - \mathbf{y})/2$ ;
- the matrix  $a$  vanishes,  $a = 0$ ;
- the entanglement entropy vanishes,  $S_1 = 0$ ;

**Entanglement entropy at vanishing interaction or vanishing density**

and maybe we should stop before getting redundant. The thing is that we are familiar with a system characterised by the above properties: it is that of a free gas of bosons in a coherent state. Even within the many-body setting, the energy of the ground state is finite: it actually vanishes, and the entanglement entropy follows.

Let us now go into the weakly interacting condensate, with a finite ground state density  $n$ . We will analyse the entanglement entropy for such a system in one and two spatial dimensions. We look therefore for the entropy between a segment of an infinite line and the rest of the line, or a circular region in an infinite 2D condensate. To do so, we translate the necessary expressions involving two-point correlation functions from a finite interval in position space to discrete momentum space, and thus we build the coming procedure.

## 4.2 Dictionary to Fourier space

We wish to determine the entanglement entropy given in terms of the eigenvalues of matrix  $a$  in Eq. (3.8). For this task it is natural to work in discrete momentum space, as a treatment of the reduced density matrix in region  $A$ . It is important to highlight that there is no physical boundary in the system, so the partition should not involve any boundary conditions. Hence, we need an expansion scheme that does not make any definite assumptions about such conditions. Here we develop this expansion scheme for one- and two-dimensional systems.

### 4.2.1 In one dimension

In the following we provide the main ideas behind the development of the Fourier expansion scheme needed in a one-dimensional situation, all the steps carried out in this section are given in greater detail in [10].

We begin by considering a finite and closed interval  $[0, \pi]$  and put forward the ansatz

$$f(z) = f_{-1} + f_0 \frac{2z - \pi}{\pi} + \sum_{n=1}^{\infty} f_n \sin(nz) \quad (4.12)$$

which allows for free boundary conditions at  $z = 0$  and  $z = \pi$ . The expansion coefficients  $f_n$  can be obtained from  $f(z)$  through the relations

$$f_{-1} = \frac{1}{2} [f(0) + f(\pi)], \quad f_0 = \frac{1}{2} [-f(0) + f(\pi)], \quad (4.13)$$

and

$$\begin{aligned} f_n &= \frac{2}{\pi} \left[ -\frac{2}{n} f_{-1} + \int_0^{\pi} dz f(z) \sin(nz) \right] && \text{for odd } n \geq 1, \\ f_n &= \frac{2}{\pi} \left[ \frac{2}{n} f_0 + \int_0^{\pi} dz f(z) \sin(nz) \right] && \text{for even } n \geq 2. \end{aligned} \quad (4.14)$$

By further defining  $s_n(z)$  as

$$\begin{aligned} s_{-1}(z) &= 1, & s_0(z) &= \frac{2z - \pi}{\pi}, \\ \text{and } s_n(z) &= \sin(nz) & \text{for } n \geq 1, \end{aligned} \quad (4.15)$$

one can write down the expansion scheme (4.12) in compact form as

$$f(z) = \sum_{n=-1}^{\infty} f_n s_n(z), \quad \text{for } z \in [0, \pi]. \quad (4.16)$$

Conversely, by defining the integration kernels  $t_n(z)$  as

$$\begin{aligned} t_{-1}(z) &= \frac{\pi}{4} [\delta(z) + \delta(z - \pi)], & t_0(z) &= \frac{\pi}{4} [-\delta(z) + \delta(z - \pi)], \\ \text{and } t_n(z) &= \left[ -\frac{1}{n} \delta(z) + \frac{(-1)^n}{n} \delta(z - \pi) + \sin(nz) \right] && \text{for } n \geq 1, \end{aligned} \quad (4.17)$$

one has the inverse relation

$$f_n = \frac{2}{\pi} \int_{0-\epsilon}^{\pi+\epsilon} dz f(z) t_n(z). \quad (4.18)$$

With (4.16) and (4.18) it is now possible to translate between a continuous position space interval and a discrete Fourier representation. The  $\epsilon$  shift of the

boundaries in (4.18) is necessary to make clear that the distributions  $\delta(z)$  and  $\delta(z + \pi)$  must be included in the integral. Keeping this in mind, we will drop all  $\epsilon$ 's when no further clarification is important.

Through a coordinate transformation  $z \rightarrow \frac{L}{\pi}z = x$ , the expansion scheme can be implemented on an interval  $[0, L]$  of arbitrary finite length  $L$ , past the specific  $[0, \pi]$  interval. This yields

$$f(x) = \frac{1}{L} \left[ f_{-1} + f_0 \frac{2x - L}{L} + \sum_{n=1}^{\infty} f_n \sin\left(\frac{n\pi}{L}x\right) \right] \quad \text{for } x \in [0, L], \quad (4.19)$$

and the inverse relation,

$$f_n = 2 \int_0^L dx f(x) t_n\left(\frac{x\pi}{L}\right). \quad (4.20)$$

The factor  $1/L$  in (4.19) has been introduced for this convention to match the standard Fourier transform when  $L \rightarrow \infty$ ,

$$\frac{1}{L} \sum_{n=1}^{\infty} f_n \sin\left(\frac{n\pi}{L}x\right) \rightarrow 2i \int_0^{\infty} \frac{dk}{2\pi} f(k) \sin(kx) \quad (4.21)$$

with  $f_n = if(k) = -if(-k)$  for  $k = n\pi/L$ .

One can additionally show that the kernels  $s_n$  and  $t_n$  satisfy the completeness and orthogonality relations on the interval  $[0, L]$ ,

$$\begin{aligned} \frac{2}{L} \sum_{n=-1}^{\infty} t_n\left(\frac{y\pi}{L}\right) s_n\left(\frac{x\pi}{L}\right) &= \delta(x - y) \\ \frac{2}{L} \int_0^L dx s_m\left(\frac{x\pi}{L}\right) t_n\left(\frac{x\pi}{L}\right) &= \delta_{mn} \end{aligned} \quad (4.22) \quad \begin{array}{l} \text{Completeness} \\ \text{and} \\ \text{orthogonality} \end{array}$$

as expected from any set of well defined expansion basis. As a natural consequence, the trace of an operator can be evaluated in the different representations,

$$\begin{aligned} \text{tr}\{\mathcal{O}\} &= \int_0^L \int_0^L dx dy \mathcal{O}(x, y) \delta(x - y) \\ &= \frac{2}{L} \int_0^L \int_0^L dx dy \mathcal{O}(x, y) \sum_{n=-1}^{\infty} s_n\left(\frac{x\pi}{L}\right) t_n\left(\frac{y\pi}{L}\right) = \sum_{n=-1}^{\infty} \mathcal{O}_{nn}, \end{aligned} \quad (4.23) \quad \begin{array}{l} \text{Operator} \\ \text{trace} \end{array}$$

where we use

$$\mathcal{O}_{mn} = \frac{2}{L} \int_0^L dx \int_0^L dy s_m\left(\frac{x\pi}{L}\right) \mathcal{O}(x, y) t_n\left(\frac{y\pi}{L}\right). \quad (4.24)$$

Alternatively one can also use

$$\overline{\mathcal{O}}_{mn} = \frac{2}{L} \int_0^L dx \int_0^L dy t_m \left( \frac{x\pi}{L} \right) \mathcal{O}(x, y) s_n \left( \frac{y\pi}{L} \right) \quad (4.25)$$

and the operator trace becomes  $\text{tr}\{\mathcal{O}\} = \sum_n \overline{\mathcal{O}}_{nn}$ . This is of fundamental interest to our work, given that matrix traces is what we will be calculating.

There is still an additional step that we can take, to move in our desired direction. Let us remember that the motivation is to obtain the values of  $a_{mn}$  from the equal-time statistical correlation functions, (4.10), which diagonal in momentum space. Therefore it simplifies things to translate the kernels  $s_n(x)$  and  $t_n(x)$  to momentum space, and bring the correlation functions directly from  $k$ -space to our discrete Fourier representation, meaning

$$[\Delta_{\phi\phi}^S]_{nl} = \int_k \tilde{s}_n(k) [\Delta_{\phi\phi}^S](k) \tilde{t}_l(k). \quad (4.26)$$

So we set to find these  $\tilde{s}_n(k)$  and  $\tilde{t}_n(k)$ .

Concretely, one can write down  $f_n$  in terms of  $\tilde{f}(k)$ ,

$$f_n = 2 \int_0^L dx f(x) t_n \left( \frac{x\pi}{L} \right) = \int_k \tilde{f}(k) \tilde{t}_n(k); \quad (4.27)$$

remembering that

$$f(x) = \int_k e^{ikx} \tilde{f}(k) \quad (4.28)$$

evidently implies

$$\tilde{t}_n(k) = 2 \int_0^L dx e^{ikx} t_n \left( \frac{x\pi}{L} \right). \quad (4.29)$$

Hence, we obtain

$$\begin{aligned} \tilde{t}_{-1}(k) &= \frac{L}{2} [1 + e^{ikL}], & \tilde{t}_0(k) &= \frac{L}{2} [-1 + e^{ikL}], \\ \tilde{t}_n(k) &= \frac{2L}{\pi} \left[ -\frac{1}{n} + \frac{(-1)^n}{n} e^{ikL} \right] + 2 \int_0^L dx e^{ipx} \sin \left( \frac{nx\pi}{L} \right) \quad \text{for } n \geq 1. \end{aligned} \quad (4.30)$$

1D kernels

By a similar procedure for  $\tilde{s}_n(k)$ , with

$$\tilde{s}_n(k) = \frac{1}{L} \int_0^L dx e^{-ikx} s_n \left( \frac{x\pi}{L} \right), \quad (4.31)$$

we find

$$\begin{aligned}\tilde{s}_{-1}(k) &= \frac{1}{ipL} [e^{ip\epsilon} - e^{-ip(L+\epsilon)}], \\ \tilde{s}_0(k) &= \frac{2}{L^2} \left[ \frac{e^{-ip(L+\epsilon)} - e^{ip\epsilon}}{k^2} \right] - \left( \frac{L+2\epsilon}{L} \right) \frac{1}{ipL} [e^{-ip(L+\epsilon)} + e^{ip\epsilon}], \\ \tilde{s}_n(k) &= \frac{1}{L} \int_0^L dx e^{-ipx} \sin\left(\frac{nx\pi}{L}\right) \quad \text{for } n \geq 1.\end{aligned}\tag{4.32}$$

**1D dual kernels**

Furthermore, by combining equations (4.22), (4.29), and (4.31) one has in terms of orthonormality

$$\int_k \tilde{s}_m(k) \tilde{t}_n(k) = \frac{2}{L} \int_0^L dx s_m\left(\frac{x\pi}{L}\right) t_n\left(\frac{x\pi}{L}\right) = \delta_{mn},\tag{4.33}$$

whilst with (4.44), (4.29), and (4.31) one arrives to

$$\begin{aligned}P_L(k, q) &= \sum_{n=-1}^{\infty} \tilde{t}_n(k) \tilde{s}_n(q) \\ &= \frac{2}{L} \sum_{n=-1}^{\infty} \int_0^L dx e^{ikx} t_n\left(\frac{x\pi}{L}\right) \int_0^L dy e^{-iqy} s_n\left(\frac{y\pi}{L}\right) \\ &= \int_0^L dx e^{i(k-q)x} = \frac{e^{i(k-q)(L+\epsilon)} - e^{-i(k-q)\epsilon}}{i(k-q)},\end{aligned}\tag{4.34}$$

**Projector**

as a completeness relation. This last expression can be understood as a projection operator that is unity in the region  $[0, L]$  and zero outside, when written in momentum space.

## 4.2.2 In two dimensions

For the two-dimensional case, we wish to transform between functions defined on a disk of radius  $R$  in continuous position space to a discrete two-dimensional Fourier representation. This is done for an arbitrary two-valued function  $\omega(r, \varphi)$ , conveniently written down in polar coordinates. We know that Bessel functions are a natural basis for translating a finite disk in position space to a discrete momentum representation, so we take this knowledge and, as done for the one-dimensional case, extend this basis of transformation kernels, in order to recover free boundary conditions at  $r = R$ . The translation of the azimuthal variable is taken care of in the usual way by

$$\omega^m(r) = \frac{1}{2\pi} \int_0^{2\pi} d\varphi \omega(r, \varphi) e^{-im\varphi},\tag{4.35}$$

**Azimuthal variable**

while for the transformation of the radial coordinate we complement the basis of Bessel functions with an additional  $s^m_0(r)$  kernel. Denoting by  $J_m(k_l^{(m)}r)$  the Bessel function of order  $m$ , with the  $l$ th zero at  $Rk_l^{(m)}$ , we write down the expansion for every fixed index  $m$  as

$$\omega^m(r) = \omega^m_0 f^m(r) + \sum_{l=1}^{\infty} \omega^m_l J_m(k_l^{(m)}r) = \sum_{l=0}^{\infty} \omega^m_l s^m_l(r), \quad (4.36)$$

introducing already the transformation basis

$$\begin{aligned} s^m_0(r) &= f^m(r), \\ s^m_l(r) &= J_m(k_l^{(m)}r) \quad \text{for} \quad l \geq 1. \end{aligned} \quad (4.37)$$

The function  $f^m(r)$  is still to be determined. To find the inverse transformation, we see in Eq. (4.36) that for  $l \neq 0$  we have

$$\omega^m_l = \frac{2}{R^2 [J_{m+1}(k_l^{(m)}R)]^2} \int_0^R r \, dr [\omega^m(r) - \omega^m_0 f^m(r)] J_m(k_l^{(m)}r); \quad (4.38)$$

while for  $l = 0$  we note that  $\omega^m_0 = \omega^m(R)/f^m(R)$ . So, without loss of generality we choose a function  $f^m(r)$  that satisfies  $f^m(R) = 1$ . With the above in mind we introduce the kernels

$$\begin{aligned} t^m_0(r) &= \frac{1}{R} \delta(r - R), \\ t^m_l(r) &= \frac{2}{R^2 [J_{m+1}(k_l^{(m)}R)]^2} \left( J_m(k_l^{(m)}r) \right. \\ &\quad \left. - \frac{1}{R} \delta(r - R) \int_0^R r' \, dr' f^m(r') J_m(k_l^{(m)}r') \right) \quad \text{for} \quad l \geq 1 \\ &= \frac{1}{R^2 [J_{m+1}(k_l^{(m)}R)]^2} \left( J_m(k_l^{(m)}r) - \frac{\delta(r - R)}{k_l^{(m)}} J_{m+1}(k_l^{(m)}R) \right), \end{aligned} \quad (4.39)$$

and obtain the general expression,

$$\omega^m_l = \int_0^{R+\epsilon} r \, dr \, \omega^m(r) t^m_l(r). \quad (4.40)$$

<sup>1</sup>This last equality comes from the future, once we have determined the shape of  $f^m(r)$ .

The behaviour at the origin  $r = 0$  should also be taken care of. In particular, we know from (4.35) and (4.36) that

$$\omega^m(0) \stackrel{(4.35)}{=} \delta^m_0 \omega(0, \varphi) \stackrel{(4.36)}{=} \omega^m_0 f^m(0) + \sum_{l=1}^{\infty} \omega^m_l \delta^m_0 \quad (4.41)$$

so  $f^m(r)$  must satisfy  $\lim_{r \rightarrow 0} f^m(r) \propto \delta^m_0$ , and  $f^m(r) = (r/R)^m$  is a perfectly suitable choice. In summary, we recover a non-vanishing function at  $r = R$  with  $\omega^m(R) = \omega^m_0$ , while at  $r = 0$

$$\begin{aligned} \omega^m(0) &= \delta^m_0 \left( \omega^m_0 + \sum_{l=1}^{\infty} \int_0^R r \, dr \, \omega^m(r) t^m_l(r) \right) \\ &= \delta^m_0 \left( \omega^m_0 + \sum_{l=1}^{\infty} \frac{2}{R^2 [J_{m+1}(k_l^{(m)} R)]^2} \int_0^R r \, dr \, \omega^m(r) J_m(k_l^{(m)} r) \right. \\ &\quad \left. - \sum_{l=1}^{\infty} \frac{2\omega^m_0}{R^2 [J_{m+1}(k_l^{(m)} R)]^2} \int_0^R r \, dr \, f^m(r) J_m(k_l^{(m)} r) \right) \\ &= \delta^m_0 (\omega^m_0 + \omega^m(0) - \omega^m_0 \delta^m_0), \end{aligned} \quad (4.42)$$

everything fits in. In the intermediate steps of (4.42) we used that

$$\delta^m_0 \sum_{l=1}^{\infty} \frac{2J_m(k_l^{(m)} r)}{R^2 [J_{m+1}(k_l^{(m)} R)]^2} = \delta^m_0 \frac{1}{r} \delta(r). \quad (4.43)$$

It is a simple exercise to verify that the kernels  $t^m_l(r)$ ,  $s^m_l(r)$  satisfy the completeness and orthonormality relations

$$\sum_{l=0}^{\infty} t^m_l(r) s^m_l(u) = \frac{1}{r} \delta(r - u), \quad \int_0^R r \, dr \, t^m_l(r) s^m_n(r) = \delta_{ln}. \quad (4.44)$$

**Completeness  
and  
orthogonality**

Therefore,  $t^m_l(r)$  and  $s^m_l(r)$  are each other's inverse matrices, and we can use them to perform unitary transformations. In particular, if we have a two-point valued function  $\omega(r, \varphi; u, \theta)$ , we can go to discrete momentum space by steps, as follows. First,

$$\omega^{mn}(r; u) = \left( \frac{1}{2\pi} \right)^2 \int_0^{2\pi} d\varphi \int_0^{2\pi} d\theta \, e^{im\varphi} \omega(r, \varphi; u, \theta) e^{-in\theta} \quad (4.45)$$

and subsequently,

$$\omega^{mn}_{lj} = \int_0^R r dr \int_0^R u du s^m_l(r) \omega^{mn}(r; u) t^n_j(u). \quad (4.46)$$

An additional comment regarding the identity in the azimuthal index basis is in order: if we transform a delta distribution defined in a disk to discrete momentum space, we get

$$\begin{aligned} \left(\frac{1}{2\pi}\right)^2 \int_0^{2\pi} d\varphi \int_0^{2\pi} d\theta e^{im\varphi} \delta(\varphi - \theta) e^{-in\theta} &= \left(\frac{1}{2\pi}\right)^2 \int_0^{2\pi} d\theta e^{i(m-n)\theta} \\ &= \frac{1}{2\pi} \delta_{mn} := \mathbb{I}_{mn} \end{aligned} \quad (4.47)$$

which defines the identity in the azimuthal space  $m, n$ ; we will use this definition throughout.

For our last step we translate the kernels  $s^m_l(r)$  and  $t^m_l(r)$  to momentum space. To do so, we remember the relation between  $\omega^m(r)$  and its momentum space representation  $\tilde{\omega}^m(k)$

$$\omega^m(r) = \int_0^\infty k dk J_m(kr) \tilde{\omega}^m(k) \quad (4.48)$$

and implement this, so that in discrete momentum space we have for (4.40)

$$\omega^{m_l} = \int_0^R r dr \int_0^\infty k dk J_m(kr) \tilde{\omega}^m(k) t^m_l(r) = \int_0^\infty k dk \tilde{\omega}^m(k) \tilde{t}^m_l(k) \quad (4.49)$$

with

$$\tilde{t}^m_l(k) = \int_0^R r dr J_m(kr) t^m_l(r). \quad (4.50)$$

In a similar manner we obtain

$$\tilde{s}^m_l(k) = \int_0^R r dr J_m(kr) s^m_l(r). \quad (4.51)$$

In this way, equation (4.46) translates to

$$\omega^{mn}_{lj} = \int_0^\infty k dk \int_0^\infty q dq \tilde{s}^m_l(k) \omega^{mn}(k; q) \tilde{t}^n_j(q). \quad (4.52)$$

The explicit shape of kernels  $\tilde{s}^m_l(k)$  and  $\tilde{t}^m_l(k)$  can be calculated to give

$$\begin{aligned} \tilde{t}^m_0(k) &= J_m(kR), \\ \tilde{t}^m_l(k) &= \frac{2J_m(kR)}{Rk_l^{(m)} J_{m+1}(k_l^{(m)} R)} \left( \frac{k^2}{k_l^{(m)2} - k^2} \right) \quad \text{for } l \geq 1, \end{aligned} \quad (4.53)$$

2D kernels

and

$$\begin{aligned}\tilde{s}^m_0(k) &= \frac{R}{k} J_{m+1}(kR), \\ \tilde{s}^m_l(k) &= \frac{Rk_l^{(m)} J_m(kR) J_{m+1}(k_l^{(m)}R)}{k_l^{(m)2} - k^2} \quad \text{for } l \geq 1.\end{aligned}\tag{4.54} \quad \text{2D dual kernels}$$

Using (4.44), (4.50), (4.51), and the completeness relation of Bessel functions in momentum space,

$$\int_0^\infty k \, dk J_m(kr) J_m(ku) = \frac{1}{r} \delta(r - u),\tag{4.55}$$

one can verify that the kernels  $\tilde{t}^m_l(k)$  and  $\tilde{s}^m_l(k)$  are normalised and orthogonal,

$$\int_0^\infty k \, dk \tilde{t}^m_l(k) \tilde{s}^m_n(k) = \delta_{ln}.\tag{4.56}$$

Regarding completeness one finds again a projector, this time on the disk of radius  $R$ ,

$$\begin{aligned}P_R^m(k, q) &= \sum_{l=0}^{\infty} \tilde{t}^m_l(k) \tilde{s}^m_l(q) \\ &= \sum_{l=0}^{\infty} \int_0^R r \, dr \int_0^R u \, du s^m_l(r) J_m(rk) J_m(uq) t^m_l(u) \\ &= \int_0^R r \, dr J_m(rk) J_m(rq) \\ &= \frac{R}{k^2 - q^2} \left[ q J_m(Rk) J_m(Rq)_{,r} - k J_m(Rq) J_m(Rk)_{,r} \right].\end{aligned}\tag{4.57} \quad \text{2D Projector}$$

## 4.3 Analytical expressions

Having obtained the above kernels, we now calculate using different methods the actual values of the matrix  $a_{mn}$ , and thereof determine entanglement entropy by diagonalising  $a_{mn}$ . This process has two steps, we first go as far as we can analytically, and afterwards implement a numerical approach to solve for integrals which do not lend themselves to analytical solutions.

### 4.3.1 For a one-dimensional system

As we know now, our main task is to obtain the matrix  $a_{mn}$  determined by the statistical correlation functions as given in (3.4). Here  $m$  and  $n$  are discrete

one-dimensional momentum indices, and the translation to this space is done by means of the kernels  $\tilde{s}_n(k), \tilde{t}_n(k)$  constructed in 4.2.1.

With the momentum representation of the equal-time statistical correlation functions given by (4.10) (we concentrate on the ground state where  $n_{\top}(k) = 0$ ) the matrix elements  $a_{mn}$  become<sup>2</sup>

$$\begin{aligned} a_{mn} + \frac{1}{4}\delta_{mn} &= \sum_{l=-1}^{\infty} [\Delta_{\pi\pi}^S]_{ml} [\Delta_{\phi\phi}^S]_{ln} \\ &= \sum_{l=-1}^{\infty} \int_p \int_q \tilde{s}_m(k) \Delta_{\pi\pi}^S(k) \tilde{t}_l(k) \tilde{s}_l(q) \Delta_{\phi\phi}^S(q) \tilde{t}_n(q) \\ &= \frac{1}{4} \int_k \int_q \tilde{s}_m(k) \sqrt{\frac{k^2}{k^2 + 2/\xi^2}} P_L(k, q) \sqrt{\frac{q^2 + 2/\xi^2}{q^2}} \tilde{t}_n(q), \end{aligned} \quad (4.58)$$

using the expression of the projector  $P_L(k, q)$  obtained in (4.34).

We can calculate the entries of (4.58) by integrating in the complex plane first over  $q$ , which has no poles on the real axis, so that we can slide the contour slightly below. Once there we divide the integral in two terms, one that converges when closing the contour above,

$$I_0^a(k) = \int_q \frac{e^{-i(k-q)\epsilon}}{i(q-k)} \sqrt{\frac{q^2 + 2/\xi^2}{q^2}} \tilde{t}_n(q), \quad (4.59)$$

and one which converges by closing below the real axis

$$I_0^b(k) = \int_q \frac{e^{i(k-q)(L+\epsilon)}}{i(k-q)} \sqrt{\frac{q^2 + 2/\xi^2}{q^2}} \tilde{t}_n(q). \quad (4.60)$$

The poles contribution from (4.59) at  $q = k$  simply gives

$$I_0^a(k)_{\text{poles}} = \sqrt{\frac{k^2 + 2/\xi^2}{k^2}} \tilde{t}_n(k) \quad (4.61)$$

so that when substituting back in, (4.58), we get the contribution from poles

**Poles  
contribution**

$$[a_{mn}]_{\text{poles}} = \frac{1}{4} \int_k \tilde{s}_m(k) \tilde{t}_n(k) - \frac{1}{4}\delta_{mn} = 0. \quad (4.62)$$

This term above would lead to a vanishing entanglement entropy.

<sup>2</sup>Note that we have interchanged the terms corresponding to  $\Delta_{\pi\pi}^S$  and  $\Delta_{\phi\phi}^S$ , so that our expressions match those in [10]. This would imply an exchange in matrix indices  $m \leftrightarrow n$ , which at the end has no effect on the solution, for what we are looking after are the eigenvalues of  $a_{mn}$ .

Now we take into account the branch cuts in the integrals (4.59) and (4.60). To do so we start by rotating  $q \rightarrow -iq = y$  and implement this change of variable in both expressions, so that (4.59) becomes

$$I_0^a(k) = -\frac{1}{2\pi} e^{-ik\epsilon} \int_{i\infty}^{-i\infty} idy \frac{e^{-y\epsilon}}{y+ik} \sqrt{\frac{2/\xi^2 - y^2}{-y^2}} \tilde{t}_n(iy) \quad (4.63)$$

which now closes to the right, and (4.60) is written as

$$I_0^b(k) = \frac{1}{2\pi} e^{ik(L+\epsilon)} \int_{i\infty}^{-i\infty} idy \frac{e^{y(L+\epsilon)}}{ik+y} \sqrt{\frac{2/\xi^2 - y^2}{-y^2}} \tilde{t}_n(iy) \quad (4.64)$$

which closes to the left. The total branch cuts contribution is therefore given by

$$I_0(k)_{bc} = \frac{1}{\pi} \int_0^{\sqrt{2}/\xi} dy e^{-y\epsilon} \frac{\sqrt{2/\xi^2 - y^2}}{y} \left[ \frac{e^{-ik\epsilon}}{y+ik} + (-1)^n \frac{e^{ik(L+\epsilon)}}{ik-y} \right] \tilde{t}_n(iy). \quad (4.65)$$

Here we have used that  $-e^{-yL} \tilde{t}_n(-iy) = (-1)^n \tilde{t}_n(iy)$ . By taking the limit  $\epsilon \rightarrow 0$  in the above expressions we arrive to

$$a_{mn} = \frac{1}{4\pi} \int_0^{\sqrt{2}/\xi} dy \frac{\sqrt{2/\xi^2 - y^2}}{y} \int_k \tilde{s}_m(k) \sqrt{\frac{k^2}{k^2 + 2/\xi^2}} \times \left[ \frac{1}{y+ik} + (-1)^n \frac{e^{ikL}}{ik-y} \right] \tilde{t}_n(iy). \quad (4.66)$$

On a next step we calculate

$$I_1(y) = \int_k \tilde{s}_m(k) \sqrt{\frac{k^2}{k^2 + 2/\xi^2}} \left[ \frac{1}{y+ik} \right] \quad (4.67)$$

and

$$I_2(y) = \int_k \tilde{s}_m(k) \sqrt{\frac{k^2}{k^2 + 2/\xi^2}} \left[ \frac{e^{ikL}}{ik-y} \right], \quad (4.68)$$

first for the case  $m = -1$ . We see that

$$I_2(y)|_{m=-1} = \int_k \frac{1}{ikL} \sqrt{\frac{k^2}{k^2 + 2/\xi^2}} \left[ \frac{e^{ikL} - 1}{ik-y} \right] = -I_1(y)|_{m=-1} \quad (4.69)$$

has no poles on the real axis, so we integrate (4.69) by taking the contour slightly below, and closing above — note that  $y \in (0, \sqrt{2}/\xi)$  guarantees that

there are also no poles on the imaginary axis. In an analogous procedure to the one before, (4.69) is integrated to the right of the complex plane to give the branch contribution

$$I_2(y)|_{m=-1} = \frac{1}{\pi L} \int_0^{\sqrt{2}/\xi} \frac{dx}{\sqrt{2/\xi^2 - x^2}} \left[ \frac{e^{-xL} - 1}{x + y} \right]. \quad (4.70)$$

In this way one arrives to the matrix row  $a_{-1n}$ ,

$$\begin{aligned} a_{-1n} &= \frac{1}{2\pi^2 L} \int_0^{\sqrt{2}L/\xi} d\bar{y} \int_0^{\sqrt{2}L/\xi} d\bar{x} \frac{1}{\bar{y}} \sqrt{\frac{2(L/\xi)^2 - \bar{y}^2}{2(L/\xi)^2 - \bar{x}^2}} \\ &\times \left[ \frac{1 - e^{-\bar{x}}}{\bar{x} + \bar{y}} \right] \tilde{t}_n \left( i \frac{\bar{y}}{L} \right), \end{aligned} \quad (4.71)$$

**Matrix row**  
 $m = -1$

setting  $\bar{y} = yL$  and  $\bar{x} = xL$ .

In a similar manner one calculates for  $m = 0$  and  $m \geq 1$ . The development is given in [10], for the final expressions to yield, correspondingly,

$$\begin{aligned} a_{0n} &= -\frac{1}{2\pi^2 L} \int_0^{\sqrt{2}L/\xi} d\bar{y} \int_0^{\sqrt{2}L/\xi} d\bar{x} \frac{1}{\bar{y}} \sqrt{\frac{2(L/\xi)^2 - \bar{y}^2}{2(L/\xi)^2 - \bar{x}^2}} \\ &\times \left[ \frac{2}{\bar{x}} \left[ \frac{e^{-\bar{x}} - 1}{\bar{x} + \bar{y}} \right] + \frac{1 + e^{-\bar{x}}}{\bar{x} + \bar{y}} \right] \tilde{t}_n \left( i \frac{\bar{y}}{L} \right) \end{aligned} \quad (4.72)$$

**Matrix row**  
 $m = 0$

and

$$\begin{aligned} a_{mn} &= \frac{m}{2\pi L} \int_0^{\sqrt{2}L/\xi} d\bar{y} \int_0^{\sqrt{2}L/\xi} d\bar{x} \frac{\bar{x}}{\bar{y}(\bar{x} + \bar{y})} \\ &\times \sqrt{\frac{2(L/\xi)^2 - \bar{y}^2}{2(L/\xi)^2 - \bar{x}^2}} \left[ \frac{1 - (-1)^m e^{-\bar{x}}}{(m\pi)^2 + \bar{x}^2} \right] \tilde{t}_n \left( i \frac{\bar{y}}{L} \right). \end{aligned} \quad (4.73)$$

**Matrix rows**  
 $m \geq 1$

In all cases  $m$  and  $n$  have to be of the same parity for  $a_{mn}$  not to vanish.

One can integrate the above expressions for  $a_{mn}$  numerically, diagonalise the latter matrix for a chosen (truncated) matrix dimension, and derive the entanglement entropy through (3.7) for an increasing value of  $L/\xi$ . An important thing to highlight is that the matrix column  $a_{m(-1)}$  has divergent elements for all (odd)  $m$ , as  $y \rightarrow 0$  in the integral. This divergence calls for an infrared (IR) cutoff  $\mu$  to be set by hand, as follows

$$\begin{aligned} a_{m(-1)} &= \frac{m}{4\pi} \int_{\mu}^{\sqrt{2}L/\xi} d\bar{y} \int_0^{\sqrt{2}L/\xi} d\bar{x} \frac{\bar{x}}{\bar{y}(\bar{x} + \bar{y})} \\ &\times \sqrt{\frac{2(L/\xi)^2 - \bar{y}^2}{2(L/\xi)^2 - \bar{x}^2}} \left[ \frac{1 - (-1)^m e^{-\bar{x}}}{(m\pi)^2 + \bar{x}^2} \right] [1 + e^{-\bar{y}}]. \end{aligned} \quad (4.74)$$

**IR regulator**

All other matrix elements remain finite. Note that  $n = -1$  corresponds to a homogeneous mode and the infrared regulator  $\mu$  introduced in (4.74) removes small momenta  $|k| < \mu/L$ .

### 4.3.2 For a two-dimensional system

Let us now go through the analogous process in a two-dimensional disk of radius  $R$ . We begin with the equal-time correlation functions (4.10) in polar coordinates

$$\begin{aligned}\Delta_{\phi\phi}^S(\mathbf{k}, \mathbf{q}) &= \frac{1}{2} \sqrt{\frac{k^2 + 2/\xi^2}{k^2}} \delta(\mathbf{k} - \mathbf{q}) \\ &= \frac{1}{2} \sqrt{\frac{k^2 + 2/\xi^2}{k^2}} \frac{\delta(k - q) \delta(\theta - \phi)}{k},\end{aligned}\quad (4.75)$$

and take care of the azimuthal variable, as instructed in section 4.2.2,

$$\begin{aligned}[\Delta_{\phi\phi}^S]^{mn}(k, q) &= \frac{1}{2} \left(\frac{1}{2\pi}\right)^2 \sqrt{\frac{k^2 + 2/\xi^2}{k^2}} \frac{\delta(k - q)}{k} \int_0^{2\pi} d\theta e^{i\theta(m-n)} \\ &= \frac{1}{2} \sqrt{\frac{k^2 + 2/\xi^2}{k^2}} \frac{\delta(k - q)}{k} \mathbb{I}_{mn} := [\Delta_{\phi\phi}^S]^m(k).\end{aligned}\quad (4.76)$$

We do so analogously for  $[\Delta_{\pi\pi}^S]^m(k)$ . This means that the matrix elements  $a^{mn}_{lj}$  can be written down as

$$\begin{aligned}a^{mn}_{lj} + \frac{1}{4} \mathbb{I}_{mn} \delta_{lj} &= \sum_{o=0}^{\infty} [\Delta_{\pi\pi}^S]^m_{lo} [\Delta_{\phi\phi}^S]^m_{oj} \mathbb{I}_{mn} \\ &= \sum_{o=0}^{\infty} \int_k \int_q \tilde{s}^m_l(k) [\Delta_{\pi\pi}^S]^m(k) \tilde{t}^m_o(k) \tilde{s}^m_o(q) [\Delta_{\phi\phi}^S]^m(q) \tilde{t}^m_j(q) \mathbb{I}_{mn} \\ &= \frac{1}{4} \int_k \int_q \tilde{s}^m_l(k) \sqrt{\frac{k^2}{k^2 + 2/\xi^2}} \mathbf{P}_R^m(k, q) \sqrt{\frac{q^2 + 2/\xi^2}{q^2}} \tilde{t}^m_j(q) \mathbb{I}_{mn} \\ &:= a^m_{lj} + \frac{1}{4} \delta_{lj},\end{aligned}\quad (4.77)$$

using the projector to region  $A$  in momentum space,  $\mathbf{P}_R^m(k, q)$  defined in Eq. (4.57). As useful as contour integration proved for the one-dimensional case, in this situation it is not possible to follow that path, given that the integrals over  $k$  and  $q$  actually diverge on the complex plane, as  $J_m(ik) = i^m I_m(k)$ ; so there is the need to resort directly to numerical methods.

Before going into that section, we wish to give the analytical result of the entropy when  $R \rightarrow 0$ , i.e. at vanishing size of region  $A$ . The matrix elements in (4.77) under a change of variables variables  $k \rightarrow kR = \bar{k}$  and  $q \rightarrow qR = \bar{q}$

can be written down as

**Matrix elements in 2D**

$$\begin{aligned}
 a^m_{lj} + \frac{1}{4}\delta_{lj} &= \frac{1}{4} \int_{\bar{k}} \int_{\bar{q}} \tilde{s}^m_l(\bar{k}) \sqrt{\frac{\bar{k}^2}{\bar{k}^2 + 2R^2/\xi^2}} \\
 &\times P_R^m(\bar{k}, \bar{q}) \sqrt{\frac{\bar{q}^2 + 2R^2/\xi^2}{\bar{q}^2}} \tilde{t}^m_j(\bar{q}) \mathbb{I}_{mn}.
 \end{aligned} \tag{4.78}$$

It is straightforward to see that in the limit  $R \rightarrow 0$  both expression under square root give unity, and orthogonality of the kernels takes care of the rest, to yield

**Entropy at  $R \rightarrow 0$**

$$\begin{aligned}
 \lim_{R \rightarrow 0} \left[ a^m_{lj} + \frac{1}{4}\delta_{lj} \right] &= \frac{1}{4} \sum_{o=0}^{\infty} \int_{\bar{k}} \int_{\bar{q}} \tilde{s}^m_l(\bar{k}) \tilde{t}^m_o(\bar{k}) \tilde{s}^m_o(\bar{q}) \tilde{t}^m_j(\bar{q}) \mathbb{I}_{mn}, \\
 &= \frac{1}{4} \sum_{o=0}^{\infty} \delta_{lo} \delta_{oj} \mathbb{I}_{mn} = \frac{1}{4} \delta_{lj} \mathbb{I}_{mn},
 \end{aligned} \tag{4.79}$$

and therefore a vanishing entanglement entropy,  $S_1 = 0$ . This is again an important result in the sense that entanglement entropy between spatial regions of a condensate of infinite extent is well behaved and not divergent, not only in the UV limit, but also in the IR region. Now let us obtain some results for a region  $A$  of finite size.

## 4.4 Numerical results

*That's why we do all the things we do. It is the work of gathering all the bones together. Then we must sit at the fire and think about which song we will use to sing over the bones, which creation hymn, which re-creation hymn. And the truths we tell will make the song.*

We here go into the resulting entanglement entropy after the implementation of numerical methods on the expressions derived in the previous sections. These results pertain of course to spatial entanglement in our nonrelativistic system, a BEC. We wish to show that the expected result of convergence at the UV and the relativistic behaviour for the low energy corner are recovered. We discuss this again in one and two spatial dimensions.

### 4.4.1 One-dimensional vacuum

When we say ‘‘vacuum’’ we of course refer to the state of zero thermal occupation for Bogoliubov quasiparticles,  $n_{\text{T}}(\mathbf{k})$ , within a condensate of finite density  $n$ . Let us look into this system, then.

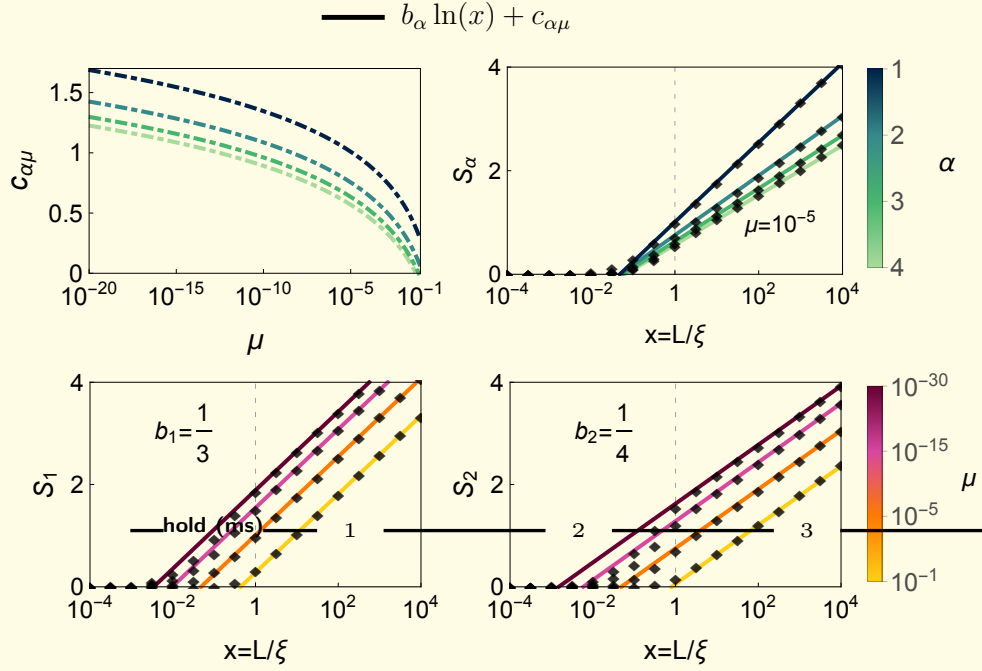


**Figure 4.1 | Entanglement entropies and cutoff dependence.** The  $x$  axis is set to logarithmic scale on all plots. On the upper left panel we show the entropy dependence on the cutoff, through its offset parameter  $c_{\alpha\mu}$ , to see its double logarithmic growth as  $\mu \rightarrow 0$ . This is given for the Rényi indices  $\alpha = \{1, 2, 3, 4\}$ . Next to it we find the entanglement entropy for the different Rényi indices at the chosen cutoff  $\mu = 10^{-5}$ , all solid lines have the shape  $b_\alpha \ln(x) + c_{\alpha\mu}$ . A more detailed exposition of the von Neumann entropy  $\alpha = 1$  and the Rényi entropy  $\alpha = 2$  is given on the bottom row, for varying values of the cutoff  $\mu$ . We note the agreement in behaviour between the numerical results (black markers) and the theoretical prediction (solid lines) for all entropies  $S_\alpha$ .

To present our results we put together several things in Figure 4.1. We first analyse the entanglement entropy dependence on the infrared regime, to find that the infrared divergence is fully contained in an offset parameter  $c_{\alpha\mu}$ , for a Rényi entanglement entropy index  $\alpha$ . We show the behaviour of this offset as a function of IR regulator  $\mu$ , for indices  $\alpha = \{1, 2, 3, 4\}$ . The panel on the upper left of Figure 4.1 demonstrates the double-logarithmic dependence of entanglement entropy with respect to IR cutoff, as expected for a one-dimensional system.

Next to that we show that our numerical result for Rényi entanglement entropies  $\alpha = \{1, 2, 3, 4\}$  is well represented by the behaviour for  $\mu \rightarrow 0$

$$S_\alpha \sim b_\alpha \ln(L/\xi) + c_{\alpha\mu}, \quad (4.80)$$

in the region  $L \geq \xi$ . We do this for a choice of IR regulator  $\mu = 10^{-5}$ . This behaviour is of course in agreement with the prediction for a relativistic one-dimensional scenario. Furthermore, the result obtained can be trivially extended

**Offset  
parameter  $c_{\alpha\mu}$**

**Relativistic  
behaviour**

to any Rényi index  $\alpha$ . We can also see that the coefficient  $b_\alpha$  in Eq. (4.80) is entirely determined by the relativistic regime ( $L \geq \xi$ ) and independent of the infrared regulator  $\mu$ . This coefficient corresponds to the result of conformal field theory calculations [49]

$$b_\alpha = \frac{c}{6\alpha}(\alpha + 1), \quad (4.81)$$

with a central charge  $c = 1$ . This is emphasised in the lower row of Figure 4.1, where we show von Neumann and Rényi  $\alpha = 2$  entanglement entropies at different values of the cutoff  $\mu$ . This summarises the behaviour in the “relativistic region”.

On the other hand, when the size of the system is below the healing length, the entanglement entropy is that of a nonrelativistic system, once the IR divergence is taken care of. This implies that for small  $L$  (large wavenumber  $k$ ), the entanglement entropy vanishes. One can also analyse the behaviour at the crossover region. From Eq. (4.80) it is clear that the value of  $c_{\alpha\mu}$  determines where precisely the crossover from nonrelativistic to relativistic entanglement entropy is located. In Figure 4.1 one can read out that  $c_{\alpha\mu}$  is close to unity for reasonable values of  $\mu$  so that the transition would take place around  $x = L/\xi = e^{-c_{\alpha\mu}/b_\alpha} \approx e^{-1/b_\alpha} \approx 1$ .

All the Rényi entanglement entropies have been calculated through Eq. (3.5) (and corresponding expression for  $\alpha = 1$ ) with the matrix  $a$  determined through the Fourier expansion scheme introduced in section 4.2.1, and truncated to a finite matrix dimension. In [10] we show the numerical result for the von Neumann entanglement entropy  $S_1$  for different choices of the (truncated) matrix dimension  $d_M$ . One can see that the numerical result agrees reasonably well for  $d_M = 10$ ,  $d_M = 20$ , and  $d_M = 100$ , which demonstrates that the expansion scheme developed in section 4.2.1 leads to convergent results for the entanglement entropy. For the numerical calculations shown in Figure 4.1 we have fixed  $d_M = 100$ , so that the correlation functions are represented by  $100 \times 100$  matrices.

In [10] we also discuss the functional behaviour of the entanglement entropy at the transition region,  $L \sim \xi$ , we find there that this behaviour might be described with reasonable accuracy by

**Crossover  
region**

$$S_\alpha \sim \frac{1}{2} \ln(h_{\alpha\mu} x + 1). \quad (4.82)$$

Here, the parameter  $h_{\alpha\mu}$  is chosen so that the values for the entanglement entropy calculated through (4.80) and (4.82) coincide at  $L = \xi$ , namely

$$c_{\alpha\mu} = \frac{1}{2} \ln(h_{\alpha\mu} + 1). \quad (4.83)$$

This gives for instance

$$h_{1\mu} = -32 \ln(3\mu)/51 \quad \text{and} \quad h_{2\mu} = -19 \ln(7\mu)/51. \quad (4.84)$$

The relation (4.83) implies that the entropy on both regions can be fitted by only one free parameter, which depends on the value of the chosen regulator  $\mu$ .

We also observe that (4.82) together with  $h_{\alpha\mu} \sim -\ln(\mu)$  and  $x = L/\xi$  leads to the same dependence on the infrared regulator as in Eq. (6.1). It is therefore likely that one must attribute the behaviour of the entanglement entropy in the crossover region to the entanglement of the homogeneous mode, namely  $\mu \rightarrow 0$ . We should note that the dependence of  $S_\alpha$  on  $\mu$  is double logarithmic, and therefore so weak that it is unlikely to be of relevance in an experimental context.

**IR  
dependence**

#### 4.4.2 Two-dimensional vacuum

Let us now look into entanglement entropies between a disk of radius  $R$  and its complementary region, within a two-dimensional condensate of infinite extent. The starting point of our numerical calculations is the shape of matrix  $a$  as written down in (4.78). While its defining integrals do converge to finite results — as one can show from the asymptotic behaviour of the kernels,  $\tilde{s}^{m_l}(k), \tilde{t}^{m_l}(k)$ , and the projector  $P_R^m(k, q)$  —, we were not able to construct a numerical procedure which would give reasonable results when taking the upper bounds to infinity. It is therefore necessary to impose an upper limit  $\bar{\mu}$  in radial momentum, with the goal of finding numerically convergent results for increasing size of the integration region. However, when doing so, two issues arise:

**Upper bound  
 $\bar{\mu}$**

- The first problem that arises has to do with the fact that in a finite region the kernels are not orthonormal anymore, i.e. (4.56) is “truncated”, so one has to take into account the appearance of spurious finite values  $\neq \delta_{ln}$  in some way.
- The second problem that arises is that, because of the change of variable  $k \rightarrow kR$ , the upper finite limit is rescaled also by  $R$ , and one cannot formally take the limit  $R \rightarrow 0$ , the result vanishes. In contrast, when the integral is taken to infinity, this limit gives back the identity matrix, as shown in Eq. (4.79).

**First issue**

**Second issue**

To solve the first issue, we determine numerically  $a_{lj}^m(R, \bar{\mu}R) + \delta_{lj}/4$  for a chosen upper bound  $\bar{\mu}R$ , with  $\bar{\mu}$  playing the role of a UV cutoff. We diagonalise this matrix and “factor out” what differs from the identity. This difference with respect to the identity is provided by the numerical calculation of  $a$  at  $R = 0$ , for the same choice of  $\bar{\mu}$ . In summary, we redefine the matrix eigenvalues as

**Solution to  
first issue**

$$\text{Diag} \left[ a_{lj}^m(R, \bar{\mu}R) + \frac{1}{4} \delta_{lj} \right] \rightarrow \frac{\text{Diag} [a_{lj}^m(R, \bar{\mu}R) + \delta_{lj}/4]}{4 \text{Diag} [a_{lj}^m(R' = 0, \bar{\mu}R) + \delta_{lj}/4]}. \quad (4.85)$$

when the denominator is larger than one. Here the variable  $\bar{\mu}R$  is explicitly written down, to stress the dependence on integration region.

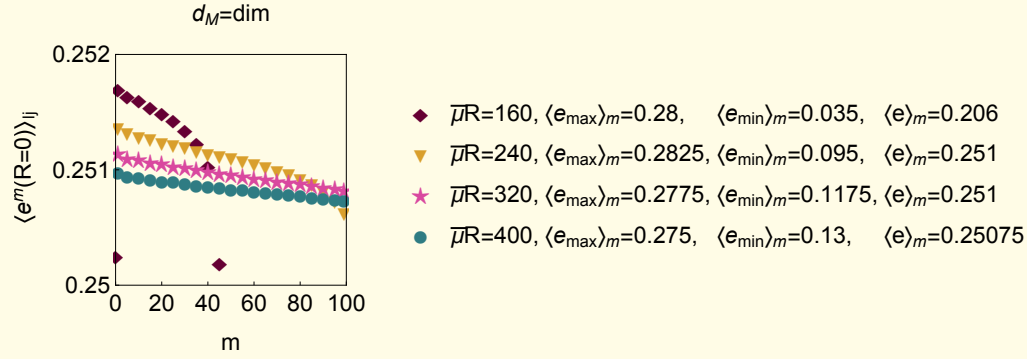


**Figure 4.2** | **Average eigenvalue** of each 30-dimensional  $a^m_{lj} + \delta_{lj}/4$  matrix at  $R = 0$ , with  $m$  running from 0 to 99; the average is done without taking the lowest eigenvalue into account. In the legends we also provide the average over all  $m$  of the largest eigenvalue and the lowest one. Furthermore the average of all eigenvalues over all  $m$  is given. To determine the latter we omitted again the lowest eigenvalue at each  $m$ . We provide the result at four different (upper) integration bounds  $\bar{\mu}R$ , to show the convergent behaviour.

#### Solution to second issue

For the second issue — which arises when looking into the behaviour of the entropy as  $R \rightarrow 0$  — we choose an upper bound which satisfies  $\bar{\mu} \gg 1/\xi$ . Since we are looking at small  $R$ , we also have  $R \ll \xi$ . Therefore  $\bar{\mu}R$  is of a reasonable size, and it yields an integration region which is both, numerically possible to handle and formally “close to infinity”. Then it is sensible to keep a constant upper bound while  $R$  acquires finite values, approaching zero. For the choice of fixed upper bound  $\bar{\mu}R = 400$  the eigenvalues at  $R = 0$  still differ from  $1/4$ , but get considerably close to it, as shown and discussed in Figure 4.2, for a  $30 \times 30$  matrix  $a$ . Therein we put forth the “average eigenvalue” of each matrix  $a^m_{lj} + \delta_{lj}/4$ , taken over the  $(l, j)$  indices. This gives one value for each index  $m$ . We further average over all indices  $m$ , to investigate the overall behaviour. We find that the lowest eigenvalue falls far from the expected value, but convergence looks promising when increasing the UV cutoff. In our numerical calculations we take any eigenvalue below  $1/4$  to be  $1/4$ , as this is a precise known lower bound of the matrix we are looking at.

We are ready to determine entanglement entropies, by means of Eq. (3.5). In Figure 4.3 we give the resulting behaviour for Rényi indices  $\alpha = \{1, 2, 3, 4\}$ . We analyse the entropies for  $R \leq \xi$  and  $R \geq \xi$  separately. For both cases we use a matrix dimension  $d_M = 30$ , and let the azimuthal index run up to  $m = 99$ . For the lower values of  $R$  we can choose a larger UV cutoff, so we implement different values of the regulator  $\bar{\mu}$  in the two different regions. With these results we can determine the analytical behaviour of the entanglement

entropies to follow

$$\begin{aligned} S_\alpha(R) &\sim A_\alpha (\ln(R + \xi) - \ln(\xi)) && \text{for } R \leq \xi, \\ S_\alpha(R) &\sim B_\alpha R + C_\alpha && \text{for } R \geq \xi. \end{aligned} \quad (4.86)$$

**Crossover  
region and  
relativistic  
behaviour**

We find therefore a logarithmic growth from  $S_\alpha = 0$  when  $R$  approaches the healing length  $\xi$ , which turns afterwards to a linear growth with  $R$ , when the radius of the disk becomes larger than  $\xi$ . This latter result is the expected area law for our two-dimensional system, with a scaling constant yet unknown, but which would be reached at convergence. It is important to emphasise that the integrals performed to obtain these results are convergent in the limit  $\bar{\mu} \rightarrow \infty$ , which implies that the entropy does remain finite in the UV. We also find, in contrast to the one-dimensional case, that the absence of an IR divergence allows for the determination of the crossover region  $R \approx \xi$  with certainty; plus we find that there is no IR divergence! — as expected for the two-dimensional case.

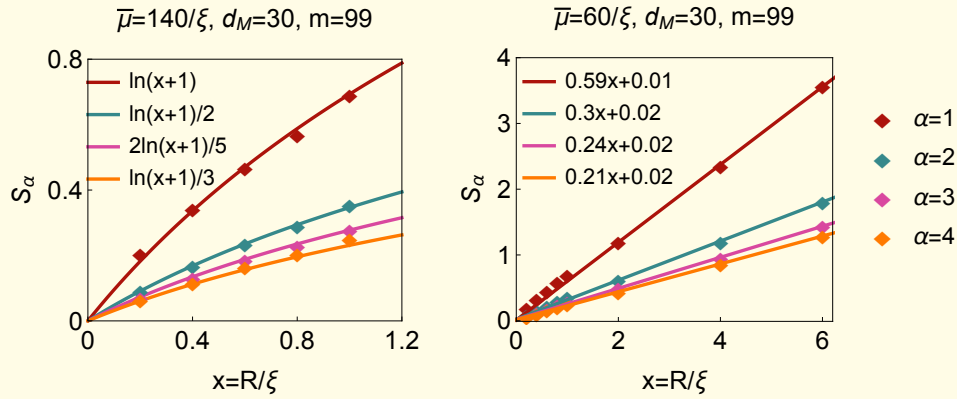


**Figure 4.3** | Rényi entanglement entropies for two different regimes of  $R$ , defined in terms of the healing length of the condensate  $\xi$ . We see a logarithmic scaling behaviour for small  $R$  and a linear one for  $R \geq \xi$ , providing thus a new result for the crossover region, and an agreement with a two-dimensional area law in the relativistic regime. The results are obtained by performing the trace in Eq. (3.5) over a matrix  $a^m_{lj}$  with  $(l, j)$  indices running from 0 to 29, to yield the matrix dimension  $d_M = 30$ , while taking the azimuthal index  $m$  up to 99. The UV cutoff is set to  $140/\xi$  for low values of  $R$ , and to  $60/\xi$  for  $R \geq \xi$ . This is done for the four Rényi indices  $\alpha$ . Numerical results are presented with discrete markers, while solid lines correspond to analytical fits.

Let us now inquire into the convergence of the numerical results for three different parameters: matrix index  $m$ , which stands for the azimuthal component of the momentum, matrix dimension  $d_M$  in radial indices  $(l, j)$ , and integration bound or UV cutoff  $\bar{\mu}$ . In all cases we will see that convergence can be reached for low  $R$ , but gets numerically challenging already at  $R \approx 10 \xi$ . We provide the

**Convergence in  $m$**  analysis for an increasing matrix index  $m$  in Figure 4.4, to find that the results converge already at  $m \sim 15$  for small  $R$ , and at  $m \sim 60$  for  $\xi \leq R \leq 10\xi$ .

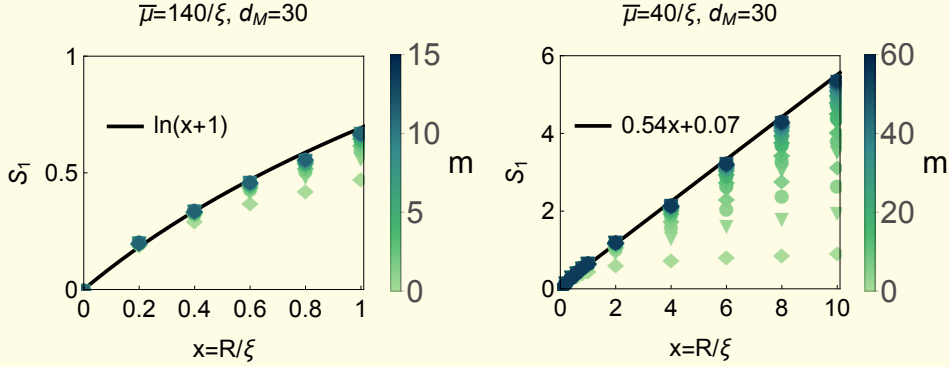


**Figure 4.4 | Convergence in azimuthal variable.** We see a convergent behaviour of the numerical results for the von Neumann entanglement entropy  $S_1$ . This is obtained at both regimes of  $R$ , for different values of  $m$ . The numerical results are given in discrete markers, while the solid lines indicate the functional behaviour of the entanglement entropy in each region. The results given are obtained by using a matrix dimension  $d_M = 30$  and two different UV regulators  $\bar{\mu}$ , depending on the size  $R$  of the entangled region  $A$ . We find an earlier convergence for lower values of  $R$  (left panel), already reached at  $m \sim 15$ .

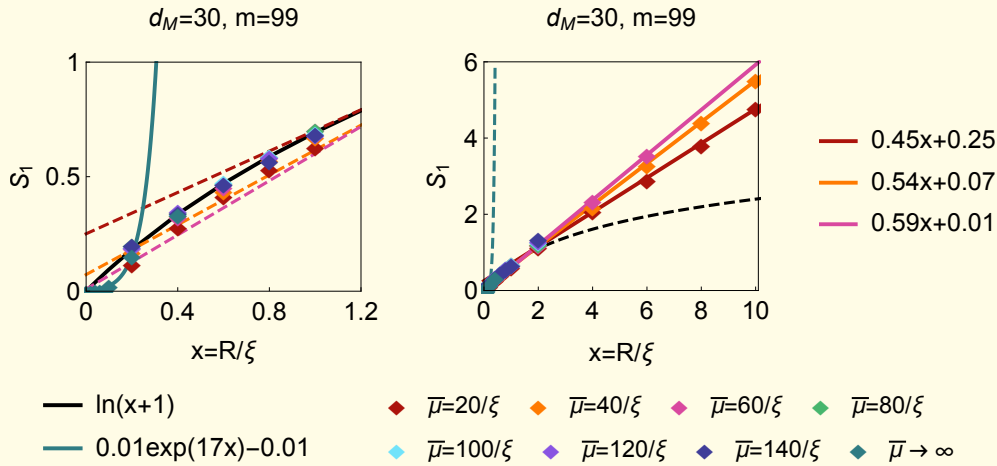


**Figure 4.5 | Convergence for the UV cutoff.** We depict with markers numerical results and with solid lines their corresponding fits. On the left we show the entanglement entropy for the region  $R \leq \xi$ , and find convergent results for increasing  $\bar{\mu}$ . The limit  $\bar{\mu} \rightarrow \infty$  is taken to calculate entanglement entropy when  $R \rightarrow 0$ , to find an exponential build up of the entropy from  $S_1(R=0) = 0$ . On the right we see the numerical limit encountered, with full convergence still to be reached. Nevertheless we can certify a two-dimensional area law with our results and appreciate a convergent tendency as the regulator  $\bar{\mu}$  increases.

To analyse the convergence regarding UV cutoff  $\bar{\mu}$  we have Figure 4.5. We again show the results at two different regimes of  $R$ . When the size of the probed region is of the order of the healing length, the UV cutoff is taken up to  $\bar{\mu} = 140/\xi$ , to find a convergent result. Therein we also analyse the build up of entanglement entropy from  $R = 0$ , with an upper bound set to  $\bar{\mu}R = 400$ . For  $R \rightarrow 0$  the latter formally corresponds to  $\bar{\mu} \rightarrow \infty$ . In this region — defined by  $R \leq 0.2\xi$  — we find an exponential growth of the von Neumann entropy with increasing region size. That is, on top of the results given in Eq. (4.86), we find the behaviour for the von Neumann entanglement entropy at  $R \rightarrow 0$ ,

$$S_1(R) \sim D_1 e^{E_1 R} - D_1 \quad \text{for } R \ll \xi. \quad (4.87)$$

When the region size  $R$  goes up to  $10\xi$ , it becomes a numerical challenge to reach convergence. Nevertheless, in the right hand side of Figure 4.5 one can see that we have obtained both, a linear behaviour of the entropy and a slope whose increase with UV cutoff is attenuated as  $\bar{\mu}$  gets larger.

Finally we look into convergence regarding matrix dimension  $d_M$  in Figure 4.6. In this case we also reached a numerical limit at  $d_M = 30$ , but found that the results for increasing matrix dimension do not present much variations, and exhibit a reasonable behaviour, taking into account the several numerical hindrances we encounter throughout the calculations.

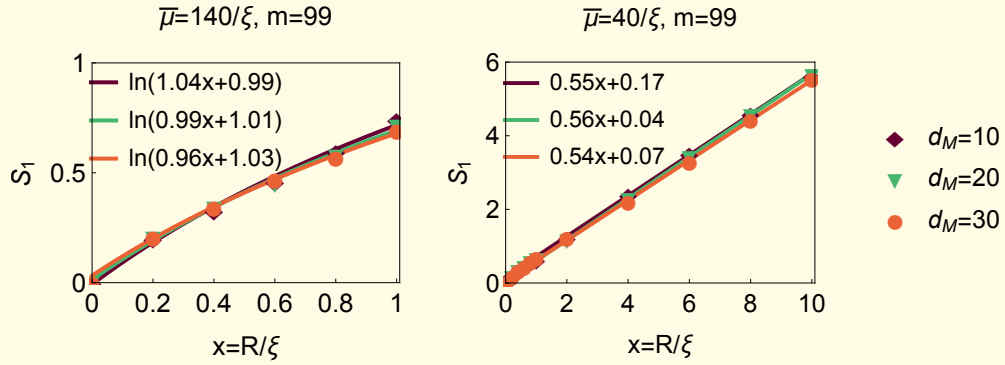


**Figure 4.6 | Convergence in matrix dimension.** We analyse the convergence for three different values of matrix dimension  $d_M$ . Again, the azimuthal variable  $m$  runs up to 99 and the UV regulator  $\bar{\mu}$  is chosen according to the size of the region  $R$ . While perfect convergence in matrix dimension is still to be achieved, one can determine with certainty the qualitative behaviour of the entanglement entropy in the two regimes of the condensate depicted herein. Numerical results are shown with discrete markers and their corresponding fits with solid lines.

Overall we have recovered the relativistic result of an area law increase of entanglement entropy for a disk of radius  $R \geq \xi$ . We have also determined the functional build up of entropy from a vanishing value at  $R = 0$ , driven initially

Convergence  
in  $\bar{\mu}$

Convergence  
in  $d_M$

by an exponential increase, to go into logarithmic growth before encountering the relativistic regime. In this way we give important results which can be experimentally tested and implemented in many-body entanglement quests. The absence of divergencies demonstrated here for a BEC is of great advantage, as universal quantities become straight forwardly accessible.

## Table-top 2 + 1 cosmology

---

We begin this chapter with a general analysis of the geometrical and dynamical aspects of FLRW cosmologies in  $d = 2 + 1$  spacetime dimensions. In the following sections we outline the theoretical model, predictions, and matching experimental outcomes regarding first, the simulation of spatially curved universes, and later the simulation of time dependent scale factors, with a special interest around the phenomenon of particle production within different types of expansion (accelerated, uniform, and decelerated).

Naturally, we are interested in the line element (2.47) with

$$\gamma_{ij} dx^i dx^j = \frac{du^2}{1 - \kappa u^2} + u^2 d\varphi^2, \quad (5.1)$$

where  $\kappa$  parametrises spatial curvature of a closed ( $\kappa > 0$ ), flat ( $\kappa = 0$ ), or open ( $\kappa < 0$ ) universe, and  $\varphi \in [0, 2\pi)$  denotes an azimuthal angle. As a reminder, we have

$$g_{00} = -1, \quad g_{0i} = g_{i0} = 0, \quad \text{and} \quad g_{ij} = a^2(t) \gamma_{ij}. \quad (5.2)$$

The shape of the metric implies that the nonvanishing Christoffel symbols in this context are [see Eq. (2.48)]

$$\begin{aligned} \Gamma^0_{11} &= \frac{a\dot{a}}{1 - \kappa u^2}, & \Gamma^0_{22} &= a\dot{a}u^2, \\ \Gamma^1_{01} &= \Gamma^1_{10} = \Gamma^2_{02} = \Gamma^2_{20} = \frac{\dot{a}}{a}, & \Gamma^2_{12} &= \Gamma^2_{21} = \frac{1}{u}, \\ \Gamma^1_{11} &= \frac{\kappa u}{1 - \kappa u^2}, & \Gamma^1_{22} &= -u(1 - \kappa u^2). \end{aligned} \quad (5.3)$$

Likewise, the Ricci tensor [see Eq. (2.49)] has the nonzero components

$$\begin{aligned} R_{00} &= -\Gamma^\lambda_{0\lambda,0} - \Gamma^\rho_{0\lambda} \Gamma^\lambda_{0\rho} = -2\frac{\ddot{a}}{a}, \\ R_{11} &= \frac{1}{1 - \kappa u^2} [\ddot{a}a + \dot{a}^2 + \kappa], & R_{22} &= u^2 [\ddot{a}a + \dot{a}^2 + \kappa], \end{aligned} \quad (5.4)$$

which yield for the Ricci scalar,

$$R = \frac{2\kappa + 4\ddot{a}a + 2\dot{a}^2}{a^2}. \quad (5.5) \quad \text{Ricci scalar}$$

Wait a second, we know this object; at least a bit. By setting  $\kappa = 0$  in (5.5) we can read out the effective mass squared (times  $-8/a^2$ ) that we derived for a spatially flat FLRW 2 + 1 situation, within the discussion of particle production [section 3.2, Table 3.1]. Interesting, right? Curvature  $\leftrightarrow$  mass. Ok, let's keep moving. With the above ingredients we obtain the components of the Einstein tensor (2.42),

$$G_{00} = \frac{\kappa + \dot{a}^2}{a^2}, \quad G_{ij} = -a\ddot{a}\gamma_{ij}, \quad (5.6)$$

in accordance with the general expression provided in (2.50). With the analog of Einstein's equations in  $d = 2 + 1$  dimensions, and the shape of the energy momentum tensor (2.51) we arrive to Friedmann's equations

$$\frac{\kappa + \dot{a}^2}{a^2} = 8\pi G_{\text{N}}\epsilon, \quad -\frac{a\ddot{a}}{a^2} = 8\pi G_{\text{N}}P. \quad (5.7)$$

In this particular case we have the conservation law (2.52) for  $D=2$

$$\dot{\epsilon} + \frac{2\dot{a}}{a}(1+w)\epsilon = 0, \quad (5.8)$$

where we have used the definition of  $w := P/\epsilon$ . This conservation law determines the evolution of the energy density in radiation, matter, and cosmological constant dominated universes respectively, as

$$\epsilon(t) = \epsilon_0 \times \begin{cases} (a_0/a(t))^3 & w = 1/2 \\ (a_0/a(t))^2 & w = 0 \\ 1 & w = -1, \end{cases} \quad (5.9)$$

in accordance with (2.53). This, together with (5.7), yields for the scale factor

**Solutions for  
the scale  
factor**

$$a(t) = a_0 \times \begin{cases} t^{2/3} & \gamma \\ t & \text{M} \\ e^{Ht} & \Lambda. \end{cases} \quad (5.10)$$

Above,  $a_0$  and  $\epsilon_0$  are the values of the scale factor and energy density at some chosen fiducial time. Also, in solving for (5.10) a vanishing spatial curvature,  $\kappa = 0$ , has been assumed. We note that a nonvanishing spatial curvature would modify these results. Particularly, a universe without any matter content,  $\epsilon = P = 0$ , would only fulfil Friedmann's equations for  $\kappa \leq 0$  to yield a linear scale factor of the form  $a(t) = \sqrt{-\kappa}t$ . With this insights into our cosmological model, let us examine how we can simulate and test the emergence of spatial curvature and expanding universes in a condensate trap.

## 5.1 Spatial curvature

As discussed in section 2.2.2, the background density distribution of the 2D condensate is determined by a given trapping potential through (2.62). In the case of harmonic and inverse harmonic traps ( $f(\mathbf{r}) = \pm r^2$ ), the former reduces to

$$n_0 = n \left( 1 \mp \frac{r^2}{R_{\text{TF}}^2} \right) = n \left( \frac{R_{\text{TF}}^2}{R_{\text{TF}}^2 \pm u^2} \right), \quad (5.11) \quad \text{Density profiles}$$

expressed also in reduced circumference coordinates ( $u, \varphi$ ), for which the FLRW line element is obtained [Eq. (2.74)]. This is true up to a certain approximation, the exact mapping to FLRW required an additional term in the trapping potential, quartic in the radial coordinate; a comparison between the density profile induced by this additional term in the potential and the one in a harmonic (inverse harmonic) trap is given in Figure 5.1. Therein we also show the geometric structure imprinted in the condensate disk by the different density distributions.

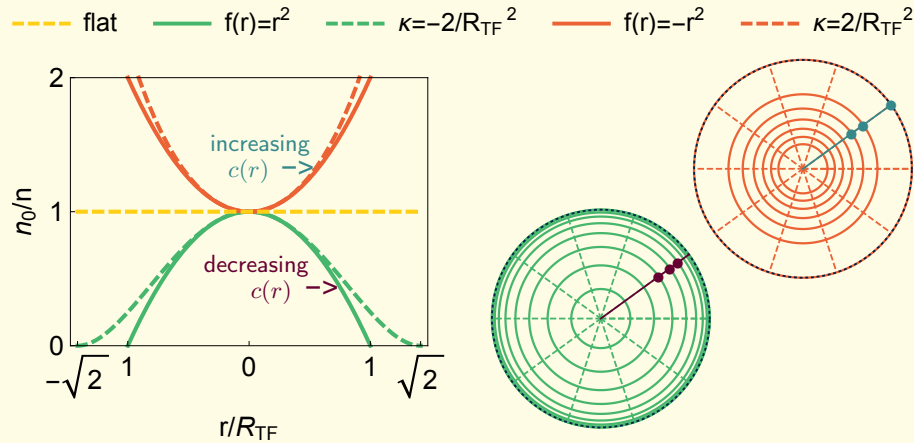


**Figure 5.1 | Density distribution and curvature** for different trapping potentials. On the left we see in solid lines the density distribution achieved through harmonic (solid green) and inverse harmonic (solid red) traps. We point to the spatial dependence of the speed of sound, which imprints the different geometries on the condensate. To the right we show with coordinate grids the emergent spatial curvature related to each of the trapping potentials. Equidistant points are depicted in each of the geometries to find, in particular, that the edges of the condensate are “infinitely” far away from the centre in a harmonic trap (open universe, hyperbolic geometry), and reachable at finite time in an inverse harmonic trap (closed universe, spherical geometry). These geometries are exact when the density distribution is the one depicted on the left panel with dashed lines.

The mere shape of the density profile alters the speed of sound towards the edges of the trap: in the case of a harmonic trap, the speed of sound decreases

as phonons propagate outwards, while it increases for the inverse harmonic trap. Since the speed of sound sets the scales for rulers, equidistant lines become more dense in the case of a decreasing speed of sound, and sparse when  $c(r)$  increases: this drives the emergent geometry. We thus obtain a manifold with intrinsic curvature corresponding to  $\kappa \mp 2/R_{\text{TF}}$  in our approximation (2.75).

### Experimental implementation

To test for the emergent curvature in harmonic and inverse harmonic trapping potentials, phonon propagation near the edges of the trap was analysed. For a given initial position, one can determine the null geodesics in the curved manifolds. When the initial position is not in the centre, these geodesics become more interesting and are certainly distinguishable for positive and negative curvatures. This was implemented experimentally, to yield the results shown in Figure 5.2. One can read out there the successful implementation and verification of the two types of curvature. Additionally, in [13] a deeper analysis was done to certify the harmonic trap as an accurate implementation of hyperbolic space.

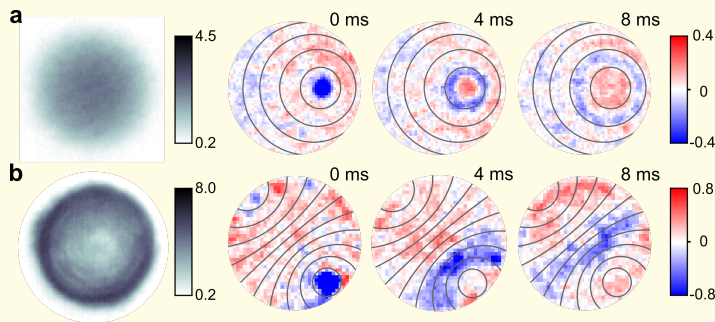


**Figure 5.2** | **Experimental outcome** for the implementation of harmonic (upper row) and inverse harmonic (lower row) traps. The overall density distribution is shown to the left. This initial distribution is perturbed close to the edges to generate a sound wave and observe its propagation. Once the background density is subtracted, one can read out the propagation of phonons within each trap. Blue signals under-density, red signals over-density, and solid lines depict the predicted propagation for sound waves in each of the emergent geometries. We can therefore appreciate a successful implementation of the geometries predicted. This figure is taken from [13], where it is further discussed.

## 5.2 Expanding universe

As we have explored in section 3.2 for an FLRW type of geometry with a time-dependent scale factor  $a(t)$ , the notions of particles and quantum field theoretic vacuum are not unique [57, 58]. Of course this situation also arises when the initial and final state have a stationary scale factor, but  $a(t)$  varies at intermediate time. This type of toy model is a close simulation of, for example, early time

cosmology, such as an inflationary epoch where  $a(t)$  evolved strongly. We now discuss particle production and the emergent measurable features in a  $d = 2 + 1$  FLRW spacetime, for a time dependent scale factor defined as,

$$a(t) = \begin{cases} a_i & \text{for } t \leq t_i & \text{region I} \\ Q|t - t_0|^\gamma & \text{for } t_i < t < t_f & \text{region II} \\ a_f & \text{for } t_f \leq t & \text{region III.} \end{cases} \quad (5.12) \quad \text{Toy model}$$

Here,  $Q$  and  $t_0$  are free parameters, and the exponent  $\gamma \geq 0$  is set to be some real number. Through the choice of  $\gamma$  one is able to simulate decelerated ( $\gamma < 1$ ), uniform ( $\gamma = 1$ ), or accelerated ( $\gamma > 1$ ) expanding cosmologies. This allows to analyse a wide variety of situations, within a regime which is experimentally accessible. The model situation is depicted in Figure 5.3.

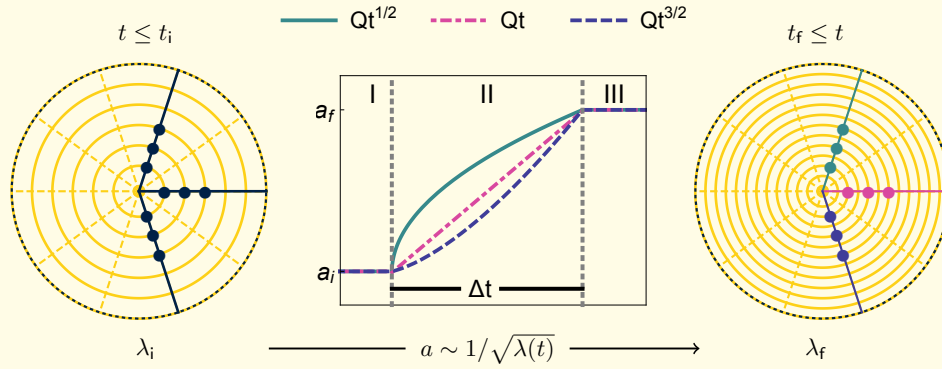


**Figure 5.3 | Polynomial expansion.** On the middle we see the time evolution of the scale factor  $a(t)$  for three different types of expansion, corresponding to a decelerated ( $\gamma = 1/2$ ), uniform ( $\gamma = 1$ ), and accelerated ( $\gamma = 3/2$ ) universe. The scale factor is shown in regions I, II, and III. In the initial and final regions (I and III) the scale factor is stationary, while in the region in between (II) it is time-dependent. The model corresponds to an expansion period of duration  $\Delta t$ . On the left we see the initial geometry of a (flat) condensate, and on the right we see the final state, once the scattering length has been altered. Events comoving with the spacetime geometry are marked with dots, to find that the distance between them has increased at final time. This is shown with coordinate grids, and due to a lower final scattering length in the condensate — linearly related to the coupling  $\lambda(t)$  through Eq. (2.57).

The theoretical predictions will of course depend on the difference between the initial and the final state; the parameter that defines them is the initial and final scale factor, correspondingly. It is then useful to introduce the concept of e-folds we acquire from cosmology. The number of e-folds in a time interval is defined simply as

$$dN_e = d \ln a(t). \quad (5.13)$$

So, in our case, with constant initial and final scale factor, we have that  $N_e = \ln(a_f/a_i)$  at the end of expansion. One can therefore analyse the effects of expansion in terms of different number of e-folds, which is done in detail in [11]. It is here important to note that, within the proposed simulation, the number of e-folds which are experimentally within reach is around  $N_e \sim 1$ . On this we base our theoretical predictions for experimental outcomes.

### Particle production

Let us now analyse particle production within the polynomial expansion scheme proposed in Eq. (5.12). As discussed in section 3.2, when the Hamiltonian is constant in time, the mode functions are oscillatory waves with a frequency  $k/a$ , normalised by a factor  $1/\sqrt{2ak}$  — see Table 3.1. Introducing the Bogoliubov transformation relating the mode functions at initial and final time, we find their shape in a universe with scale factor set by (5.12) to follow,

$$v_k(t) = \begin{cases} v_k^{\text{I}}(t) = e^{-ikt/a_i}/\sqrt{2a_i k} & \text{in region I} \\ v_k^{\text{II}}(t) = \text{solution to the mode equation} & \text{in region II} \\ v_k^{\text{III}}(t) = (\alpha_k^* e^{-ikt/a_f} - \beta_k e^{ikt/a_f})/\sqrt{2a_f k} & \text{in region III.} \end{cases} \quad (5.14)$$

As a reminder, in region I the vacuum is defined as  $\hat{d}|0\rangle_{\hat{d}} = 0$ , while in region III we have  $\hat{c}|0\rangle_{\hat{c}} = 0$ . The Bogoliubov coefficients can be determined by solving the mode equation in region II and using the appropriate boundary conditions. In appendix D we go through the derivation for  $\gamma = 1/2$  in coordinate time and for  $\gamma = 1$  in conformal time, to show the difference in these approaches. We redirect the reader to [11] for the analytical expressions of Bogoliubov coefficients for  $\gamma = 2/3$  and  $\gamma = 3/2$ .

Ok, we can obtain the Bogoliubov coefficients, so what now? As we have been promising, we want some measurable quantities related to these coefficients: here is where two-point functions come into play. Let us place ourselves at the end of expansion, i.e., at times  $t \geq t_f$ , and let us introduce the rescaled density contrast

### Density contrast

$$\delta_c(t, u, \varphi) = \sqrt{\frac{n_0(u)}{n^3}} [n_F(t, u, \varphi) - n_0(u)]. \quad (5.15)$$

Here  $n_F(t, u, \varphi) = |\Phi(t, u, \varphi)|^2$  denotes the full condensate density,  $n_0(u)$  the background density, and  $n$  the density in the centre of the trap. In this way, the rescaled density contrast is dimensionless. Let us substitute with  $|\Phi(t, u, \varphi)|^2$  from (2.69) and expand to linear order in the fluctuating fields to relate fields

and density contrast as,

$$\begin{aligned}\delta_c(t, \mathbf{u}) &= \sqrt{\frac{n_0(u)}{n^3}} \left[ \left( \phi_0(t, \mathbf{u}) - \frac{\dot{\phi}(t, \mathbf{u})}{2\sqrt{mc^2}} \right)^2 + m\phi^2(t, \mathbf{u}) - n_0(u) \right] \\ &\approx -\sqrt{\frac{n_0^2(u)}{n^3}} \left[ \frac{\dot{\phi}(t, \mathbf{u})}{\sqrt{mc^2}} \right] = -\sqrt{\frac{m}{\lambda_f^2 n^3}} \dot{\phi}(t, \mathbf{u})\end{aligned}\quad (5.16)$$

using the expression of the speed of sound at final time  $c^2 = n_0(u)\lambda_f/m$ . We can directly see that the equal-time two-point correlation function for density contrast and the one for time derivative of fields are related by

$$\mathcal{G}_{nn}(t; u, u', \varphi, \varphi') = \langle \delta_c(t, u, \varphi) \delta_c(t, u', \varphi') \rangle = \frac{m}{\lambda_f^2 n^3} \mathcal{G}_{\dot{\phi}\dot{\phi}}(t, L), \quad (5.17)$$

where

$$\mathcal{G}_{\dot{\phi}\dot{\phi}}(t, L) = \frac{1}{2} \langle \{ \dot{\phi}(t, u, \varphi), \dot{\phi}(t, u', \varphi') \} \rangle_c. \quad (5.18)$$

Here we have used that, as a consequence of spatial homogeneity and isotropy, all two-point correlation functions depend on spatial coordinates only through the (comoving) distance  $L$  between the two spatial positions  $\mathbf{u}$  and  $\mathbf{u}'$ . The density contrast correlation function therefore acquires the symmetries of the acoustic FLRW universe.

Let us calculate then  $\mathcal{G}_{\dot{\phi}\dot{\phi}}$  in momentum space. We start with the expansion of the fields in terms of mode functions in region III,

$$\dot{\phi}_{\mathbf{k}}(t) = \dot{v}_k(t) \hat{d}_{\mathbf{k}} + \dot{v}_k^*(t) \hat{d}_{-\mathbf{k}}^\dagger, \quad \dot{v}_k^{\text{III}}(t) = -i \sqrt{\frac{k}{2a_f^3}} (\alpha_k^* e^{-ikt/a_f} + \beta_k e^{ikt/a_f}) \quad (5.19)$$

so that

$$\begin{aligned}\frac{1}{2} \langle \{ \dot{\phi}_{-\mathbf{k}}(t) \dot{\phi}_{\mathbf{k}}(t) \} \rangle_{\hat{d}} &= |\dot{v}_k(t)|^2 \left( 1 + \langle \hat{d}_{-\mathbf{k}}^\dagger \hat{d}_{-\mathbf{k}} \rangle_{\hat{d}} + \langle \hat{d}_{\mathbf{k}}^\dagger \hat{d}_{\mathbf{k}} \rangle_{\hat{d}} \right) \\ &= \frac{k}{2a_f^3} (1 + 2|\beta_k|^2 + 2 \operatorname{Re} [\alpha_k \beta_k e^{2ikt/a_f}]) (1 + 2N_k^{\hat{d}}) \\ &:= \frac{k}{a_f^3} \left( \frac{1}{2} + N_k + \Delta N_k(t) \right) := \frac{k}{a_f^3} S_k(t).\end{aligned}\quad (5.20)$$

**Spectrum of fluctuations**

We find in the above expression the expected occupation number of phonon excitations per mode

$$N_k := N_k^{\hat{d}} + |\beta_k|^2 (1 + 2N_k^{\hat{d}}). \quad (5.21)$$

**Final occupation**

Defined therein are also the spectrum of fluctuations,  $S_k(t)$ , as the momentum space representation of the two-point correlation function, and the time-dependent contribution

**Time  
dependence**

$$\begin{aligned} \Delta N_k(t) &:= \left(1 + 2N_k^{\hat{d}}\right) \operatorname{Re} \left[\alpha_k \beta_k e^{2ikt/a_f}\right] \\ &= \left(1 + 2N_k^{\hat{d}}\right) |\alpha_k \beta_k| \cos \left(\frac{2k}{a_f}t + \theta_k\right). \end{aligned} \quad (5.22)$$

Additionally, we have introduced the phase corresponding to the momentum mode  $k$ ,

**Phase**

$$\theta_k = \operatorname{Arg}(\alpha_k \beta_k), \quad (5.23)$$

which will prove to be an important quantity for the comparison between theory and experiment. Both, the phase  $\theta_k$  and the spectrum of fluctuations  $S_k(t)$  are discussed in Figure 5.4. On top of these notions, we find the initial occupation

**Initial  
occupation**

$$N_k^{\hat{d}} = \langle \hat{d}_{\mathbf{k}}^\dagger \hat{d}_{\mathbf{k}} \rangle_{\hat{d}}, \quad (5.24)$$

which induces the general shape of the final spectrum, subject to stimulated particle production [63]. Of course, if the initial state is simply  $|0\rangle_{\hat{d}}$ , the above reduces to the phenomenon of particle production in vacuum states.

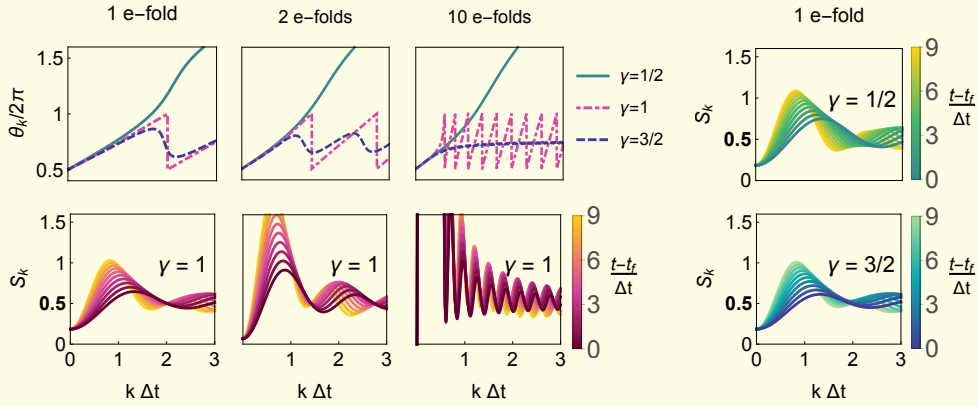


**Figure 5.4** | **Phase and spectrum evolution after expansion** for an initial vacuum state subject to a polynomial expansion of duration  $\Delta t$ . In the first three panels, upper row, we show the acquired phase after expansion as a function of wave number  $k$  [cf. Eq. (5.23)] for decelerated ( $\gamma = 1/2$ ), uniform ( $\gamma = 1$ ), and accelerated ( $\gamma = 3/2$ ) expansion, for various e-fold numbers. In the remaining panels we depict the evolution of the spectrum after expansion has ceased, for a time lapse of  $9\Delta t$ . The spectrum evolves in time with a frequency set by the dispersion relation  $\omega_k = k$ , and an initial phase  $\theta_k$ . When  $\gamma = 1$  one obtains nodes at  $\beta_k = 0$ , related to the phase jumps found in the upper row. Furthermore, the type of expansion encoded in  $\gamma$  does not have a big influence on the shape of the spectra, so that the phase becomes a relevant parameter to certify different types of expansion in an experimental context.

In the experimental context we will consider an initial thermal state, so that the initial occupation number is determined through the Bose-Einstein distribution as

$$N_k^{\hat{d}}(T) = \frac{1}{e^{\omega_k^{\hat{d}}/T} - 1} \quad (5.25)$$

for a given temperature  $T$ . In the following, to set a temperature scale, we use the critical temperature  $T_c$  of an ideal gas in an anisotropic trap. In particular, we consider a ratio between longitudinal and radial trapping frequencies that elicit the emergence of a 2D condensate [64]. This critical temperature is given by

$$T_c = \omega \left( \frac{N}{\zeta(2)} \right)^{1/2}, \quad (5.26)$$

where  $N$  is the total number of atoms, and  $\omega$  is the radial trapping frequency.

To analyse the two-point density contrast correlation function (5.16) we must go back to position space. We naturally do so through a Bessel transform

**Position  
space**

$$\mathcal{G}_{\hat{\phi}\hat{\phi}}(t, L) = \frac{1}{2\pi} \int_0^\infty k \, dk \, J_0(kL) \mathcal{G}_{\hat{\phi}\hat{\phi}}(t, k), \quad (5.27)$$

taking into account that the azimuthal variable is integrated to  $\delta_{m0}/2\pi$ . We apply this directly to the density contrast in position space — putting together (5.17) and (5.20) —, and obtain

$$G_{nn}(t, L) = \frac{a_f}{nm} \int_0^\infty dk \frac{k^2}{2\pi} J_0(kL) S_k(t), \quad (5.28)$$

with the expression for the scale factor  $a_f^2 = m/n\lambda_f$  determined in (2.71).

At this point it is important to note that a two-point correlation function of fields as defined in (5.18) shows an ultraviolet divergence. This can be cured through the use of test or window functions, which act as a regulator. We are therefore formally working with smeared-out fields

$$\tilde{\phi}(t, \mathbf{r}) = \int_{\mathbf{r}'} W(\mathbf{r} - \mathbf{r}') \phi(t, \mathbf{r}'); \quad \int_{\mathbf{r}'} W(\mathbf{r}') = 1, \quad (5.29)$$

by means of a normalised window function  $W(\mathbf{r} - \mathbf{r}')$ . We end up with a regularised expression for the rescaled density contrast correlation function

$$G_{nn}(t, L) = \frac{a_f}{nm} \int_0^\infty dk \frac{k^2}{2\pi} J_0(kL) S_k(t) \tilde{f}_G(k), \quad (5.30)$$

where  $\tilde{f}_G(k) = \tilde{W}^*(k) \tilde{W}(k)$  corresponds to the absolute square of the Fourier transformed window function. In the following we work with a window function

of Gaussian form in position space (as a function of the comoving distance), which in momentum space yields

$$\tilde{f}_G(k) = \tilde{W}^*(k)\tilde{W}(k) = e^{-w^2k^2}, \quad (5.31)$$

for a spatially flat scenario. In the context of a Bose-Einstein condensate, a regularisation arises naturally as the readout of the density contrast is limited by the precision of the measurement apparatus. Moreover, the acoustic regime we work on is a low momentum effective description that loses validity in the ultraviolet region.

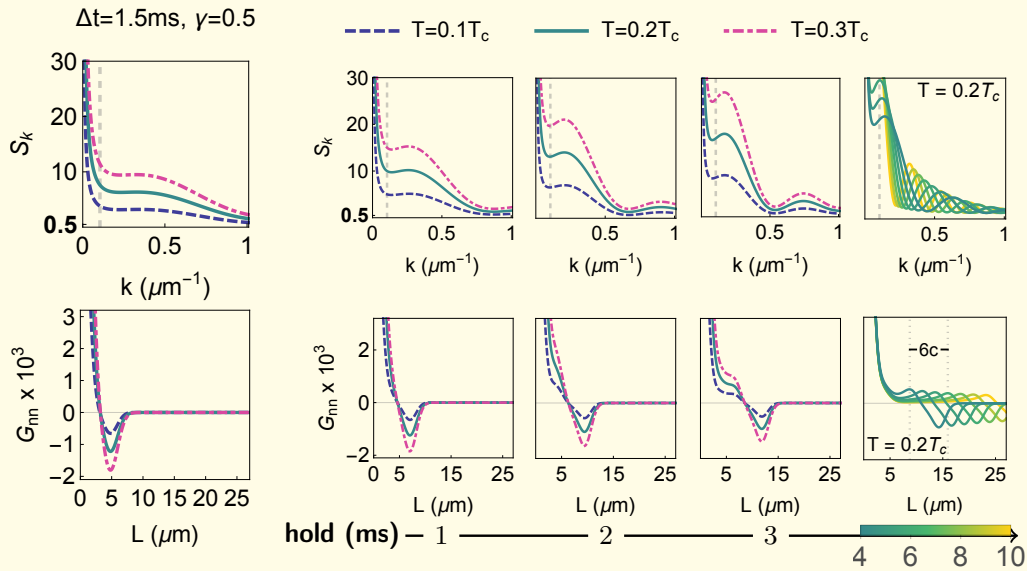


**Figure 5.5 | Analysis of stimulated particle production** in an experimental context. In this case the number of excited low momenta is large, due to the Bose-Einstein distribution of a thermal state, in contrast to particle production from the vacuum. Different temperatures are compared, to find larger occupation at greater temperatures, as expected. On the two-point density contrast side we find a strong anticorrelation peak at short distances, which evolves with time after expansion. The correlation and anticorrelation peaks propagate through the condensate at twice the speed of sound, as indicated through dotted lines in the bottom right panel; this propagation was also experimentally detected. The results shown were obtained through convolution with a Gaussian window function of standard deviation  $w = 0.8 \mu\text{m}$ , corresponding to the estimated experimental precision. Moreover, one can see that the two-point density contrast converges at long times to a thermal state, plus a finite contribution from the excited modes, determined by  $|\beta_k|^2$ . In all the momentum space plots a grey vertical dashed line indicates the experimental low  $k$  limit at inverse condensate size.

Of less experimental interest, but nevertheless relevant, are the equal-time two-point correlation functions of the field  $\phi$

$$\mathcal{G}_{\phi\phi}(t, L) = \frac{1}{a_f} \int_0^\infty \frac{dk}{2\pi} J_0(kL) \left( \frac{1}{2} + N_k(t) - \Delta N_k(t) \right), \quad (5.32)$$

and the mixed correlation functions,

$$\mathcal{G}_{\phi\dot{\phi}}(t, L) = \mathcal{G}_{\dot{\phi}\phi}(t, L) = \frac{1}{a_f^2} \int_0^\infty k \frac{dk}{2\pi} J_0(kL) \text{Im} [\alpha_k \beta_k e^{2ikt/a_f}]. \quad (5.33)$$

Discussion and numerical results around these objects are given in [11].

Now we turn to the experimental simulation of the properties we have discussed above. For the following results we employ SI units; the corresponding expressions in SI units can be found in [12]. The experimental parameters used for the theoretical predictions are given in appendix E. Let us go directly into the predictions and comparison with experimental outcomes.

### Simulation

In Figure 5.5 we show the spectrum of fluctuations after expansion for a decelerated expansion lasting 1.5ms. Three different temperatures are given, to demonstrate the effect of the initial state on the result at final time. The divergence of the spectrum at  $k \rightarrow 0$  is due to the Bose-Einstein thermal distribution, and its shape in this regime is therefore dominated by the initial occupation. The experimental setting we compare to has an initial temperature  $T \sim 0.2T_c$ , so we give greater focus to the analysis of those results. Plots for the rescaled two-point density contrast are also provided, to analyse the correlation and anti-correlation peaks and their propagation in time. As these involve phonons in the trap, the correlations propagate with a velocity corresponding to twice the speed of sound. In Figure 5.5 our results are derived using a Gaussian window function of standard deviation  $w = 0.8 \mu\text{m}$ . Details for different choices of standard deviation are given in [12].

We provide Figure 5.6 to show some of the experimental outcomes for the simulated expansion. Depicted therein is the predicted behaviour for the phase after expansion defined in (5.23) as a function of wavenumber  $k$ , together with the experimental outcome in discrete markers. We can see the agreement at different types of simulated expansion, which certifies a successful implementation of the quantum simulator. In particular, the phase jumps observed for a uniform expansion ( $\gamma = 1$ ) predicted in (D.21) were recovered in the experiments. Next to that result we find the experimental outcome for the two-point density contrast, highlighting also the peak propagation after the expansion has ceased. The experiment was done for two different expansion durations  $\Delta t$ . The discussion around the experimental implementation, and a detailed analysis of the results is extended in [13]. With this we conclude our current exposition on theory and experiment around a quantum simulator for relativistic fields in curved spacetimes with two-dimensional traps.

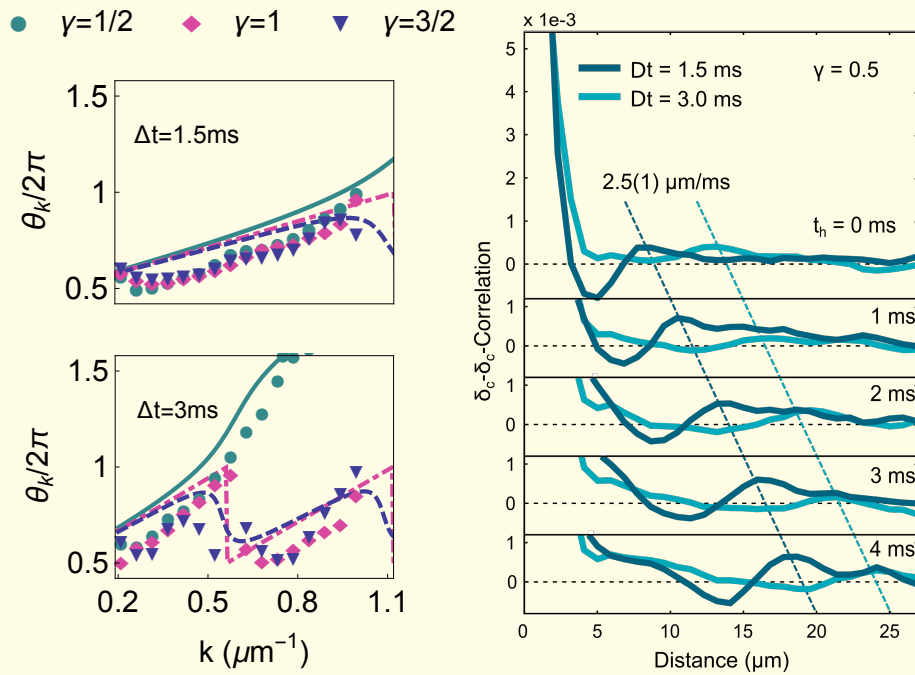


**Figure 5.6 | Agreement with experiments.** On the left we show the predicted phases for momentum modes for two different expansion durations  $\Delta t$ . The theoretical predictions are provided with lines while the experimental outcomes are depicted with markers. It can be seen that the effects of decelerated, uniform, and accelerated expansion were in fact detected in the experimental setting. On the right the experimental result for the two-point density contrast is given, again for two expansion durations, in the case of a decelerated expansion. Propagation of the correlation peaks at twice the speed of sound was verified. The figure on the right hand side is taken from [13] and is further discussed there.

## Concluding remarks

---

*O Faculty of Appearances, when someone falls asleep and dreams, he may hear many accounts of the early formation of the cosmos and the evolution of human and nonhuman life forms... However, when that person wakes up the next morning, it turns out that all those perceived appearances and reports were nothing but his own appearances emerging from and disappearing back into his own nature.*

In this work we have explored two main topics: entanglement in nonrelativistic QFTs, and the implementation of two-dimensional BECs as quantum simulators for relativistic fields in curved spacetimes.

We have tackled challenges regarding numerics to be able to determine entanglement entropies, and arrived to the desired results and known predictions for the relativistic region of the condensate, while obtaining new predictions for the build up of entanglement entropy from its vanishing nonrelativistic value at  $R = 0$ . In particular, for the one-dimensional system we find an agreement with the calculations developed in [65] for entanglement entropy within the Lieb-Liniger model [66, 67]. Furthermore, we found that entanglement entropies in BECs are naturally regulated in the UV, while exhibiting an IR divergence for the one-dimensional scenario. As the IR is within the relativistic region of the condensate, this divergence is actually expected in our inquiry [54], and its behaviour matches that of the literature. An intuitive physical explanation of this phenomenon is discussed in [10], in particular, in [68] it was argued that the homogeneous or zero mode is actually responsible for IR divergences because its amplitude is not restricted energetically. The literature result [69] finds an infrared divergence in entanglement entropy for a free one-dimensional relativistic scalar theory proportional to

$$\frac{1}{2} \ln(-\ln(mR)), \quad (6.1)$$

where  $m$  is a small mass with  $m \rightarrow 0$  and  $R$  a characteristic length scale. Besides introducing a small mass  $m$ , there are other ways to regularise the IR sector, for us it was convenient to introduce an infrared regulator at the momentum

scale  $\mu/L$  by hand. A finite temperature also provides a physical IR regulator, as shown in [70].

Regarding the simulation of curved spacetimes, we built a theoretical procedure through which an acoustic FLRW metric with freedom in choice of spatial curvature can be experimentally implemented. Experimental collaboration gave place for testing our theoretical construct. We provided quantities to be explored in an experimental context to certify the geometries that were predicted, and found fruitful results in the experiments performed.

Both of the topics explored here can give rise to a fascinating area of inquiry when put together. In particular, one can look into entanglement in cosmological horizons, relate what was given here to the notion that entanglement between modes with opposite wave numbers can be witnessed in a two-mode squeezed state, recently observed experimentally in [71] within a homogeneous two-dimensional Bose-Einstein condensate. Explore also things as Page curvature, entanglement of Hawking pairs, and other horizon physics in cosmology, as all the former questions suddenly become experimentally accessible.

## Noninteracting BEC in a box



Although this is textbook material [25], we want to go through the logical steps and ingredients behind Bose-Einstein condensation to put forward the most important quantities and features of this phase of matter. This is best described in the grand canonical ensemble, where the macroscopic fixed parameters are the temperature  $T$  and chemical potential  $\mu$ . The partition function is given by

$$Z = \sum_{N'=0}^{\infty} \sum_q P_{N'}(E_q), \quad (\text{A.1})$$

where

$$P_{N'}(E_q) = e^{(\mu N' - E_q)/T} \quad (\text{A.2})$$

is the probability of the system to be in a state of  $N'$  particles with total energy  $E_q$ . For the ideal gas, the many-body Hamiltonian is given by a sum over the one-particle hamiltonian,

$$\hat{H} = \sum_i \hat{h}_i. \quad (\text{A.3})$$

This naturally has the eigenstates,

$$|q\rangle \propto \prod_i (\hat{a}_i^\dagger)^{n_i} |0\rangle \quad (\text{A.4})$$

with total particle number and energies,

$$N' = \sum_i n_i, \quad E_q = \sum_i \epsilon_i n_i, \quad (\text{A.5})$$

where  $\epsilon_i$  is the energy of each single-particle state.

Let us go through the thermodynamics. We have the grand canonical potential,

$$\Omega = -\frac{\ln Z}{T} = E - TS - \mu N, \quad (\text{A.6})$$

so that the entropy and the total number of particles are determined through

$$S = -\frac{\partial \Omega}{\partial T} \quad \text{and} \quad N = -\frac{\partial \Omega}{\partial \mu}, \quad (\text{A.7})$$

respectively. In particular, for the free gas one obtains the Bose-Einstein distribution, to yield

**Number of particles**

$$N = \sum_i \frac{1}{e^{(\epsilon_i - \mu)/T} - 1} = \sum_i \bar{n}_i. \quad (\text{A.8})$$

Here is where the mechanism of condensation starts to creep in. Notice that the chemical potential is restricted by the condition  $\mu < \epsilon_i$  in order to have  $\bar{n}_i > 0$ . If the chemical potential gets close to the lowest energy,  $\mu \rightarrow \epsilon_0$ , then the occupation  $\bar{n}_0$  becomes macroscopically large. We rewrite (A.8) as

$$N = \bar{n}_0 + \sum_{i \neq 0} \bar{n}_i := N_0 + N_T, \quad (\text{A.9})$$

**Thermal component**

where  $N_0$  is the lowest energy occupation and  $N_T$  is the number of particles outside the condensate, the thermal component. The absence of a condensate implies that  $N_T \leq N$ . For the lowest possible chemical potential,  $\mu = \epsilon_0$  one can define the critical temperature as that which yields  $N_T = N$ , this implies

$$N = N_T(T_c, \mu = \epsilon_0) = \frac{V}{\lambda_{T_c}^3} g_{3/2}(e^{\mu/T}), \quad (\text{A.10})$$

where the last result is calculated by putting the gas in a 3D box of volume  $V$ . Here the energies are given by  $\epsilon_{\mathbf{k}} = \mathbf{k}^2/2m$  and the sum over states in (A.9) is taken to the continuum — calculated as an integral over momentum. We introduced above the thermal wavelength  $\lambda_T = \sqrt{2\pi/mT}$  and the Bose function  $g_q$ . This gives the result for the critical temperature of a 3D condensate in a box

**Critical temperature**

$$T_c = \frac{2\pi}{m} \left( \frac{n}{g_{3/2}(1)} \right)^{2/3} \quad (\text{A.11})$$

and the condensate fraction,

**Condensate fraction**

$$N_0(T) = N \left[ 1 - \left( \frac{T}{T_c} \right)^{3/2} \right], \quad (\text{A.12})$$

macroscopic at low temperatures,  $T < T_c$ . A corresponding analysis can be done for different trapping potentials and boundary conditions, giving place to interesting scenarios. Dimensionality is one particular case of this.

## Lower dimensional BEC

---

As in this work we focus on one- and two-dimensional Bose-Einstein condensates, we cannot obviate the discussion around this topic. We wish here to set the regimes in which our calculations and conclusions are valid.

While Hohenberg's theorem [72] about the absence of long-range-order in one- and two-dimensional systems is taken as a demonstration of the absence of BEC in such settings, it can be shown that symmetry breaking and therefore macroscopic occupation of the lowest one-particle energy state is possible in these regimes [26, 26]. Furthermore, harmonic trapping inducing pancake shapes is a well understood setting for achieving quasi-two-dimensional condensates, while an additional stronger confinement leading to a quasi-one-dimensional cigar shape is a questionable setting for the onset of condensation [64]. In the latter case, the safe treatment of the confined free gas of bosons is carried out in [66, 67] and known as the "Lieb-Liniger model". It is also known that in this one-dimensional geometry the Bogoliubov approximation is valid at low interaction strength  $\lambda$ , and that one branch of the spectrum follows the Bogoliubov dispersion relation. Our results for entanglement entropy in a one-dimensional BEC actually coincide with those of [65], where the Rényi  $\alpha = 2$  entanglement entropy for the Lieb-Liniger model was calculated. The coincidence is of course when weak interactions are taken into account in the latter.

Regarding the construction put forth to build the simulator, the pancake trapping is performed within the Thomas-Fermi approximation, which is still effectively three dimensional, and gives rise to the experimental setting discussed here. Nevertheless, as there is still strong confinement in the  $z$  direction, we are able to apply a two-dimensional treatment at the level of the action, concerned with the introduction of a two-dimensional coupling constant, related to the scattering length through Eq. (2.57).

In general shapes of the trapping potential, the thermodynamical treatment has to be done accordingly. Particular quantities to define this regime involve the relation between the trapping frequencies in each direction, and the density of the condensate. The speed of sound, the chemical potential, the critical temperature, and the coupling strength all depend on the regime one is working on. Extensive discussions can be found for example in [25, 64].



## Horizon problem and inflation

---

For a neat discussion on the horizon problem and its solution, one can turn to [these lecture notes](#). Let us here present a short summary of the way modern cosmology addresses it [73, 74].

In horizon physics one has two important concepts: particle horizon and event horizon. Defined from an event in spacetime  $p$ , the former is the region of spacetime that can have an influence over this event, and the latter is the region in spacetime which can be influenced by  $p$ . These influence regions are set by the speed of light, putting the rules of causality at work.

The evolution of spacetime through merely radiation, matter, and dark energy dominated epochs, implies causally disconnected patches in the cosmic microwave background (CMB) hypersurface, at time  $t = t_{\text{rec}}$ . That is, an evolution from the Big Bang singularity, happening at the equal-time hypersurface set by  $t = 0$ , implies that the hypersurface at time  $t_{\text{rec}}$  is divided in regions which have never been allowed to interchange information between them, given that their particle horizons do not overlap. For this reason, physicists are challenged to understand the observations of a uniform and isotropic radiation, that of the CMB.

The model of inflation solves this problem, by assuming a period of rapid accelerated expansion right after the Big Bang, with a number of e-folds of around 60 to be achieved by the recombination epoch, where the CMB comes from. This expansion is supposed to be driven by a scalar field, known as the inflaton. Discussion around this topic is extensive, and of course out of our present scope.

## Bogoliubov coefficients for polynomial expansion

Let us start with a scale factor with exponent  $\gamma = 1/2$  and the corresponding mode equation in region II (setting  $t_0 = 0$  and considering  $0 < t$ ),

**Solution for  $\gamma = 1/2$**

$$a(t) = Q\sqrt{t} \quad \rightarrow \quad \ddot{v}_k + \frac{1}{t}\dot{v}_k + \frac{\mathbf{k}^2}{Q^2 t}v_k = 0. \quad (\text{D.1})$$

The general form of the mode equation can be found in Table 3.1. The mode functions are to satisfy the boundary conditions

$$\left( v_k^{\text{II}}(t) \stackrel{!}{=} v_k^{\text{I}}(t) \right) \Big|_{t=t_i} \quad \text{and} \quad \left( \dot{v}_k^{\text{II}}(t) \stackrel{!}{=} \dot{v}_k^{\text{I}}(t) \right) \Big|_{t=t_i} \quad (\text{D.2})$$

at initial time, and those

$$\left( v_k^{\text{III}}(t) \stackrel{!}{=} v_k^{\text{II}}(t) \right) \Big|_{t=t_f} \quad \text{and} \quad \left( \dot{v}_k^{\text{III}}(t) \stackrel{!}{=} \dot{v}_k^{\text{II}}(t) \right) \Big|_{t=t_f} \quad (\text{D.3})$$

at final time.

It is useful to remember that we start with,

$$v_k^{\text{I}}(t) = \frac{1}{\sqrt{2ka_i}} e^{-ikt/a_i} \quad (\text{D.4})$$

in region I. The general solution to the mode equation in region II is given by

$$v_k^{\text{II}}(t) = A_k J_0 \left( 2 \frac{|\mathbf{k}| \sqrt{t}}{Q} \right) + B_k Y_0 \left( 2 \frac{|\mathbf{k}| \sqrt{t}}{Q} \right), \quad (\text{D.5})$$

where  $J_0$  and  $Y_0$  are Bessel functions of the first and second kind, respectively. Implementing the boundary conditions (D.2), the coefficients  $A_k$  and  $B_k$  evaluate to

$$\begin{aligned} A_k &= \frac{\pi \sqrt{\omega_k^{\text{I}} t_i}}{\sqrt{2Q}} e^{-i\omega_k^{\text{I}} t_i} \left[ iY_0(2\omega_k^{\text{I}} t_i) - Y_1(2\omega_k^{\text{I}} t_i) \right], \\ B_k &= -\frac{\pi \sqrt{\omega_k^{\text{I}} t_i}}{\sqrt{2Q}} e^{-i\omega_k^{\text{I}} t_i} \left[ iJ_0(2\omega_k^{\text{I}} t_i) - J_1(2\omega_k^{\text{I}} t_i) \right], \end{aligned} \quad (\text{D.6})$$

where we have introduced the frequency in region I,  $\omega_k^I = k/a_i$ . Again,  $J_1$  and  $Y_1$  are Bessel functions of the first and second kind.

We define for each region  $\nu_k^I := \omega_k^I t_i$  and  $\nu_k^{III} := \omega_k^{III} t_f$ , plug the coefficients (D.6) into the solution (D.5), remember that the mode function in region III is given by

$$v_k^{III}(t) = \frac{1}{\sqrt{2a_f k}} (\alpha_k^* e^{-ikt/a_f} - \beta_k e^{ikt/a_f}), \quad (D.7)$$

implement the boundary conditions (D.3), and obtain

$$\alpha_k^* = \frac{\pi \sqrt{\nu_k^I \nu_k^{III}}}{2} e^{i(\nu_k^{III} - \nu_k^I)} \left\{ [iY_0(2\nu_k^I) - Y_1(2\nu_k^I)] [J_0(2\nu_k^{III}) - iJ_1(2\nu_k^{III})] \right. \\ \left. - [iJ_0(2\nu_k^I) - J_1(2\nu_k^I)] [Y_0(2\nu_k^{III}) - iY_1(2\nu_k^{III})] \right\} \quad (D.8)$$

**Bogoliubov coefficients** and

$$\beta_k = \frac{\pi \sqrt{\nu_k^I \nu_k^{III}}}{2} e^{-i(\nu_k^{III} + \nu_k^I)} \left\{ [iJ_0(2\nu_k^I) - J_1(2\nu_k^I)] [Y_0(2\nu_k^{III}) + iY_1(2\nu_k^{III})] \right. \\ \left. - [iY_0(2\nu_k^I) - Y_1(2\nu_k^I)] [J_0(2\nu_k^{III}) + iJ_1(2\nu_k^{III})] \right\}. \quad (D.9)$$

Our job is done.

**Solution for  $\gamma = 1$  in conformal time**

Let us now investigate the case  $\gamma = 1$  in conformal time. The corresponding mode equation is [see Table 3.1]

$$v_k'' + (\mathbf{k}^2 + M^2(\eta)) v_k = 0, \quad (D.10)$$

with

$$M^2(\eta) = -\frac{Q^2}{4} \left[ \Theta(\eta - \eta_i) \Theta(\eta_f - \eta) + \frac{2}{Q} (\delta(\eta - \eta_i) - \delta(\eta_f - \eta)) \right] \quad (D.11)$$

So, the mode functions in conformal time are to satisfy the boundary conditions

$$\left( v_k^{II}(\eta) \stackrel{!}{=} v_k^I(\eta) \right) \Big|_{\eta=\eta_i} \quad \text{and} \quad \left( v_k^{II'}(\eta) \stackrel{!}{=} v_k^{I'}(\eta) + \frac{Q}{2} v_k^I(\eta) \right) \Big|_{\eta=\eta_i} \quad (D.12)$$

at initial conformal time, and

$$\left( v_k^{III}(\eta) \stackrel{!}{=} v_k^{II}(\eta) \right) \Big|_{\eta=\eta_f} \quad \text{and} \quad \left( v_k^{III'}(\eta) \stackrel{!}{=} v_k^{II'}(\eta) - \frac{Q}{2} v_k^{II}(\eta) \right) \Big|_{\eta=\eta_f} \quad (D.13)$$

at final conformal time. In this case we start with the mode function expressed in conformal time as

$$v_k^I(\eta) = \frac{1}{\sqrt{2k}} e^{-ik\eta} \quad (\text{D.14})$$

in region I. The general solution to the mode equation (D.10) in region II is given by

$$v_k^{II}(\eta) = A_k e^{-h\eta} + B_k e^{h\eta} \quad \text{with} \quad h = \sqrt{\frac{Q^2}{4} - k^2} \quad (\text{D.15})$$

Implementing the boundary conditions (D.12), the coefficients  $A_k$  and  $B_k$  evaluate to

$$\begin{aligned} A_k &= \frac{1}{2\sqrt{2k}} e^{(-ik+h)\eta_i} \left( 1 - \frac{Q}{2h} + \frac{ik}{h} \right) \\ B_k &= \frac{1}{2\sqrt{2k}} e^{-(ik+h)\eta_i} \left( 1 + \frac{Q}{2h} - \frac{ik}{h} \right). \end{aligned} \quad (\text{D.16})$$

The mode function in conformal time in region III is given by

$$v_k^{III}(\eta) = \frac{1}{\sqrt{2k}} (\alpha_k^* e^{-ik\eta} - \beta_k e^{ik\eta}) \quad (\text{D.17})$$

so we substitute with (D.16) into the solution (D.15), implement the boundary conditions (D.13), and obtain

$$\alpha_k^* = \frac{1}{2h} e^{ik(\eta_f - \eta_i)} [(h + ik)e^{-h(\eta_f - \eta_i)} + (h - ik)e^{h(\eta_f - \eta_i)}] \quad (\text{D.18})$$

and

$$\beta_k = \frac{Q}{4h} e^{-ik(\eta_f + \eta_i)} [e^{-h(\eta_f - \eta_i)} - e^{h(\eta_f - \eta_i)}]. \quad (\text{D.19})$$

Let us analyse this last result a bit. First of all, for a linear scale factor  $a(t) = Qt$  we have

$$\eta_f - \eta_i = \frac{1}{Q} \ln \left( \frac{t_f}{t_i} \right) = \frac{N_e}{Q} \quad (\text{D.20})$$

expressed in terms of the e-fold number [see Eq. (5.13)]. This will simplify our expressions a bit. Now, we can see in (D.19) that for imaginary values of  $h$  (that is for  $k > Q/2$ ) we obtain an oscillatory function  $\beta_k$  with zeroes at

$$\frac{hN_e}{Q} = in\pi, \quad \rightarrow \quad k = Q \sqrt{\frac{n^2 \pi^2}{N_e^2} + \frac{1}{4}} \quad (\text{D.21})$$

where we have substituted for  $h$  with (D.15). This of course yields for  $\alpha_k$  just a phase, so that  $|\alpha_k|^2 = 1$ . Those  $k$  modes are therefore not excited by the process of particle production in this type of expansion. This result also yields a phase jump of  $\pi$  in  $\theta_k$  as defined in (5.23), and further explored in Figure 5.4.

**Bogoliubov  
coefficients**

## Experimental implementation

---

The two-dimensional condensate implemented in the experiments is composed of potassium-39 atoms, with an approximate occupation of  $N_0 = 23,000$  atoms. Confinement in the  $z$ -direction is achieved with a trapping frequency of  $\omega_z = 3.2\pi$  kHz, while the radial trapping frequency  $\omega(t)$  is dynamically adjusted between 23 and 7 Hz. This gives rise to a two-dimensional harmonic trap, with a Thomas-Fermi radius of the condensate around  $25 \mu\text{m}$  for the curvature measurements and  $30 \mu\text{m}$  for the expansion measurements. An inverse trapping potential, and thus positive spatial curvature, is configured by means of a digital micromirror device [75]. The scattering length is adjusted utilising the Feshbach resonance at  $562.2 \pm 1.5$  G [34]. For the analysis of wave packet propagation (Figure 5.2) the scattering length is set to  $100 a_0$  for the hyperbolic geometry, and to  $200 a_0$  for the spherical one. In the expansion experiments the scattering length is ramped from  $400 a_0$  to  $50 a_0$ . Imaging resolution is  $1 \mu\text{m}$ . Further details are given in [13]

In correspondence with the experimental implementation, and within the error bounds, the parameters used for the theoretical predictions are: a condensate density of  $n = 16.6$  atoms/ $\mu\text{m}^2$ , together with an initial scattering of  $350 a_0$  and a final one of  $50 a_0$ . This determines the coupling and, thereafter, the scale factor. We take an imaging resolution of  $0.8 \mu\text{m}$  and determine a two-dimensional critical temperature at initial time of  $T_c = 192.8$  nK.

# Bibliography

---

- [1] Barceló C, Liberati S, and Visser M, Analogue gravity [Living Rev Relativ](#) **14**, 3 (2011).
- [2] Visser M, Barceló C, and Liberati S, Analogue models of and for gravity [Gen Relativ Gravit](#) **34**, 1719 (2002).
- [3] Novello M, Visser M, and Volovik GE (eds), [Artificial Black Holes](#) (World Scientific Publishing 2002).
- [4] Gibbons GW and Hawking SW, Cosmological event horizons, thermodynamics, and particle creation [Phys Rev D](#) **15**, 2738 (1977).
- [5] Page DN, Information in black hole radiation [Phys Rev Lett](#) **71**, 3743 (1993).
- [6] Srednicki M, Entropy and area [Phys Rev Lett](#) **71**, 666 (1993).
- [7] Bombelli J, Koul RK, Lee J, and Sorkin RD, Quantum source of entropy for black holes [Phys Rev D](#) **34**, 373 (1986).
- [8] Hawking SW, Particle creation by black holes [Comm Math Phys](#) **43**, 199 (1975).
- [9] Unruh WG, Experimental black-hole evaporation? [Phys Rev Lett](#) **46**, 1351 (1981).
- [10] Sánchez-Kuntz N and Floerchinger S, Spatial entanglement in interacting Bose-Einstein condensates [Phys Rev A](#) **103**, 043327 (2021).
- [11] Sánchez-Kuntz N, Parra-López Á, Tolosa-Simeón M, Haas T, and Floerchinger S, Scalar quantum fields in cosmologies with  $2 + 1$  spacetime dimensions [Phys Rev D](#) **105**, 105020 (2022).
- [12] Tolosa-Simeón M, Parra-López Á, Sánchez-Kuntz N, Haas T, Viermann C, Sparrn M, Liebster N, Hans M, Kath E, Strobel H, Oberthaler MK, and Floerchinger S, Curved and expanding spacetime geometries in Bose-Einstein condensates [Phys Rev A](#) **106**, 033313 (2022).

- 
- [13] Viermann C, Sparn M, Liebster N, Hans M, Kath E, Strobel H, Parra-López Á, Tolosa-Simeón M, Sánchez-Kuntz N, Haas T, Floerchinger S, and Oberthaler MK, Quantum field simulator for dynamics in curved spacetime [arXiv:2202.10399](#), (2022).
- [14] Barceló C, Liberati S, and Visser M, Probing semiclassical analog gravity in Bose-Einstein condensates with widely tunable interactions [Phys Rev A](#) **68**, 053613 (2003).
- [15] Fedichev PO and Fischer UR, Gibbons-Hawking effect in the sonic de Sitter space-time of an expanding Bose-Einstein-condensed gas [Phys Rev Lett](#) **91**, 240407 (2003).
- [16] Fedichev PO and Fischer UR, “Cosmological” quasiparticle production in harmonically trapped superfluid gases [Phys Rev A](#) **69**, 033602 (2004).
- [17] Fischer UR, Quasiparticle universes in Bose–Einstein condensates [Mod Phys Rev A](#) **19**, 1789 (2004).
- [18] Fischer UR and Schützhold R, Quantum simulation of cosmic inflation in two-component Bose-Einstein condensates [Phys Rev A](#) **70**, 063615 (2004).
- [19] Uhlmann M, Xu Y, and Schützhold R, Aspects of cosmic inflation in expanding Bose-Einstein condensates [New J Phys](#) **7**, 248 (2005).
- [20] Calzetta EA and Hu BL, Early universe quantum processes in BEC collapse experiments [Int J Theor Phys](#) **44**, 1691 (2005).
- [21] Jain P, Weinfurtner S, Visser M, and Gardiner CW, Analog model of a Friedmann-Robertson-Walker universe in Bose-Einstein condensates: Application of the classical field method [Phys Rev A](#) **76**, 033616 (2007).
- [22] Weinfurtner S, Jain P, Visser M, and Gardiner CW, Cosmological particle production in emergent rainbow spacetimes [Class Quantum Gravity](#) **26**, 065012 (2009).
- [23] Prain A, Fagnocchi S, and Liberati S, Analogue cosmological particle creation: Quantum correlations in expanding Bose-Einstein condensates [Phys Rev D](#) **82**, 105018 (2010).
- [24] Altland A and Simons B, [Condensed Matter Field Theory](#) (Cambridge University Press 2010).
- [25] Pitaevskii L and Stringari S, [Bose–Einstein Condensation and Superfluidity](#) (Oxford University Press 2016).

- 
- [26] Sütő A, Bose-Einstein condensation and symmetry breaking [Phys Rev A](#) **71**, 023602 (2005).
- [27] Sütő A, Equivalence of Bose-Einstein condensation and symmetry breaking [Phys Rev Lett](#) **94**, 080402 (2005).
- [28] Yukalov VI, Bose-Einstein condensation and gauge symmetry breaking [Laser Phys Lett](#) **4**, 632 (2007).
- [29] Lieb EH, Seiringer R, and Yngvason J, Bose-Einstein condensation and spontaneous symmetry breaking [Rep Math Phys](#) **59**, 389 (2007).
- [30] Landau LD and Lifshitz EM, [Quantum Mechanics: Non-relativistic Theory](#) (Pergamon Press 1977).
- [31] Zee A, [Quantum Field Theory in a Nutshell](#) (Princeton University Press 2010).
- [32] Ratra B and Peebles PJE, Inflation in an open universe [Phys Rev D](#) **52**, 1837 (1995).
- [33] Ratra B, Inflation in a closed universe [Phys Rev D](#) **96**, 103534 (2017).
- [34] D'Errico C, Zaccanti M, Fattori M, Roati G, Inguscio M, Modugno G, and Simoni A, Feshbach resonances in ultracold 39K [New J Phys](#) **9**, 223 (2007).
- [35] Reeh H and Schlieder S, Bemerkungen zur unitärequivalenz von lorentz-invarianten feldern [Il Nuovo Cimento](#) **22**, 1051 (1961).
- [36] Witten E, APS Medal for Exceptional Achievement in Research: Invited article on entanglement properties of quantum field theory [Rev Mod Phys](#) **90**, 045003 (2018).
- [37] Summers SJ and Werner R, The vacuum violates Bell's inequalities [Phys Lett A](#) **110**, 257 (1985).
- [38] Summers SJ and Werner R, Maximal violation of Bell's inequalities is generic in quantum field theory [Commun Math Phys](#) **110**, 247 (1987).
- [39] Landau LJ, On the violation of Bell's inequality in quantum theory [Phys Lett A](#) **120**, 54 (1987).
- [40] Landau LJ, On the non-classical structure of the vacuum [Phys Lett A](#) **123**, 115 (1987).
- [41] Benedict E and Pi SY, Entanglement entropy of nontrivial states [Ann Phys](#) **245**, 209 (1996).

- 
- [42] Holzhey C, Larsen F, and Wilczek F, Geometric and renormalized entropy in conformal field theory [Nucl Phys B](#) **424**, 443 (1994).
- [43] Casini H and Huerta M, Lectures on entanglement in quantum field theory [arXiv:2201.13310v1](#), (2022).
- [44] Chandran SM and Shankaranarayanan S, One-to-one correspondence between entanglement mechanics and black hole thermodynamics [Phys Rev D](#) **102**, 125025 (2020).
- [45] Eisert J and Plenio MB, Introduction to the basics of entanglement theory in continuous-variable systems [Int J Quantum Inf](#) **01**, 479 (2003).
- [46] Berges J, Floerchinger S, and Venugopalan R, Dynamics of entanglement in expanding quantum fields [J High Energy Phys](#) **2018**, 145 (2018).
- [47] Eisert J, Cramer M, and Plenio MB, Colloquium: Area laws for the entanglement entropy [Rev Mod Phys](#) **82**, 277 (2010).
- [48] Cramer M, Eisert J, Plenio MB, and Dreißig J, Entanglement-area law for general bosonic harmonic lattice systems [Phys Rev A](#) **73**, 012309 (2006).
- [49] Calabrese P and Cardy J, Entanglement entropy and conformal field theory [J Phys A Math Theor](#) **42**, 504005 (2009).
- [50] Ryu S and Takayanagi T, Aspects of holographic entanglement entropy [J High Energy Phys](#) **2006**, 045 (2006).
- [51] Amico L, Fazio R, Osterloh A, and Vedral V, Entanglement in many-body systems [Rev Mod Phys](#) **80**, 517 (2008).
- [52] Riera A and Latorre JI, Area law and vacuum reordering in harmonic networks [Phys Rev A](#) **74**, 052326 (2006).
- [53] Vidal G, Latorre JI, Rico E, and Kitaev A, Entanglement in quantum critical phenomena [Phys Rev Lett](#) **90**, 227902 (2003).
- [54] Mallayya K, Tibrewala R, Shankaranarayanan S, and Padmanabhan T, Zero modes and divergence of entanglement entropy [Phys Rev D](#) **90**, 044058 (2014).
- [55] Korepin VE, Universality of entropy scaling in one dimensional gapless models [Phys Rev Lett](#) **92**, 096402 (2004).
- [56] Calabrese P and Cardy J, Entanglement entropy and quantum field theory [J Stat Mech Theory Exp](#) **2004**, P06002 (2004).

- 
- [57] Parker L, Quantized fields and particle creation in expanding universes. I *Phys Rev* **183**, 1057 (1969).
- [58] Birrell ND and Davies PCW, *Quantum Fields in Curved Space* (Cambridge University Press 1982).
- [59] Weinberg S, *Cosmology* (Oxford University Press 2008).
- [60] Mukhanov V and Winitzki S, *Introduction to Quantum Effects in Gravity* (Cambridge University Press 2007).
- [61] Simon C, Natural entanglement in Bose-Einstein condensates *Phys Rev A* **66**, 052323 (2002).
- [62] Floerchinger S, Variational principle for theories with dissipation from analytic continuation *J High Energy Phys* **9**, 99 (2016).
- [63] Calzetta EA and Hu BLB, *Nonequilibrium Quantum Field Theory* (Cambridge University Press 2008).
- [64] Dalfovo F, Giorgini S, Pitaevskii LP, and Stringari S, Theory of Bose-Einstein condensation in trapped gases, *Rev Mod Phys* **71**, 463 (1999).
- [65] Herdman CM, Roy PN, Melko RG, and Del Maestro A, Spatial entanglement entropy in the ground state of the Lieb-Liniger model *Phys Rev B* **94**, 064524 (2016).
- [66] Lieb EH, Exact analysis of an interacting Bose gas. II. The excitation spectrum *Phys Rev* **130**, 1616 (1963).
- [67] Lieb EH and Liniger W, Exact analysis of an interacting Bose gas. I. The general solution and the ground state *Phys Rev* **130**, 1605 (1963).
- [68] Unruh WG, Comment on "Proof of the quantum bound on specific entropy for free fields" *Phys Rev D* **42**, 3596 (1990).
- [69] H Casini H and Huerta M, Entanglement entropy in free quantum field theory *J Phys A Math Theor* **42**, 504007 (2009).
- [70] Solodukhin SN, Entanglement entropy of black holes *Living Rev Relativ* **14**, 8 (2011).
- [71] Chen CA, Khlebnikov S, and Hung CL, Observation of quasiparticle pair production and quantum entanglement in atomic quantum gases quenched to an attractive interaction *Phys Rev Lett* **127**, 060404 (2021).
- [72] Hohenberg PC, Existence of long-range order in one and two dimensions *Phys Rev* **158**, 383 (1967).

- 
- [73] Guth AH, Inflationary universe: A possible solution to the horizon and flatness problems [Phys Rev D](#) **23**, 347 (1981).
- [74] Linde AD, A new inflationary universe scenario: A possible solution of the horizon, flatness, homogeneity, isotropy and primordial monopole problems [Phys Lett B](#) **108**, 389 (1982).
- [75] Saint-Jalm R, Castilho PCM, Le Cerf É, Bakkali-Hassani B, Ville JL, Nascimbene S, Beugnon J, and Dalibard J, Dynamical symmetry and breathers in a two-dimensional Bose gas [Phys Rev X](#) **9**, 021035 (2019).

# Agradecimientos

---

First of all, I want to extend my deep gratitude to Prof. Dr. Stefan Flörchinger, whose highly professional yet human support throughout all projects made possible the successful completion of this work. At the same time, this work would not have been what it is without the close collaboration of Tobias Hass, Mireia Tolosa-Simeón, and Álvaro Parra-López, all great minds to whom I regard with admiration. I also want to thank Simon Brunner and Feodor Konomaev, who gave me the opportunity to learn from their personal projects, and to discuss our common ground continuously. For not only fun discussions but also important practical solutions to numerical issues, I want to thank Alaric Erschfeld. Furthermore, I would like to mention other members of the group whose support and joy always brought a bright side to the routinely task of research: Aleksas, Eduardo, Neil, Lars, Daniel, Andreas, Lara, Natalie, thank you for your continuous inputs to discussion. I would like to thank Chris for his companionship since my arrival to Heidelberg, both as a friend and insightful colleague.

A special mention goes to Celia Vierman, Nikolas Liebster, Marius Sparn, Maurus Hans, Elinor Kath, Helmut Strobel, and Markus Oberthaler, for their willingness and trust in embarking to a committed collaboration between theory and experiment.

I want to thank all the tutors, teachers, students, staff, which keep this place running and full of life, allowing us to have a complete and fulfilled learning experience. Very importantly, I want to thank my official scholarship providers: the Deutscher Akademischer Austauschdienst (DAAD, German Academic Exchange Service) under the Länderbezogenes Kooperationsprogramm mit Mexiko: CONACYT Promotion, 2018 (57437340).

On another note: thank you Carlos for your ever present ears, company, and support, Emilian, for your closeness, letza, for the fun saliditas juntas, Aristeia, for your bright smile, my neighbours, who make me feel at home. In all, the people around me that have supported long winters far from my root system. Here I also include all my sanghas, who are here everyday through their loving members: Veerle, Maria, Emilio, Balp, Carlos, Adri, Atenea, Yon, Alma, Anaíd, Rodrigo, and the list goes on... thank you all for your natural loving hearts. Now would be the turn to thank a long list of teachers who gave me the precise instructions in the precise moments, to grow in all possible areas of my life. A special mention to Eduardo Nahmad, my early years mentor physics-wise, and to Alan Wallace, my beacon in life. All the rest remain in my heart, they know

they are there, no mention required.

Now that we have extended all around the world, I go to my Mexican crew, magos, hermanas, amores. Pilar, gracias amor de mis vidas por tu luz y guía. Andrea, gracias por las charlas extendidas y reflexiones entre risas. Annie, gracias por estar, volver, renacer y ser ante mis ojos. Paola, sí, no estás en la sangha, pero estás acá, como mujer, compañera, fiel guerrera y exploradora de caminos (ya estoy llorando, creo que sólo era cosa de cambiar a español). Leo, hermanito de amor, gracias siempre. Nelson, por los cíclicos retornos de la magia. Fabian, por tu padrísima presencia, de buenas o de malas. Rubén, por la lírica y consistente compañía. Quique, por los compartires extensos. Eli, hermana más allá del tiempo, gracias por tu esencia y fuerza. Tania, gemelita del juego y la alegría, gracias por tus pócimas secretas.

Paso a mi papá. Ay no, que lloro otra vez. Hay cosas que las lágrimas expresan mejor que las palabras. La fragilidad diciendo: "gracias por estar, no sé qué haría, qué hubiera hecho, sin tí". Gracias por el apoyo, la reflexión, la sabiduría, el aprendizaje, los abrazos, la formación, la exploración, la libertad, la confianza, la fé, el mundo. Las puertas, los caminos, los libros, los pensamientos, la no verdad, la verdad, la mística, el espíritu y los fundamentos que nos ayudan a no perdernos. Gracias María por estar con nosotros con tu ligereza y fortaleza iguales.

Paso a mi mamá. Sin dejar de llorar y transformando mis lágrimas de un tipo de llanto a otro, escenifica este río en mi rostro la gratitud a la vida (*que me ha dado tanto, me ha dado la risa y me ha dado el llanto*). Pero mamá, ¿no era necesario tanto sacrificio! La gratitud de tenerte ya era inmensa antes de todo: después de tu accidente entendí mejor el significado del infinito. ¿Era momento de entenderlo? No lo sé, pero camino con la confianza de que el Universo sabe que sí. Se agarró de un alma fuerte como la tuya para darnos lecciones a todos a tu alrededor. Para animarnos a explorar profundidades más adversas y paisajes más temidos. Para encontrar en ellos tesoros perdidos, y comunicarlos al tiempo que viene, vendrá. Todo nos prepara. Gracia mamá por ser esa fuerza de preparación constante y persistente en mi vida: desde antes de nacer, en cada uno de mis palpitaes, hasta la eternidad. Gracias por el impulslo vital que imprimes en mí y que ahora es mío. Gracias por tu apoyo, compañía y complicidad en todo momento.

A Roberto. Tú podrías haber estado allá arriba en la categoría de maestros: en tí, nuestro vínculo y nuestras conversaciones encuentro siempre lecciones y cosas que aprender. Retos, dificultades, retos superados, obstáculos vencidos, nuevos objetivos. Gracias por los objetivos compartidos, por la solidaridad y todo el sostén y soporte.

A mi tío Memo, por ser el centro de fuerza de una pequeña familia, que tuvo sus orígenes en un Norte mexicano. Por la paternalidad, la atención, la disposición y todos los cuidados. Gracias por la escucha, el espacio, la presencia.

Gracias por estar.

Santos, Marcela, Fer, Xime, Valentina, Mónica, ¿qué se creen que se iban a librar? No, pero ya no estoy llorando, eso sí. Ahora sólo tengo una sonrisa al recordar la calidez (ay no, ahí viene el llanto)... la calidez que le traen a mi vida. Gracias a cada uno de ustedes, saben lo que son para mí, en mis alegrías y gozos.

Daria, topo de amor y luz (\*risas\*). Cómo te quiero, cómo te admiro, cómo te extraño y cómo nos hacen falta tantas pláticas. Gracias por la inspiración, la confianza, todos los vaivenes. Que vengan más, por favor.

Por último quiero mencionar a todes les que no menciono, pero que han dejado en mi cuerpo y mi ser marcas, cicatrices, caminos, pistas, linternas, oscuridades, semillas, canales, lagos, estanques, grietas, arrecifes, mareas, precipicios, cuevas, constelaciones, montañas, nubes, chubascos, cielos despejados, lunas menguantes. Si algún día temí tanta naturaleza suelta, tanto barranco peligroso, hoy (entre llanto ahorita), he aprendido a prepararme un té, un chocolate caliente, una bebida refrescante — dependiendo la estación — y salir a admirar el paisaje, al final hermoso en su majestuosidad. Gracias por las cicatrices. Gracias Julie por ser mi guía en la exploración de este mundo maravilloso. Gracias llanto por seguir llenando de agua las grietas, para que podamos seguir sanando y fluyendo en el nuevo saber, de nuevos horizontes. Gracias vida por tu compasión infinita. Y es así que logro terminar este proyecto hoy, que aunque parece sólo de física, es mucho más que eso, es sobre el misterio de nuestra humanidad. Gracias humanidad por permitirme echar un vistazo.